LEAD ARTICLE

Acta Cryst. (1996). A52, 509–560

Crystallography of Quasiperiodic Crystals

AKIJI YAMAMOTO

National Institute for Research in Inorganic Materials, Tsukuba 305, Japan. E-mail: yamamoto@nirim.go.jp

(Received 24 October 1995; accepted 4 March 1996)

Abstract

The aim of this review is to describe many approaches to modulated crystals and quasicrystals developed in two decades after the introduction of higher-dimensional crystallography in a unified way. Much attention is focused on higher-dimensional crystallography of quasicrystals, which is under development. After discussions on symmetries of modulated crystals and methods of their structure analysis, many subjects on the analysis of quasicrystals are discussed, which include methods of generating quasiperiodic tilings, their diffraction patterns, similarity transformations, indexing problems, point density of quasicrystals, phason distortion, relations between quasicrystals and their crystalline approximants, model constructions, Patterson, refinement and maximum-entropy methods for quasicrystals, and superstructures in quasicrystals. In particular, the theories for octagonal, decagonal, dodecagonal and icosahedral quasicrystals are given in detail.

1. Introduction

Two decades have passed since the introduction of higher-dimensional crystallography for modulated crystals (modulated structures) and a decade since the discovery of quasicrystals. There exist three kinds of quasiperiodic structures to which higher-dimensional crystallography is applicable. The modulated structure is the oldest one, which was found in 1929 by Dehlinger. The so-called composite crystals were discovered in the 1970's (Makovicky & Hyde, 1981) and quasicrystals were found in 1984 (Shechtman, Blech, Gratias & Cahn, 1984). In particular, the discovery of quasicrystals extended the applicability of higher-dimensional space groups to non-crystallographic cases. The first quasicrystal found forced us to reconsider the concept of crystals. A quasicrystal shows no translational periodicity along any direction in three-dimensional (3D) space but has Bragg spots in the diffraction pattern. Furthermore, the rotational symmetry is non-crystallographic, including fivefold axes. The basis for understanding such a peculiar structure lies in higher-dimensional crystallography, which was introduced for incommensurately modulated structures.

In 1974, de Wolff proposed the description of a modulated structure in 4D space (de Wolff, 1974). This is based on the fact that the (X-ray) diffraction pattern of a crystal is the Fourier spectrum of its electron density. The first remark on the diffraction pattern is that it is indexable with n (>3) vectors as $\mathbf{h} = \sum_{i=1}^{n} h_i \mathbf{b}_i^*$, where $\mathbf{h}$ is the diffraction vector in 3D space, $\mathbf{b}_i^*$ ($i = 1, 2, \ldots, n$) are the basis vectors to index the diffraction vectors with generalized Miller indices $h_1, h_2, \ldots, h_n$. This implies that the location of diffraction spots is related to an n-dimensional lattice. In fact, the diffraction spots can be regarded as the projection of the nD reciprocal-lattice points onto 3D space. The diffraction spots then suggest a periodic structure in nD space. From the properties of the Fourier transformation, the intersection of electron density at the subspace normal to some direction is obtained from the diffraction pattern projected onto the subspace along that direction. The irrational (gradient) intersection of the periodic electron density leads to an aperiodic structure in the intersection. Thus, the modulated structure which has lost a period along some direction can be expressed as an irrational 3D intersection of a periodic structure in nD space. The symmetry of such a crystal in nD space will be given by the space group in nD space. The space groups in 4D space were calculated in the 1970's (Brown, Bülow, Neubüser, Wondratschek & Zassenhaus, 1978).

On the other hand, another remark is reflected in the classification of nD space groups for modulated structures. In the diffraction pattern of modulated structures, we can easily recognize prominent reflections constructing a 3D lattice. These so-called main reflections are accompanied by weak satellite reflections. This means that there exists an average structure with 3D periodicity and a weak perturbation from it. This restricts the possible point group within the crystallographic ones

After obtaining his Master's degree at Tokyo Institute of Technology, Dr A. Yamamoto obtained his doctorate at Kyoto University by studies of modulated structure analyses based on superspace groups. Since then, he has worked on methods of structure analyses of modulated structures and composite crystals, and has more recently been developing the method of structure analysis of quasicrystals based on a description in higher-dimensional space.

because the main reflections have to be transformed into themselves by it. Therefore, it is convenient to distinguish the three axes in nD space from the others. This leads to a finer classification of nD space groups. They are called superspace groups. The theory of superspace groups was introduced by Janner & Janssen (1977, 1979, 1980*a*). The first structure analyses of incommensurate and commensurate modulated structures based on 4D crystallography were given by van Aalst, den Hollander, Peterse & de Wolff (1976) and Valentine, Cavin & Yakel (1977). Yamamoto (1982*a*) derived a general structure-factor formula based on nD crystallography.

Another kind of crystal shows different diffraction patterns, in which two or more sets of 3D lattices with periods incommensurate to each other are seen. This implies that the crystal consists of two or more substructures with different periods at least along one direction. These are called chimney-ladder structures, misfit-layer structures, vernier structures or composite crystals. The diffraction patterns of composite crystals are also indexable with n (>3) vectors and generalized Miller indices. For the same reason as in modulated structures, their point group is crystallographic and the symmetry is specified by a superspace group (Janner & Janssen, 1980*a*,*b*). The classification of this superspace group should be different from that of modulated structures but it is not established yet. In any case, the structure can be analyzed on the basis of an nD space group or appropriate superspace group. Such structure analyses were made by Kato (1990) and van Smaalen (1991).

In contrast to these two kinds of crystal, there are no prominent reflections constructing a 3D sublattice in quasicrystals. Their diffraction pattern shows a non-crystallographic symmetry. The essential difference between the quasicrystals and the modulated structures or the composite crystals exists in these two points. Usually, quasicrystals are defined by a structure showing diffraction patterns with diffraction spots having non-crystallographic point symmetry. Examples of the diffraction patterns of a modulated structure and a composite crystal are shown in Fig. 1, which are compared with the typical diffraction patterns of quasicrystals in Fig. 2. All the cases can equally be indexed by more than three vectors and integers (Miller indices) as shown in §2.

Since the discovery of a quasicrystal in an Al–Mn alloy in 1984, extensive studies have been made to clarify the structure of this unusual material, which has long-range translational order and non-crystallographic rotational symmetry. Several important ideas for understanding such diffraction properties have, however, been shown in studies long before this discovery. A basic concept is a modern n-dimensional ($n > 3$) crystallography introduced by de Wolff in 1974 to interpret the diffraction patterns of the modulated structure. The root of the structural studies of quasicrystal structures comes from the Penrose tiling shown in the same year (Penrose, 1974, 1977). This is a 2D space filling with two kinds of tile without gaps, the vertices of which were shown later to give many sharp spots with tenfold symmetry in its optical diffraction pattern (Mackay, 1981). In both cases, mathematical theories have been developed to extend the first primitive ideas. In 1984, the year of the discovery of the quasicrystal, the theory of symmetry of incommensurately modulated structures and the description of their structures in n-dimensional (nD) space had almost been established. On the other hand, a mathematical theory of Penrose tiling had been given by de Bruijn 3 years before the discovery of the quasicrystal (de Bruijn, 1981) and its extension to

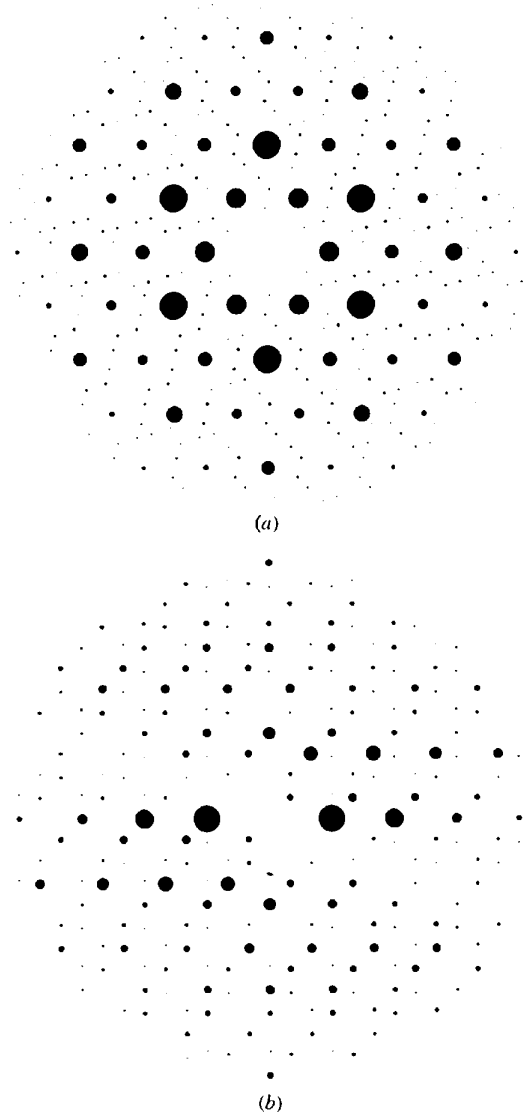

Fig. 1. Examples of diffraction patterns of modulated and composite crystals. (*a*) a^*b^* plane of the 2D modulated structure 1*T*-TaS_2. (*b*) b^*c^* plane of the composite crystal $[Ba]_x[(Pt, Cu)O_3]$.

the 3D Penrose tiling with icosahedral symmetry was published just before the discovery (Kramer & Neri, 1984). Thus, as soon as the first report by Shechtman *et al.* was published, the diffraction patterns of the 3D Penrose tiling were given (Duneau & Katz, 1985; Katz & Duneau, 1986), clarifying that the first quasicrystal found is related to the 3D Penrose tiling and the nD crystallography was extended to include quasicrystals (Bak, 1986; Janssen, 1986). According to this theory, the symmetries of quasicrystals can be given by space groups in nD space and their structures are represented by 3D sections of periodic structures (crystals) in nD space. This is quite similar to the description of modulated structures. Therefore, we can treat quasicrystals in a similar manner.

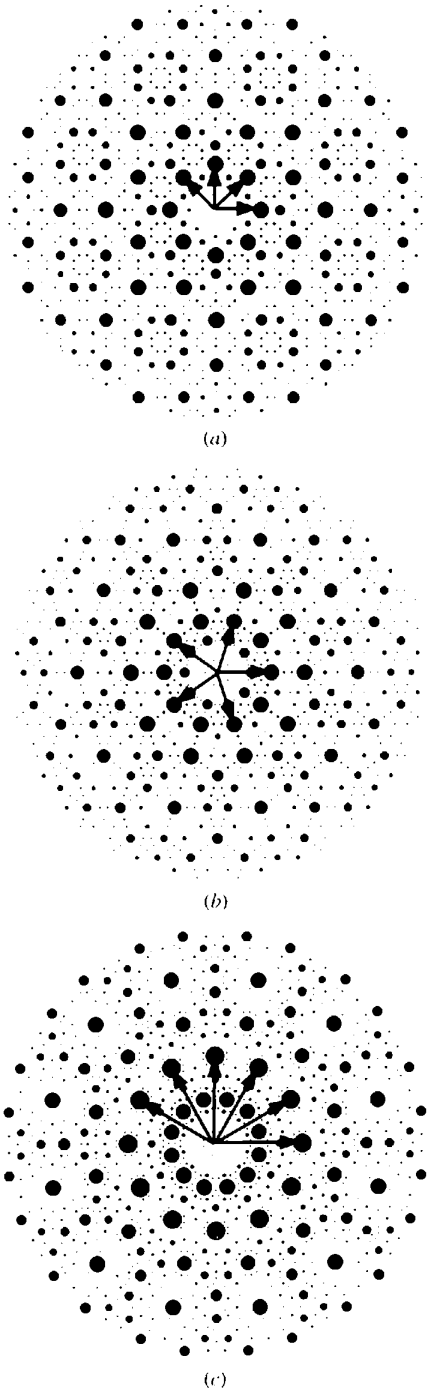

Fig. 2. Diffraction patterns of (*a*) octagonal Penrose, (*b*) Penrose and (*c*) Stampfli tilings. Arrows show vectors needed for indexing. Four of them are independent in (*b*) and (*c*).

Further important progress in experimental studies has been made by the discoveries of new kinds of quasicrystal and stable quasicrystal. New quasicrystals with octagonal, decagonal and dodecagonal symmetries have been found in Al-based alloys and Cr–Ni (Wang, Chen, & Kuo, 1987; Bendersky, 1985; Ishimasa, Nissen & Fukano, 1985) but these necessitate rapid cooling from the melt to obtain quasicrystal phases. These are called polygonal quasicrystals and have a period along one axis (8- 10- or 12-fold axis) but no period in the 2D subspace perpendicular to it. In 1986, the *T* phase in the Al–Cu–Li system, which was found in 1955 (Hardy & Silcock, 1955), was proved to be an icosahedral phase (Matthew & Elser, 1986). This is an equilibrium phase so that it is stable. This enabled us to grow single-domain quasicrystals (Dubost, Lang, Tanaka, Stainfort & Audier, 1986). The quality of the quasicrystals was, however, not very high so that the number of observed reflections was less than 100. Very high quality stable quasicrystals were first found in icosahedral Al–Cu–Fe (*i*-Al–Cu–Fe) and *i*-Al–Cu–Cr quasicrystals (Tsai, Inoue & Masumoto, 1987, 1989). These materials show a superstructure in 6D space with the face-centered icosahedral lattice (Ishimasa, Fukano & Tsuchimori, 1988; Ebalard & Spaepen, 1989). A superstructure was also found recently in decagonal Al–Ni–Co (*d*-Al–Ni–Co) (Edagawa, Ichihara, Suzuki & Takeuchi, 1992).

There are several methods to obtain quasiperiodic tilings. These are classified into four categories, which are called the inflation–deflation method (IDM), dual method (DM), projection method (PM) and section method (SM). The first two methods do not use nD space explicitly. In order to understand the symmetry of generated tilings, however, the corresponding structures in the nD space have to be known because the symmetry of quasicrystals is expressed by that of crystals in the nD space, which gives the quasiperiodic tilings as intersections in 2D or 3D external (physical, parallel) space. It is also necessary to know their diffraction patterns, which are regarded as the projections of the nD reciprocal lattice along the internal (complementary, perpendicular) space.

Such methods of generating quasiperiodic tilings with non-crystallographic symmetries and the decorations of them have extensively been considered since the optical diffraction pattern of the Penrose tiling is quite similar to

the electron diffraction pattern of decagonal Al–Mn and the diffraction intensity of the 3D Penrose tiling resembles that of icosahedral Al–Mn. However, their point density was too small compared with that of the real quasicrystal. It was shown that important information on the decoration can be obtained from a crystal structure with nearly the same chemical composition, which is called a crystalline approximant (Elser & Henley, 1985; Henley & Elser, 1986). The structure of the crystalline approximant is related with that of the quasicrystal by a linear phason strain (Socolar, Lubensky & Steinhardt, 1986) or a rotation in nD space (Kramer, 1987). The latter is essentially equivalent to the former so that we discuss only the former in the following. This method provides a crystalline approximant structure from a model of a quasicrystal by introducing an appropriate phason strain. This was applied to obtain atom positions of σ phase from a small number of atom positions in nD space without using a model in nD space (Wang & Kuo, 1988). The periodic structures obtained from quasiperiodic tilings were considered in decagonal cases (Niizeki, 1991). It was shown that the structure of the R phase can be derived from a model of icosahedral Al–Cu–Li (Yamamoto, 1992*b*). Since the direct determination of quasicrystal structures is difficult, the structure of the crystalline approximant gives important information for the model construction. The aim of this paper is to describe the subjects mentioned above in a unified way.

The arrangement of this paper is as follows. We discuss nD crystallography of modulated structures and composite crystals in §§2 and 3. In §4, the indexing problems in quasicrystals are discussed. In §§5 and 6, typical quasiperiodic tilings are derived for octagonal, decagonal, dodecagonal and icosahedral quasicrystals. The symmetry of a quasicrystal is given by an nD space group as shown in §7. A derivation of symmetry operators from the space-group symbols will be given in §8. The morphology of quasicrystals is discussed in §9. The structure factor of quasicrystals in several approximations will be shown in §10. In §11, the method of calculating the point density and frequency of subpatterns of the tilings will be described. The quasicrystal structure has to be described by a finite number of parameters. This problem is discussed in §12. In real quasicrystals, the defects specific to quasicrystals are observed in almost all cases. This so-called phason distortion is considered in §13. It leads to crystalline approximants under special conditions. Effects of a random phason in diffraction patterns are also discussed. In §14, the several structure determination methods proposed so far are discussed. The modeling of quasicrystals are given in the succeeding two sections. The quasiperiodic tilings discussed in §§5 and 6 do not always give the atom positions of quasicrystals but just give the framework of their structures. There are many atoms in other positions. Therefore, modifications or simple decorations of quasiperiodic tilings will be treated in §15 and decorations for cluster models will be explained in §16. The refinement method is given in §17. In the refinement stage, a modification of the model may be necessary. This is assisted by the difference Fourier map or the maximum-entropy method. The latter is discussed in §18. Typical tilings can be classified into the normal structure and its superstructure. This is shown in §19.

2. Quasiperiodic structures

It is known that there exist three kinds of quasiperiodic structure (aperiodic crystal) mentioned above. Among them, the incommensurate modulated structure is the simplest one. This is a crystal distorted periodically with a period that is incommensurate to that of the crystal. The composite crystal can be regarded as a general form of the modulated structure. Because of the interaction between substructures, one substructure is modulated with the period of the other. Thus, there exist two or more interpenetrating modulated substructures in a crystal. Examples of the modulated structure and composite crystals are shown in Figs. 3 and 4, which give the diffraction patterns of Fig. 1. These two have the average structures that are responsible for the main reflections. We consider them for comparison with quasicrystals, which have no main reflections constructing a three-dimensional (3D) lattice. Therefore, it is not appropriate to consider the quasicrystal as a modulated structure.

2.1. *1D analogs*

We compare 2D representations of 1D analogs of the three structure types in order to grasp common and different points among them. Fig. 5(*a*) shows the standard representation of the modulated structure. The 'atom' is continuous along the internal (complementary,

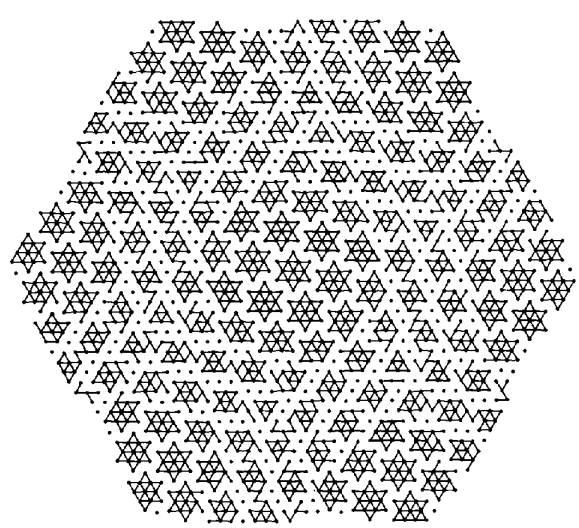

Fig. 3. Ta layer of the modulated structure of 1*T*-TaS_2. Atom clusters are denoted by solid lines.

perpendicular) space V^i and displaces along the external (physical, parallel) space V^e. The displacement (modulation function) has a periodicity along the internal space. The atom position in the external space is given by an intersection of this 2D periodic structure (crystal) with the 1D external space (horizontal line). Similarly, the composite crystal can be given by an intersection of a 2D crystal shown in Fig. 5(*b*), where two kinds of atom are present, each of which is continuous along one of the edges of the square lattice. In contrast, in the quasicrystal shown in Fig. 5(*c*), the atom is continuous in a limited range and has a jump parallel to the external space at some points (dotted lines). The continuous part is called an occupation domain (acceptance domain, window, atom surface). In these cases, their symmetry is specified by the 2D space group $p2$ since only twofold axes are present at the lattice points regardless of symmetries of the lattices. The 1D composite crystal shown above is not realistic because the interatomic distance becomes zero at the origin. In 2D composite crystals that are represented in 3D space, this can be avoided if their coordinates of the additional axis are different. For the modulated structures and composite crystals, there are two recent review papers (Yamamoto, 1993*b*; van Smaalen, 1995), so that we discuss them only briefly here.

In these 1D examples, the quasicrystal cannot be distinguished from the other two by the symmetry, though real quasicrystals can. However, their characteristic features are clearly different from each other. They are reflected in the diffraction patterns (Fig. 6). There exist prominent main reflections that are arranged periodically in the external space V^e in Fig. 6(*a*) and two sets of

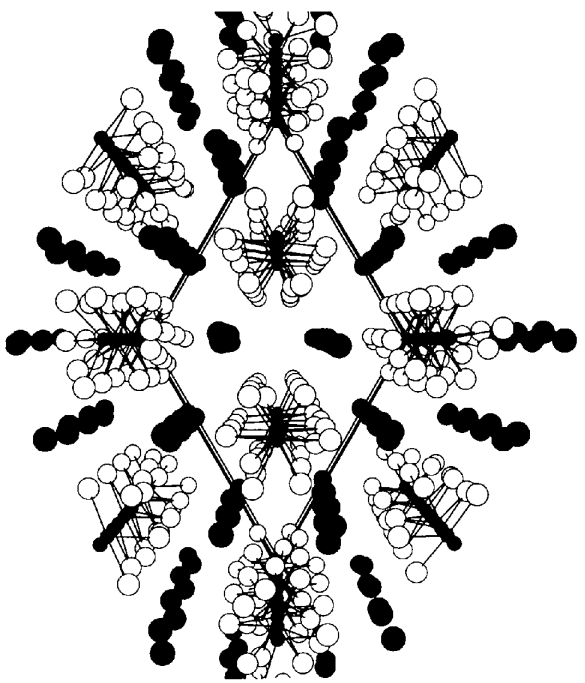

Fig. 4. The perspective view of the composite crystal $[Ba]_x[(Pt, Cu)O_3]$. Solid, shaded and open circles represent Pt/Cu, Ba and O atoms.

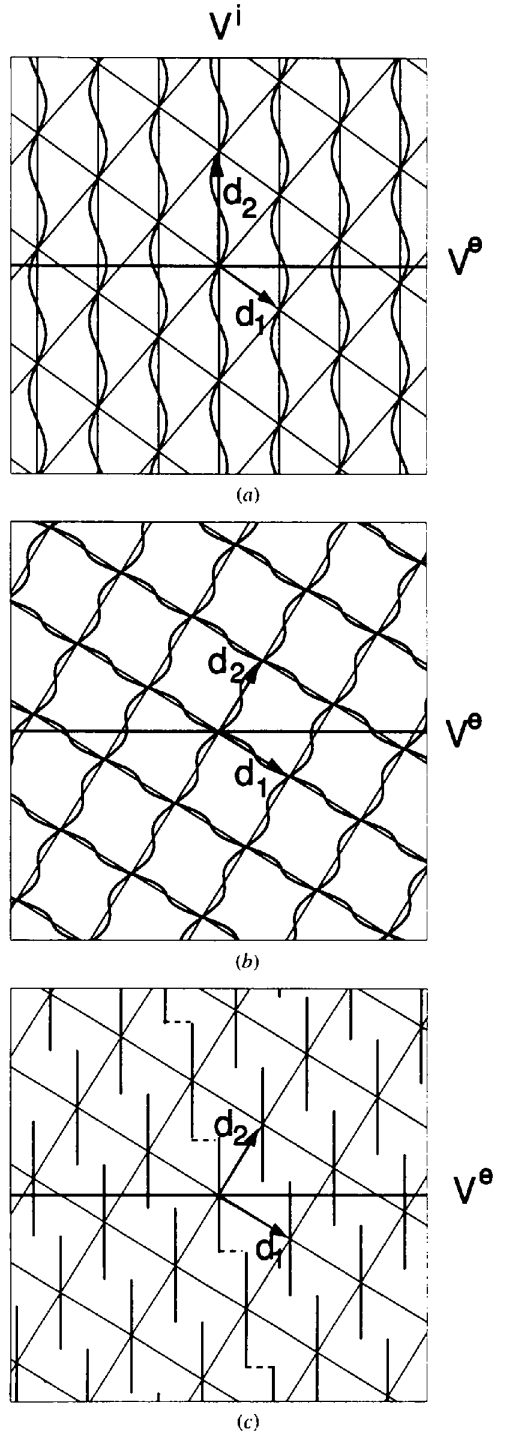

Fig. 5. The 2D representations of three quasiperiodic structures in 1D space: (*a*) modulated crystal, (*b*) composite crystal and (*c*) quasicrystal.

main reflections along the two lines passing through the origin in Fig. 6(*b*) but the prominent reflections have no period in Fig. 6(*c*). If we recognize these differences, we can distinguish the three cases by the diffraction patterns. This means that even in quasicrystals we can consider structures with crystallographic point groups. This definition of quasicrystals is somewhat ambiguous compared to the usual one, where the quasicrystal is defined as a structure with a non-crystallographic point group. This problem will be discussed again later. The difference of the former two lies not in the symmetry but in the diffraction intensity distribution. If two (or more) sets of main reflections exist, it is a composite crystal, otherwise it is a modulated structure. Keeping these characteristics in mind, we compare their modulation functions. An important point is that the above representations are not unique but there exists an infinite number of equivalent representations for the same structures. Consider the shear strain that keeps the external space (horizontal line) invariant. Examples are shown in Fig. 7. Note that one substructure in the composite crystal can be considered as a modulated structure with a sawtooth modulation function shown by thick and dotted lines (Fig. 7*b*). There are two cases depending on the relative average periods. Let the atoms parallel to the internal space V^i be the first substructure and the ones oblique to it the second. If the first substructure has an average period shorter than that of the second, the modulation function is a single-valued function in some range and without value in the other (Fig. 7*b*) while, in the opposite case, it has two values in some region. Such an example is shown in Fig. 8, where the structure in V^e is the same as in Fig. 7(*b*) but the substructure with the longer period is chosen as the first substructure. In the diffraction patterns of real modulated and composite crystals shown in Fig. 1, the modulated structure (Fig. 1*a*) is 2D modulated so that five vectors are necessary to index the diffraction pattern. This is an example of modulated structures caused by the charge density waves that are seen in transition-metal chalcogenides (Willson, DiSalve & Mahajan, 1975). The other one (Fig. 1*b*) is an example of typical misfit-layer structures seen also in transition-metal chalcogenides (Yamamoto, 1993*b*; van Smaalen, 1995).

In the above examples, we consider only the location of atoms. The shift of the atom position from the average structure is called a displacive modulation. There exists another kind of modulation, which is called an occupational or substitutional modulation. This is usually accompanied by the displacive modulation but, in some cases, the displacive modulation is small. In the occupational modulation, the occupation probability of an atom changes depending on the position. Substitutional modulation often occurs in alloys, where an atom site is occupied by two atoms and their occupation probabilities change with the position. Usually, the displacive modulation in alloys is small but not negligible

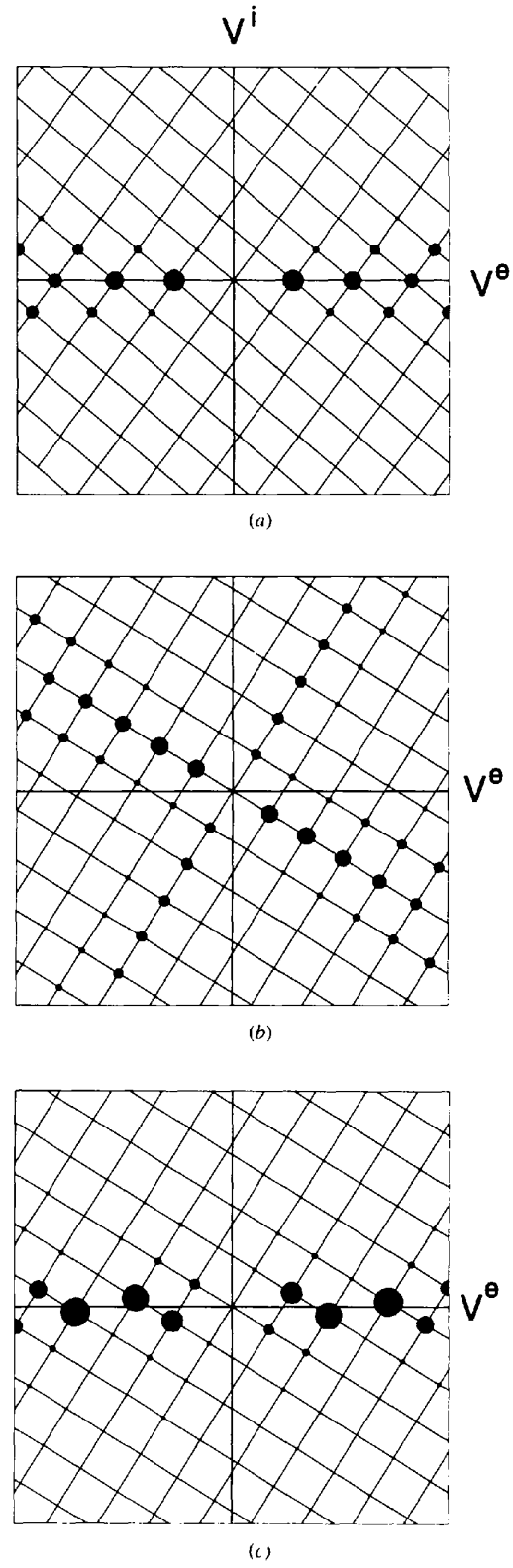

Fig. 6. Diffraction patterns of the three quasiperiodic structures shown in Fig. 5: (*a*) modulated crystal, (*b*) composite crystal and (*c*) quasicrystal.

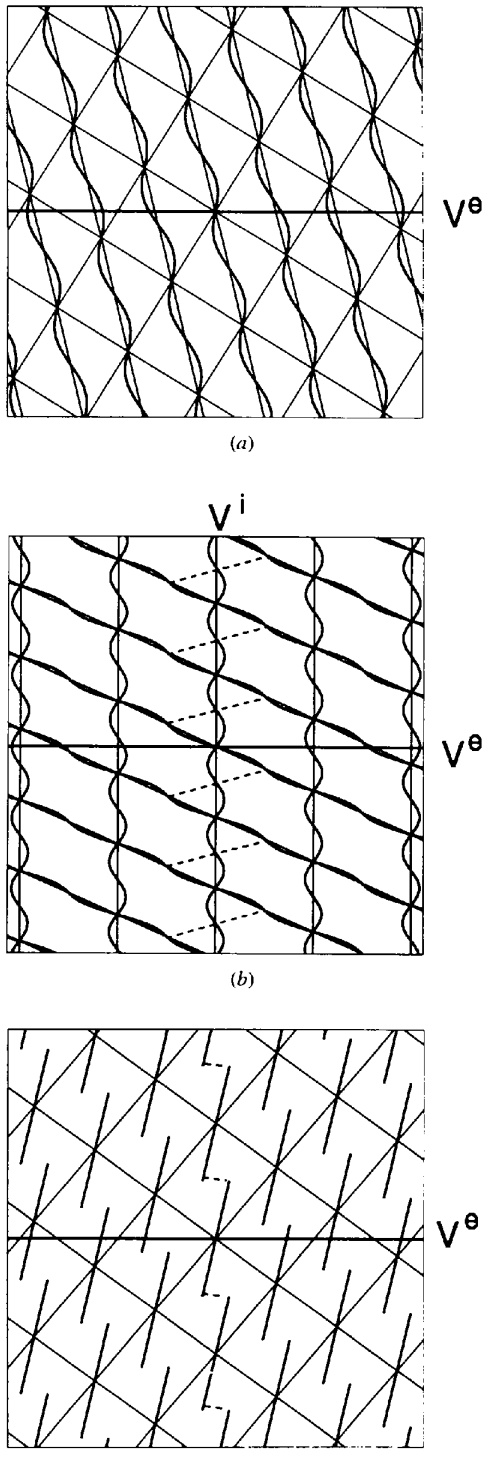

Fig. 7. Other representations of 1D quasiperiodic structures: (*a*) modulated crystal, (*b*) composite crystal and (*c*) quasicrystal. These have the same structure as in Fig. 5 in the external space, so that they are equivalent to the representations shown in Fig. 5. The dotted lines in (*b*) denote the jump of modulation function of one substructure when the modulation function of the substructure is regarded as the standard representation.

(Yamamoto, 1982*b*). On the other hand, the polytype of SiC can be regarded as a commensurately modulated structure with a pure occupational modulation, where the displacive modulation can be ignored (Yamamoto, 1981; Yamamoto & Inoue, 1982). As mentioned before, all quasicrystals found so far are alloys except for $Ta_{63}Te_{37}$, which was found quite recently (Krumeich, Conrad & Harbrecht, 1994), so that substitutional modulation may occur in an occupation domain. In general, the temperature factor is also dependent on the position (temperature-factor modulation) because the local environment is generally different and depends on the position.

2.2. *Structure factor*

For the structure-factor calculations, several formulas have been proposed. In the following, we neglect the occupational and temperature-factor modulations for simplicity. Since the structure is periodic in 2D space, the structure factor is given by the Fourier integral of the electron density over the unit cell. This has simple forms for all cases. Those for the modulated and composite crystals are similar to that of the quasicrystals when they are expressed in the following form. For the reflection with the diffraction vector $\mathbf{h} = h_1\mathbf{d}_1^* + h_2\mathbf{d}_2^*$ ($\mathbf{d}_1^*$ and $\mathbf{d}_2^*$ being the unit vectors of 2D reciprocal space), this is

$$F(\mathbf{h}) = \sum_{\mu} \sum_{\{R|\mathbf{t}\}^{\mu}} f^{\mu}(\mathbf{h}^e) p^{\mu} \exp[-B^{\mu}(h^e)^2/4] \times \exp[2\pi i \mathbf{h} \cdot (R\bar{\mathbf{x}}^{\mu} + \mathbf{t})] g_0^{\mu}(R^{-1}\mathbf{h}), \quad (1)$$

where the average position, temperature factor and occupancy of the μth independent atom are represented by $\bar{\mathbf{x}}^{\mu}$, B^{μ} and p^{μ}. $g_0^{\mu}(\mathbf{h})$ and $f^{\mu}(\mathbf{h}^e)$ are the Fourier integral of the modulation function and atomic scattering factor of the μth atom at the diffraction vector $\mathbf{h}$ and its

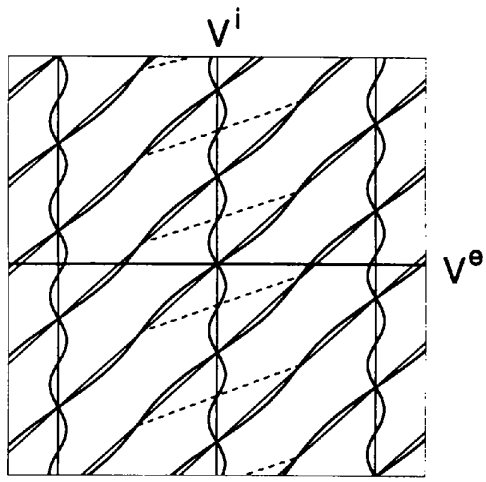

Fig. 8. Another representation of the composite crystal. This is equivalent to Fig. 7(*b*).

external space component $\mathbf{h}^e$. The sum of $\{R|\mathbf{t}\}^\mu$ runs over the symmetry operators of the space group that create new atoms in a unit cell from the independent ones. They agree with the coset representatives of the site-symmetry group.

The form of the Fourier integral is different in each case because of the difference in modulation functions. In the modulated structure in Fig. 5(*a*), there is one atom in the unit cell of 2D space and its modulation function is given by

$$x_1^1 = \bar{x}_1^1 + \mathbf{d}_1^* \cdot \mathbf{u}^1 \sin(2\pi\bar{x}_2^1) = \bar{x}_1^1 + \Delta x_1^1, \quad (2)$$

where x_1 and x_2 are the coordinates of atoms with respect to the unit vectors $\mathbf{d}_1$ and $\mathbf{d}_2$ of the 2D lattice (Fig. 5), $\bar{x}_1^1$ is the coordinate of the average position, which is represented by vertical lines in Fig. 5(*a*), $\mathbf{u}$ is the amplitude of the displacement wave parallel to the external space. In a simple sinusoidal modulation wave as in the present case, the structure factor is given by the Bessel function (Yamamoto, 1982*a*):

$$\begin{aligned} g_0^1(\mathbf{h}) &= \int_0^1 \mathrm{d}\bar{x}_2 \exp[2\pi i(h_1\Delta x_1^1 + h_2\bar{x}_2)] \\ &= J_{-h2}(2\pi\mathbf{h}\cdot\mathbf{u}^1), \end{aligned} \quad (3)$$

where J_m is the Bessel function of order m. On the other hand, in the composite structure, the unit cell accommodates two atoms, so that μ takes values 1 and 2 in (1). For the first atom, the modulation function has the same expression as (2). For the second atom,

$$x_2^2 = \bar{x}_2^2 + \mathbf{d}_2^* \cdot \mathbf{u}^2 \sin(2\pi\bar{x}_1^2) = \bar{x}_2^2 + \Delta x_2^2 \quad (4)$$

and

$$\begin{aligned} g_0^2(\mathbf{h}) &= (a_1/a_2)\int_0^1 \mathrm{d}\bar{x}_1 \exp[2\pi i(h_1\bar{x}_1 + h_2\Delta x_2^2)] \\ &= (a_1/a_2)J_{-h1}(2\pi\mathbf{h}\cdot\mathbf{u}^2), \end{aligned} \quad (5)$$

where a_1 and a_2 are the average periods of the first and second substructures in the external space.

It should be noted that (2)–(5) are independent of the difference in the representations in Figs. 5, 7 and 8. Note that the Bessel function depends only on the external component of the diffraction vector $\mathbf{h}$ and the order, which is the satellite index. The structure factors of the main reflections are given by $J_0(2\pi\mathbf{h}\cdot\mathbf{u})$, while those of the kth-order satellites are given by $J_k(2\pi\mathbf{h}\cdot\mathbf{u})$. This means that the intensity of the main reflection decreases with the increase of the external component of $\mathbf{h}$, while the satellite intensity increases. Such a tendency is seen in Figs. 6(*a*) and (*b*). Another important point is that the displacive modulation gives second- and higher-order satellites even when the modulation wave is harmonic as in the present case. They are called diffraction harmonics. In contrast to the displacive modulation, the occupational or substitutional modulation does not give the diffraction harmonics. This case is discussed later.

For the quasicrystal, g_0^1 can be given by

$$g_0^1(\mathbf{h}) = \int_{-r}^{r} \mathrm{d}t \exp(2\pi h^i t) = 2r \sin(2\pi h^i r)/2\pi h^i r, \quad (6)$$

where $2r$ is the length of the atom along the internal space (the size of the occupation domain) and h^i is the internal component of the diffraction vector $\mathbf{h}$. The right-hand side of (6) indicates that the intensity decreases with the internal components of the diffraction vector.

Consider a pure occupational modulation,

$$p^\mu(\bar{x}_2) = p_0^\mu + p_1^\mu \cos(2\pi\bar{x}_2 + \varphi), \quad (7)$$

which represents the continuous change of the occupation probability along the second axis without accompanying the displacive modulation. Then the structure factor becomes

$$\begin{aligned} F(\mathbf{h}) = \sum_\mu \sum_{\{R|\mathbf{t}\}^\mu} & f^\mu(\mathbf{h}^e)\exp[-B^\mu(h^e)^2/4] \\ & \times \exp[2\pi i\mathbf{h}\cdot(R\bar{\mathbf{x}}^\mu + \mathbf{t})]g_0^\mu(R^{-1}\mathbf{h}) \end{aligned} \quad (8)$$

and

$$\begin{aligned} g_0^\mu(\mathbf{h}) &= \int_0^1 \mathrm{d}\bar{x}_2\, p^\mu(\bar{x}_2)\exp(2\pi i h_2\bar{x}_2) \\ &= \begin{cases} p_0^\mu & \text{for } h_2 = 0 \\ p_1^\mu \exp(\mp i\varphi)/2 & \text{for } h_2 = \pm 1 \\ 0 & \text{otherwise.} \end{cases} \end{aligned} \quad (9)$$

This means that the Fourier amplitude p_0 contributes only to the main reflections and p_1 to the first-order satellite reflections. This is because the structure factor depends linearly on the occupation probability. This causes a problem in the determination of the occupational modulation waves including higher harmonics. Since the kth-order Fourier amplitude of the occupation probability contributes only the kth-order satellite reflection, its intensity is independent of the phase shift φ. Therefore, we cannot determine the phase shift, which is necessary for the determination of the modulation wave. Fortunately, the real occupational modulation is accompanied by the displacive modulation. Then the intensities of the satellite reflections depend on the phase shift and they can be determined. It should be noted that, if the displacive modulation is weak, the occupational modulation wave with wrong phases may give a small R factor for the satellite reflections. The final result has to be checked by the fact that the occupational modulation wave is within a physically reasonable range ($0 \le p \le 1$).

As a special case of the commensurate occupational modulation, we consider the SiC polytype. This provides many long-period structures. The lattice is either hexagonal or rhombohedral. This can be regarded as a layer structure with the same stacking interval where the Si and C atoms are located in each layer at one of three special positions $(0,0,z)$, $(1/3,2/3,z)$ or $(2/3,1/3,z)$ of the hexagonal unit cell. If Si takes one of these positions, C is always located at the same positions but with $z+\Delta z$. Therefore, the determination of the polytype structure is reduced to the determination of the Si position. The occupational probability of these positions is either one or zero. Thus, we have a sequence of zero and one along the c axis, which can be recognized as an occupational modulation wave. The modulation wave is given in terms of Fourier series. We cannot, however, determine the phase shift of each Fourier term because of the reason mentioned above. The problem is solved by using the penalty function (Yamamoto, 1981; Yamamoto & Inoue, 1982), which restricts the occupation probability of each site within a physically reasonable range.

In real modulated structures, there are several atoms in the nD unit cell and the modulation function may be anharmonic. Then the Fourier integral $g_0(\mathbf{h})$ does not have a simple analytic form any more but can be calculated numerically. The structure factor of a general anharmonic modulation has been given (Yamamoto, 1982*a*), which can be expanded in terms of the products of many Bessel functions (Petříček, Coppens & Becker, 1985). The structure factor of composite crystals is the weighted sum of the structure factor of the modulated substructures as $\sum_{\nu=1}^{m}(V^\nu/V^1)F^\nu(\mathbf{h})$, where V^ν is the unit-cell volume of the νth average substructure and $F^\nu(\mathbf{h})$ is the structure factor of the modulated substructure. A least-squares-refinement program based on the general structure-factor formula was written by Yamamoto (1982*a*) and programs applicable to composite crystals by Kato (1990), Petříček, Maly, Coppens, Bu, Cisarova & Frost-Jenssen (1991) and Yamamoto, Takayama-Muromachi, Izumi, Ishigaki & Asano (1992).*

2.3. *Symmetry*

The symmetry of the modulated and composite crystals is given by a space group of higher-dimensional space so that, in the present case, the space group is given by a 2D space group. This is also applicable to the quasicrystals. A characteristic feature for such quasiperiodic structures is that their space groups only necessitate a part of 2D space groups. For example, the space groups with square and hexagonal lattices do not appear, since the first and second axes are equivalent in these cases, while they are not equivalent in the quasiperiodic structures. The condition for their point groups is that they are $(1+1)$-reducible. In real quasiperiodic structures in 3D space, which can be represented as an nD crystal, the point groups are $(3+d)$-reducible, where $d=n-3$ is the dimension of the internal space. This means that the matrix representation of the rotation operator in 2D (nD) space becomes a $(1+1)$ block diagonal [$(3+d)$ block diagonal] matrix by an appropriate transformation, or there exist two subspaces, each of which is invariant under the point group. For modulated and composite crystals, another condition comes from the incommensurability between the axes. In nD cases, the external components of additional d axes are incommensurable with those of the first three axes. A similar condition excludes space groups with a rectangle lattice in the present 2D case. Thus, the allowed space groups in 2D are only $p1$ and $p2$, which are represented by the superspace-group symbols $1(\alpha)1$ and $\bar{1}(\alpha)\bar{1}$ (see below).

In fictitious modulated structures in 2D space with 1D modulation, the same condition excludes orthorhombic, tetragonal, hexagonal and cubic 3D space groups and only the triclinic and monoclinic space groups are related with the symmetry of such structures as shown by de Wolff (1974). Furthermore, in order to distinguish between main and satellite reflections, a classification finer than that for usual space groups (or nD space groups in general cases) was introduced. The space groups classified by such an equivalence relation are called superspace groups. In fact, 15 triclinic and monoclinic 3D space groups are classified into 22 $(2+1)$D superspace groups.

3. Modulated and composite crystals

3.1. *Superspace-group symbols*

The symbol of the $(3+d)$D superspace group consists of the symbol of a 3D space group of the average structure and additional symbols. In the following, we consider only $(3+1)$D cases. There are two types of symbol, one-line and two-line symbols. In the one-line symbol, the superspace group is expressed by the 3D space-group symbol followed by the modulation wave vector and the translation along the additional axis. For example, consider two superspace-group symbols, $P3_112(1/3,1/3,\gamma)$ and $R32(0,0,\gamma)t0$. These mean that their average structures have the space groups $P3_112$ and $R32$ and the wave vectors of the modulation waves are $\frac{1}{3}\mathbf{a}^*+\frac{1}{3}\mathbf{b}^*+\gamma\mathbf{c}^*$ and $\gamma\mathbf{c}^*$, where a Greek letter represents an irrational number and the hexagonal unit vectors $\mathbf{a}^*$, $\mathbf{b}^*$, $\mathbf{c}^*$ are used to express the wave vector in the rhombohedral case. (If the lattice of the average structure is centered, the wave vector is represented by the unit-vector components with respect to the centered lattice.) The former superspace group has no intrinsic

* A program system for modulated and composite crystals written by the author can be obtained *via* the Internet by anonymous ftp (ftp.nirim.go.jp/pub/sci/REMOS).

part of the translation along the fourth axis, while the latter has a 1/3 translation along the fourth axis for the threefold rotation. If the intrinsic parts of the translation along the fourth axis accompanied by the operators in the symbol are all zero, they are neglected as in the first symbol.† The same superspace groups are represented also by $R^{P3_1}_{1\,1\bar{1}}{}^{12}_{}$ and $P^{R32}_{t\,\bar{1}}$. The two-line symbol consists of the prefix representing the rational part of the modulation wave and the space-group symbol in the upper line and the intrinsic translation along the fourth axis corresponding to the operators in the space-group symbol (de Wolff, Janssen & Janner, 1981) in the lower line. If this is zero, 1 or $\bar{1}$ is written in the lower line according to whether the rotation operator transforms the irrational component of the wave vector into itself or its inversion. In the present case, twofold rotation in the ab plane inverts $\mathbf{k} = \gamma\mathbf{c}^*$ into $-\mathbf{k}$, so that the corresponding symbol in the lower line is $\bar{1}$. The prefixes *A*, *B*, *C*, *L*, *M*, *N*, *U*, *V*, *W* and *R* represent the rational components $(1/2, 0, 0)$, $(0, 1/2, 0)$, $(0, 0, 1/2)$, $(1, 0, 0)$, $(0, 1, 0)$, $(0, 0, 1)$, $(0, 1/2, 1/2)$, $(1/2, 0, 1/2)$, $(1/2, 1/2, 0)$ and $(1/3, 1/3, 0)$ in the modulation wave vector. The intrinsic parts of the translation along the fourth axis, $\pm\frac{1}{2}$, $\pm\frac{1}{3}$, $\pm\frac{1}{4}$ and $\pm\frac{1}{6}$ are represented by *s*, *t*, *q* and *h* in both symbols. The superspace groups are not equivalent if the space groups of the average structures are not equivalent to each other as usual 3D space groups. Therefore, some superspace groups may be equivalent to each other under the equivalence relation of nD space groups. In fact, these two superspace groups are equivalent as the 4D space group.

If the wave vector is located at the Brillouin zone boundary of the average structure, it has a rational component of 1/2, 1/3 or 1. The last one appears only in the centered lattice. In the first two cases, we use new centered lattices in 4D space. In the first case, the corresponding axis is doubled or the reciprocal unit vector is halved, except for the tetragonal lattice with the wave vector $(1/2, 1/2, \gamma)$. Then, the centered lattice gives the reflection conditions for general reflections [see Table 9.8.3.6 in Janssen, Janner, Looijenga-Vos & de Wolff (1992)]. The second one appears only in the trigonal system with the form $(1/3, 1/3, \gamma)$. In this case, we take the new axes $a^{*\prime} = \frac{1}{3}(\mathbf{a}^* + \mathbf{b}^*)$, $b^{*\prime} = \frac{1}{3}(-\mathbf{a}^* + 2\mathbf{b}^*)$ and $\mathbf{c}^{*\prime} = \mathbf{c}^*$. Then, the reflection condition for this centered lattice is given by $h_1 - h_2 - h_4 = 3n$ for general reflections $h_1h_2h_3h_4$. In the exceptional tetragonal case with the wave vector $(1/2, 1/2, \gamma)$, we take $a^{*\prime} = \frac{1}{2}(\mathbf{a}^* + \mathbf{b}^*)$, $b^{*\prime} = \frac{1}{2}(-\mathbf{a}^* + \mathbf{b}^*)$ and $\mathbf{c}^{*\prime} = \mathbf{c}^*$. The reflection condition for general reflections then becomes $h_1 + h_2 + h_4 = 2n$. For these cases, the new a and b axes in the standard setting are rotated by 30 and 45° from the original ones.

The superspace group of composite crystals can be specified by a superspace group of modulated structures (Janner & Janssen, 1980*b*). However, there exist many cases where the superspace group of one modulated substructure is not equivalent to that of the other substructure. In $Ba_x(Cu, Pt)O_3$, the two average substructures have space groups $P31c$ and $R3m$, which are clearly non-equivalent as 3D space groups, so that corresponding 4D superspace groups of modulated substructures, $P31c(1/3, 1/3, \gamma_1)$ and $R3m(0, 0, \gamma_2)0s$, are not equivalent as superspace groups but equivalent as 4D space groups. Thus, the equivalence relation for superspace groups of composite crystals must be different from that for the superspace groups of modulated structures. One possibility is to use an nD space group but this cannot take into account the existence of main and satellite reflections, which is the characteristic feature of composite crystals. Yamamoto (1992*a*) proposed the combined use of two superspace-group symbols for composite crystals with two substructures. In this symbol, the superspace group of $Ba_x(Cu, Pt)O_3$ is represented by $P31c(1/3, 1/3, \gamma_1)$: $R3m(0, 0, \gamma_2)0s$. A similar superspace group $P3_112(1/3, 1/3, \gamma_1)$: $R32(0, 0, \gamma_2)t0$ appears in the inclusion compound with 1,10-dibromodecane, which is the combination of the two superspace groups discussed above. In this notation, a limited setting (unified setting) is used to remove an ambiguity of the symbol. The wave vector of one modulated substructure is chosen among the reciprocal-lattice vectors of the other. Then the treatment of the composite structure becomes similar to that of the modulated structure. In particular, the introduction of completely new symbols for composite structures is not necessary but necessitates several additional prefixes in the two-line symbol (Yamamoto, 1992*a*). The unified setting, however, may require a non-standard setting for the unit cell of the average structure and for the superspace group. For example, the body-centered lattice or face-centered lattice may be necessary for monoclinic or triclinic cases [see Table 1 in Yamamoto (1993*b*)].* The choice of the modulation wave may lead to the rational component like $(1, 1/2, 0)$, for which the prefix of the two-line symbol was not given. The extended prefix necessary for superspace groups of composite

† The intrinsic part of the translation is the part that is invariant under the shift of the origin. For example, in the operator $\{\sigma_z|1/2, 1/2, 1/2\}$, the intrinsic part is $\frac{1}{2}\mathbf{a} + \frac{1}{2}\mathbf{b}$ since, if we choose the origin at $\frac{1}{4}\mathbf{c}$, this becomes $\{\sigma_z|1/2, 1/2, 0\}$. Note that if the rotation operator inverts some axes, the corresponding translation components are not intrinsic but specify the location of the symmetry element.

* In this table, the superspace group M^{Fm2m}_{111} : M^{Fm2m}_{111} of $[M_1X]_x$ [M = (Pb, Ta, S), (Sm, Ta, S) and (Bi, Ta, Se)] should be read as X^{Fm2m}_{111} : X^{Fm2m}_{111}. The superspace groups of $[M_3CrX_3]_x[M_3X]_y[Cr_7X_{12}]$ for (M, X) = (Ba, Se), (Sr, S), (Eu, S), (Pb, S) is $P^{P6_3/m}_{p.ss.\ 2}$: $P^{P6_3/m}_{p.ss.\ 2}$: $P^{P6_3/m}_{p.ss.\ 2}$, where *.ss.* below 6_3 means that the sixfold screw axis does not change the second and third wave vectors and the corresponding shifts along the fourth and fifth axes are both 1/2 while 2 below m shows that the mirror plane inverts both wave vectors. The superspace group of $[Br]_x[TTF]$ should be replaced by $P^{C2/m}_{1\ 1}$: $P^{C2/m}_{1\ 1}$.

structures or for non-standard settings of superspace groups are given by Yamamoto (1992*a*). The added symbols are *D*, *E*, *F*, *G*, *H*, *I*, *X*, *Y* and *Z* for (1/2, 1, 0), (1/2, 0, 1), (0, 1/2, 1), (1, 1/2, 0), (1, 0, 1/2), (0, 1, 1/2), (0, 1, 1), (1, 0, 1) and (1, 1, 0). The symbol is applicable to almost all composite structures found so far. There is one exceptional case, $Hg_{3-x}AsF_6$, in which there exist two Hg substructures and one Hg substructure is related to the other by the symmetry operator in the nD space group. This symmetry operator is not included in the superspace group of each substructure. This reminds us of the groupoid symmetry in normal crystals. In some cases, the space-group symmetry cannot give the true diffraction symmetry of crystals. This is known as diffraction enhancement. The general theory of diffraction enhancement has been given by Sadanaga & Ohsumi (1979). They showed that the symmetry of crystals in a category can be given by a groupoid, which is a set of symmetry operators of substructures and operators transforming one substructure into the other. The former constructs a space group and is called the kernel of the groupoid, while the latter is called the hull. Such a case appears in the commensurate phase (locked-in phase) of $NbTe_4$ (Yamamoto, 1985*b*). This consists of four $(NbTe_4)_\infty$ columns parallel to the tetragonal c axis, which are located at $(0, 0, z)$, $(0, 1/2, z)$, $(1/2, 0, z)$ and $(1/2, 1/2, z)$ (Bronsma, van Smaalen, de Boer, Wiegers, Jellinek & Mahy, 1987; Budkowski, Prodan, Marinković, Kucharczyk, Uszyński & Boswell, 1989). The second and third columns are obtained from the first one by the translations of $\{E|0, 1/2, 1/3\}$ and $\{E|1/2, 0, 1/3\}$ and the fourth one with $\{E|1/2, 1/2, 2/3\}$. They are not included in the space group but special extinction rules suggest the existence of such operators. In the case of $Hg_{3-x}AsF_6$, the situation is slightly different because the kernel and the hull construct a higher-dimensional space group. The groupoid includes the group, so that this can be considered as a special case of the groupoid symmetry. It is noted that elements of the hull can be used in the usual refinement program. Therefore, the analysis based on the groupoid symmetry is applicable to $Hg_{3-x}AsF_6$ and $NbTe_4$.

The superspace groups of 1D modulated structures are listed by de Wolff, Janssen & Janner (1981) (see also Yamamoto, Janssen, Janner & de Wolff, 1985). Their symmetry operators and superspace groups equivalent to them are available *via* the Internet from the author (http://www.nirim.go.jp/~yamamoto). Provisional tables of superspace groups and symmetry operators for 2D modulated structures are also available from the same WWW site. In some settings of the unit vectors of a 1D modulated structure, the superspace-group symbol is not present in the table of de Wolff, Janssen & Janner (1981) or in *International Tables for Crystallography* (Janssen, Janner, Looijenga-Vos & de Wolff, 1992). This is however equivalent to one superspace group in the table. In particular, we may encounter one superspace group related to the different choice of the modulation wave vector. This is discussed by Yamamoto, Janssen, Janner & de Wolff (1985). In such a case, we can find the superspace group in the standard setting by the different choice of the unit vector and/or wave vectors as discussed below.

3.2. *Superspace-group determination*

As is clear from the symbol of the superspace group, the space group of the average structure has to be determined by diffraction patterns of main reflections. The wave vector is also easily found from the diffraction pattern. Finally, we have to determine the intrinsic part of the translation along the fourth axis. This is obtained from the reflection conditions or extinction rules. In order to consider the reflection conditions, we have to use an appropriate centered cell for the cases where the wave vector is located at the Brillouin-zone boundary and, as a result, the wave vector includes rational components as discussed above. If such a setting is not a standard one, we can interchange the unit vectors $\mathbf{a}^*$, $\mathbf{b}^*$, $\mathbf{c}^*$. In *International Tables for Crystallography* (Janssen, Janner, Looijenga-Vos & de Wolff, 1992), the axes are chosen so that the irrational component of the wave vector is parallel to the $\mathbf{c}^*$ axes in the axial monoclinic, orthorhombic, tetragonal and hexagonal/trigonal systems. In the planar monoclinic system, the wave vector is chosen as $(\alpha, \beta, 0)$. Another setting is possible by adding a reciprocal-lattice vector of the average structure to the wave vector. This sometimes leads to a superspace group with standard setting having different reflection conditions. The superspace group of the standard setting will be found by such a procedure. Finally, the symmetry operators of the superspace groups are obtained from the author's table mentioned above or can be calculated from the symbol since the symbol consists of the generator of the group. The determination of the superspace groups of composite crystals is somewhat complicated (see Yamamoto, 1992*a*, 1993*b*; van Smaalen, 1995). The superspace group can also be determined by convergent-beam electron diffraction (Terauchi, Takahashi & Tanaka, 1994).

3.3. *Structure determination*

For the modulated and composite crystals, the trial-and-error method is useful in particular for one-dimensionally modulated structures. This is because the average structure can be analyzed by conventional methods and the modulation is a weak perturbation. Thus, the least-squares method is applicable to the determination of modulation functions. The determination of the modulated crystals (or composite crystals) can be made in two steps. First, the average structure (or average substructure) is determined by using only main reflections (or main reflections of each substructure).

Since the average structure is a 3D periodic structure, any techniques for conventional crystals are applicable. It should be noted, however, that the temperature factor of the average structure is affected by the presence of the displacive modulation and we may have large temperature factors. This will be reduced when the displacive modulation is taken into account. The effect of the displacive modulation in the temperature factor is usually anisotropic, since the displacement of atoms is in general anisotropic. In composite crystals, the relative positions of average substructures are determined by the reflections common to the substructures.

In many cases, the refinement method is efficient to determine the modulated or composite crystal structures. In particular, it is successfully used in 1D modulated structures. In this case, the Fourier amplitude corresponding to prominent satellite reflections is refined first. Usually, the first-order satellite reflections are strongest compared with the higher-order ones. Then, we can refine the first-order Fourier amplitude first starting from an appropriate initial value and add the Fourier amplitude of the next-strongest satellites. This is based on the fact that the nth-order Fourier amplitude of the modulation function contributes mainly to the nth-order satellite reflections. If the atoms are located at the special position in the average structure, the form of its modulation functions are generally constrained because of the site symmetry in the superspace group. Such constraint conditions are discussed by Yamamoto (1982*b*,*c*). The form of the restriction depends on the transformation properties of the modulation function because they are different for a scalar, a polar and an axial vector, and a tensor. The restriction comes from the fact that the modulation functions have to be invariant under the site symmetry. For example, let the modulation function of the displacement $\mathbf{u}(\bar{x}_4)$ be invariant for $\{R|\tau\}$. This condition is written as

$$\mathbf{u}(\bar{x}_4) = R\mathbf{u}(\{R|\tau\}^{-1}\bar{x}_4) = R\mathbf{u}(\pm\bar{x}_4 \mp \tau_4), \quad (10)$$

when $R\mathbf{k} = \pm\mathbf{k}$, where τ_4 is the fourth component of the nonprimitive translation τ. The action of the rotation R on the displacement vector $\mathbf{u}$ is the same as in the usual 3D space group since the rotation matrix in the standard setting is $(3 + 1)$ block diagonal and the first 3×3 part is the same as the matrix in the 3D space group of the average structure. [Note that a and b axes for $\mathbf{k} = (1/3, 1/3, \gamma)$ in the trigonal and $\mathbf{k} = (1/2, 1/2, \gamma)$ in the tetragonal cases are rotated in the standard setting as mentioned above.]

The restriction of the modulation wave is also applicable to composite crystals. The composite structure is a general case where there exist several modulated substructures in a crystal as mentioned above. We can choose the standard setting for each modulated substructure when we consider that substructure (see Figs. 7*b* and 8). As shown in §2.2, the structure factor does not depend on the setting. Thus, the possible modulation waves for each substructure can be obtained by considering the superspace group of that substructure and the site symmetry. Several other methods have been developed to obtain the modulation functions. The Patterson or partial Patterson function in 4D space was used for modulated structures by Steurer (1987). The direct method was introduced by Xiang, Fan, Wu, Li & Pan (1990). The maximum-entropy method (MEM) was employed for known structures and its possibility in structure determination was discussed (Steurer, 1991). They were applied to 1D modulated structures.

In our experience, the selection of initial Fourier amplitude seems not such a serious problem for 1D modulated structures. The procedure mentioned above gives smooth convergence of the R factor in many cases. On the other hand, in some 2D or 3D modulated structures, the situation is different. If we choose a wrong amplitude, the correct result may not be obtained. This is due to the following. In the 1D case, the sine (or cosine) wave with positive and negative amplitudes with the same absolute value is equivalent since this is equivalent to the phase shift of the modulation wave by π and the first structure is overlapped by the second by an appropriate shift in the external space. On the other hand, in the 2D case, there exist two modulation waves for one atom and their wave vectors are generally oriented in different directions. Then the change of the sign of the amplitude may cause a different structure. For example, consider the 2D modulated hexagonal structure with modulation wave $\cos[2\pi\bar{x}_4] + \cos[2\pi\bar{x}_5] + \cos[2\pi(\bar{x}_4 + \bar{x}_5)]$, where the modulation wave vectors are $(\alpha, 0, 0)$ and $(0, \alpha, 0)$. This is not equivalent to $-\cos[2\pi\bar{x}_4] - \cos[2\pi\bar{x}_5] - \cos[2\pi(\bar{x}_4 + \bar{x}_5)]$, since these functions cannot be overlapped by any phase shift, giving essentially different structures. In such a case, we need to know the correct sign or to try both cases. The Patterson and direct methods may be efficient in such cases but no attempt has been made so far.

In some organic compounds, the refinement encounters a difficulty because the number of parameters is not small compared to the number of observed reflections. Then it may be efficient to use a rigid-molecule approximation, where the internal motion of the molecule is neglected. The motion of the molecule is specified by six parameters, three for the translation of the rigid molecule and three for the small rotation around an axis. If the rotation is small, the displacement of all atoms in a molecule can be specified by an axial vector ω by the vector product $\omega \times \mathbf{r}^\mu$, where $\mathbf{r}^\mu$ is the positional vector of the μth atom in the molecule from its center of gravity. Such an approximation was implemented by Petříček, Coppens & Becker (1985) in their refinement program *JANA*. This is not applicable to large rotational motions. Such a large motion was observed recently in hexamethylenetetramine suberate (Gaillard, Paciorek & Chapuis, 1995). This shows the diffraction pattern

Table 1. *Modulated crystals with 1D modulations and their superspace groups*

Compound	One-line symbol	Two-line symbol	References
$LiTe_3$	$R\bar{3}m(00\gamma)0s$	$P\,{}^{R\bar{3}m}_{1\ s}$	Valentine, Cavin & Yakel (1977)
ζ-$[NH_3C_3H_7]_2MnCl_4$	$P2_1/b(0\beta0)0s$	$P\,{}^{P2_1/b}_{0\ s}$	Harris, Larsen, Lebech & Achiwa (1994)
MA_xTe_2 (M = Nb, Ta, A = Si, Ge)	$Pnma(00\gamma)s00$	$P\,{}^{Pnma}_{s\,1\,1}$	Evain, van der Lee, Monconduit & Petříček (1994); van der Lee, Evain, Monconduit, Brec & van Smaalen (1994)
$NbGe_{0.4}Te_2$	$P2_1/n(0\beta\gamma)$	$P\,{}^{P2_1/n}_{1\ 1}$	van der Lee, Evain, Mansuetto, Monconduit, Brec & Rouxel (1994)
γ-$[NH_3C_3H_7]_2 \cdot MnCl_4$	$Abma(\alpha01)$	$N\,{}^{Abma}_{1\,11}$	Depmeier (1981); Meyer, Paciorek, Schenk, Chapuis & Depmeier (1994)
$Na_4TiP_2O_9$	$P2/c(\alpha\beta0)0s$	$P\,{}^{P2/c}_{1\ s}$	Maximov, Bolotina, Simonov, Petříček & Schulz (1994)
$Na_{4.5}FeP_2O_8$	$Bmcm(0\frac{1}{2}\gamma)s00$	$B\,{}^{Bmcm}_{s\,1\,1}$	Bolotina, Maximov, Tamazyan & Petříček (1995)
$TaSi_{0.36}Te_2$	$Pnma(00\gamma)s00$	$P\,{}^{Pnma}_{s\,1\,1}$	van der Lee, Evain, Monconduit, Brec, Rouxel & Petříček (1994)
$Y(Ba, Sr)_2Cu_{2.5}B_{0.5}O_x$	$Pmmm(0\beta\frac{1}{2})$	$C\,{}^{Pmmm}_{1\,1\,1}$	Li, Li & Zhao (1993)
$K_{0.3}MoO_3$	$C2/m\ (0\beta\frac{1}{2})s0$	$C\,{}^{C2/m}_{s\ 1}$	Schutte & de Boer (1993*b*)
$Rb_{0.3}MoO_3$	$C2/m\ (0\beta\frac{1}{2})s0$	$C\,{}^{C2/m}_{s\ 1}$	Schutte & de Boer (1993*b*)
$LaMo_5O_{14}$	$C2ca(0\beta0)$	$P\,{}^{C2ca}_{1\,1\,1}$	Leligny, Labbe, Ledesert, Hervieu, Raveau & McCarroll (1993)
$Cu_{3-x}Te_2$	$Pmmm(0\beta\frac{1}{2})$	$C\,{}^{Pmmm}_{1\,1\,1}$	Schutte & de Boer (1993*a*)
$Ni_{3-x}Te_2$	$Pmmm(\alpha00)00s$	$P\,{}^{Pmmm}_{1\,1\,s}$	Schutte & de Boer (1993*a*)
$Bi_{2.08}Sr_{1.84}CuO_{6-x}$	$A2/a(\alpha0\gamma)$	$P\,{}^{A2/a}_{1\ 1}$	Leligny, Durcok, Labbe, Ledesert & Raveau (1992)
$(1-x)Ta_2O_5 \cdot xWO_3$	$Cmmm(0\beta0)s00$	$P\,{}^{Cmmm}_{s\,1\,1}$	Schmid, Withers & Thompson (1992)
$ZrO_{2-x}F_{2x}$	$Cmmm(0\beta0)s00$	$P\,{}^{Cmmm}_{s\,1\,1}$	Thompson, Withers & Kepert (1991)
$La_{1.16}Mo_8O_{16}$	$I4(00\gamma)$	$P\,{}^{I4}_{1}$	Leligny, Labbe, Ledesert, Raveau, Valdez & McCarroll (1992)
$Nb_2Zr_{x-2}O_{2x+1}$	$Amma(\alpha10)0s0$	$M\,{}^{Amma}_{1\,s\,1}$	Withers, Thompson & Hyde (1991)
$Yb_{3-x}S_4$	$Pnma(0\beta0)00s$	$P\,{}^{Pnma}_{1\,1s}$	Withers, Hyde, Prodan & Boswell (1990)
Mo_8O_{23}	$P2/c(\alpha\frac{1}{2}\gamma)$	$B\,{}^{P2/c}_{1\ 1}$	Komdeur, de Boer & van Smaalen (1990)
$Ta_{0.72}Nb_{0.28}Te_4$	$P4/ncc(00\gamma)$	$P\,{}^{P4/ncc}_{1\ 11}$	Kucharczyk, Budkowski, Boswell, Prodan & Marinković (1990)
$[NH_3(C_3H_7)]_2 \cdot CuCl_4$	$Pbca(00\gamma)ss0$	$P\,{}^{Pbca}_{s\,s1}$	Doudin & Chapuis (1990)
α-PbO	$C2mb(00\gamma)$	$P\,{}^{C2mb}_{1\,11}$	Hedoux, Grebille & Garnier (1989)
$SC(NH_2)_2$	$Pnma(0\beta0)s00$	$P\,{}^{Pnma}_{s\,11}$	Zúñiga, Madariaga, Paciorek, Pérez-Mato, Ezpeleta & Etxebarria (1989)
ε-$[NH_3(C_3H_7)]_2 \cdot MnCl_4$	$Abma(0\beta0)s00$	$P\,{}^{Abma}_{s\,10}$	Steurer & Depmeier (1989)
$TaTe_4$	$P4/ncc(00\gamma)$	$P\,{}^{P4/ncc}_{1\ 11}$	Budkowski, Prodan, Marinković, Kucharczyk, Uszyński & Boswell (1989)
$Bi_2(Sr,Ca)_3Cu_2O_{8+x}$	$Bbmb(0\beta1)$	$N\,{}^{Bbmb}_{1\,11}$	Yamamoto, Hirotsu, Nakamura & Nagakura (1989)
$Bi_2Sr_3Fe_2O_{9+x}$	$Fmmm(0\beta1)00s$	$N\,{}^{Fmmm}_{1\,1\,s}$	Perez, Leligny, Grebille, Labbe, Groult & Raveau (1995)
γ-Na_2CO_3	$C2/m(\alpha0\gamma)$	$P\,{}^{C2/m}_{1\ 0}$	Meyer, Paciorek, Schenk & Chapuis (1995); van Aalst, den Hollander, Peterse & de Wolff (1976)
$KFeF_3$	$Amma(0\beta0)00s$	$P\,{}^{Amma}_{1\,1\,s}$	Sciau & Grebille (1989)
Cs_2CdBr_4	$Pnma(\alpha00)0ss$	$P\,{}^{Pnma}_{1\,s\,s}$	Speziali & Chapuis (1989)
$AuTe_2$	$C2/m(\alpha0\gamma)0s$	$P\,{}^{C2/m}_{1\ s}$	Schutte & de Boer (1988)
$A(Al, Si)_4O_8$ A = (Na, Ca)	$P\bar{1}(\alpha\beta\gamma)$	$P\,{}^{P\bar{1}}_{1}$	Yamamoto, Nakazawa, Kitamura & Morimoto (1984); Steurer & Jagodzinski (1988)
$ZrTiO_4$	$Pbc2_1(0\beta0)$	$P\,{}^{Pbc2_1}_{1\,11}$	Yamamoto, Yamada, Ikawa, Fukunaga, Tanaka & Marumo (1991)
CuAuII	$Fmmm(0\beta0)$	$N\,{}^{Fmmm}_{1\,11}$	Yamamoto (1982*b*)
$NaNO_2$	$Immm(\alpha00)$	$P\,{}^{Immm}_{1\,s\,1}$	Yamamoto (1985*a*)
$BaMnF_4$	$P2_1nb(\alpha\frac{1}{2}\frac{1}{2})0qq$	$U\,{}^{P2_1nb}_{1\,qq}$	Sciau, Lapasset, Grebille & Berar (1988)
$SC(NH_2)_2$	$Pnma(0\beta0)$	$P\,{}^{Pnma}_{1\,11}$	Gao, Gajhede, Mallinson, Petříček & Coppens (1988)
$DMM(TCNQ)_2$	$P\bar{1}(\alpha\beta\gamma)$	$P\,{}^{P\bar{1}}_{1}$	Steurer, Visser, van Smaalen & de Boer (1987)
α-U	$P2/m(\frac{1}{2}\beta\gamma)$	$A\,{}^{P2/m}_{1\ 1}$	van Smaalen & Haas (1985); van Smaalen & George (1987)
$NiTe_4$	$P4/mcc(\frac{1}{2}\frac{1}{2}\gamma)$	$W\,{}^{P4/mcc}_{1\,111}$	Prodan & Boswell (1987)

Table 1. *(cont.)*

Compound	One-line symbol	Two-line symbol	References
α-CuNSal·Cu($C_8H_8NO_2$)$_2$	$Iba2(\alpha 00)$	$P\begin{smallmatrix}Iba2\\1\,1\,1\end{smallmatrix}$	Steurer & Adlhart (1983*a*)
α-NiNSal·Ni($C_8H_8NO_2$)$_2$	$Iba2(\alpha 00)$	$P\begin{smallmatrix}Iba2\\1\,1\,1\end{smallmatrix}$	Steurer & Adlhart (1983*b*)
Biphenyl	$Pa(0\beta 0)$	$P\begin{smallmatrix}Pa\\1\end{smallmatrix}$	Baudour & Sanquer (1983)
$Ba_{0.8}M_8O_{16}$ M = (Ti, V, Cr)	$I4/m(00\gamma)$	$P\begin{smallmatrix}I4/m\\1\,1\,\bar{1}\end{smallmatrix}$	Xiang, Fan, Wu, Li & Pan (1990)

Table 2. *Modulated crystals with 2D or 3D modulations and their superspace groups*

Compound	One-line symbol	Two-line symbol	References
TTF-TCNQ	$P2_1/c$ $(\alpha\beta 0)$	$P\begin{smallmatrix}P2_1/c\\c\,m\,m\end{smallmatrix}$	Coppens, Petříček, Levendis, Larsen, Paturle, Yan & LeGrand (1987)
Mo_2S_3	$P\bar{1}(\alpha\beta\gamma)(\lambda\mu\nu)$	$P\begin{smallmatrix}P\bar{1}\\p2\end{smallmatrix}$	Schutte, Disselborg & de Boer (1993)
$BaNiP_2$	$P6_3mc(\alpha\alpha 0)$	$P\begin{smallmatrix}P6_3mc\\p6\;mm\end{smallmatrix}$	van der Lee, van Smaalen, Wiegers & de Boer (1991)
$Au_{2+x}Cd_{1-x}$	$P6_3/mmc(\alpha\alpha 0)$	$P\begin{smallmatrix}P6_3/mmc\\p6\;1\,mm\end{smallmatrix}$	Yamamoto (1983*b*)
1*T*-TaS_2	$P\bar{3}(\alpha\beta\frac{1}{3})$	$T\begin{smallmatrix}P\bar{3}\\p6\end{smallmatrix}$	Yamamoto (1983*a*)
ε-CuSb	$P6_3/mmc(\alpha\alpha 0)$	$P\begin{smallmatrix}P6_3/mmc\\p6\;1mm\end{smallmatrix}$	Motai, Watanabe & Hashimoto (1993)
$Fe_{1-x}O$	$Fm\bar{3}m(\alpha 00)$	$P\begin{smallmatrix}Fm\bar{3}m\\Pm\bar{3}m\end{smallmatrix}$	Yamamoto (1982*a*,*b*)
$V_6Ni_{16}Si_7$	$Im\bar{3}m(\alpha\alpha 1+\alpha)$	$N\begin{smallmatrix}Im\bar{3}m\\Fm\bar{3}m\end{smallmatrix}$	Withers, Feng & Lu (1990)
$Cu_2S\cdot S_2$	$Fm\bar{3}m(\alpha\alpha\alpha)$	$P\begin{smallmatrix}Fm\bar{3}m\\Fm\bar{3}m\end{smallmatrix}$	Ohmasa, Hiraga, Tomeoda & Ueda (1995)

Table 3. *Composite crystals and their superspace groups; the substructures are enclosed by brackets*

Compound	One-line symbol	Two-line symbol	References
$[LaS]_x[CrS_2]$	$C\bar{1}(\alpha 1+\beta\gamma) : C\bar{1}(\alpha 1+\beta\gamma)$	$M\begin{smallmatrix}P\bar{1}\\1\end{smallmatrix} : M\begin{smallmatrix}P\bar{1}\\1\end{smallmatrix}$	Kato (1990)
$[LaS]_x[NbS_2]$	$Cm2a(\alpha_1 1\frac{1}{2}) : Fm2m(\alpha_2 10)$	$I\begin{smallmatrix}Cm2a\\1\,1\,1\end{smallmatrix} : M\begin{smallmatrix}Fm2m\\1\,1\,s\end{smallmatrix}$	van Smaalen (1991)
$[PbS]_x[TiS_2]$	$C2/m(01\gamma_1)s0 : C2_1/m(01\gamma_2)$	$M\begin{smallmatrix}C2/m\\s\,1\end{smallmatrix} : M\begin{smallmatrix}C2_1/m\\1\,\bar{1}\end{smallmatrix}$	van Smaalen (1991)
$[SnS]_x[NbS_2]$	$Cm2a(\alpha_1 10) : Cm2m(\alpha_2 10)$	$M\begin{smallmatrix}Cm2a\\1\,1\,1\end{smallmatrix} : M\begin{smallmatrix}Cm2m\\1\,1\,s\end{smallmatrix}$	van Smaalen (1989)
$[PbS]_x[VS_2]$	$F2(\alpha_1 10) : Cm(\alpha_2 1\frac{1}{2})$	$M\begin{smallmatrix}F2\\1\end{smallmatrix} : I\begin{smallmatrix}C2\\1\end{smallmatrix}$	van Smaalen (1989)
$[Sr]_x[TiS_3]$	$P31c(\frac{1}{3}\frac{1}{3}\gamma_1) : R3m(00\gamma_2)$	$R\begin{smallmatrix}P31c\\1\,1\,1\end{smallmatrix} : P\begin{smallmatrix}R3m\\1\,s\end{smallmatrix}$	Onoda, Saeki, Yamamoto & Kato (1993)
$[Ba]_x[TiS_3]$	$P31c(\frac{1}{3}\frac{1}{3}\gamma_1) : R3m(00\gamma_2)$	$R\begin{smallmatrix}P31c\\1\,1\,1\end{smallmatrix} : P\begin{smallmatrix}R3m\\1\,s\end{smallmatrix}$	Ukei, Yamamoto, Watanabe, Shishido & Fukuda (1993)
$[Sr_2Cu_2O_3][CuO_2]_x$	$A2_1ma(01\gamma_1) : A2_1ma(01\gamma_2)$	$M\begin{smallmatrix}A2_1ma\\1\,s\,\bar{1}\end{smallmatrix} : M\begin{smallmatrix}A2_1ma\\1\,s\,\bar{1}\end{smallmatrix}$	Ukei, Shishido & Fukuda (1994)
$[Ba]_x[FeS_2]$	$I4mm(10\gamma_1)1ss : I4bm(10\gamma_2)1ss$	$L\begin{smallmatrix}I4mm\\1\,s\,s\end{smallmatrix} : L\begin{smallmatrix}I4bm\\1\,s\,s\end{smallmatrix}$	Onoda & Kato (1991)
$[BiSe]_x[TaSe_2]$	$Fm2m(\alpha_1 00) : Pm2m(\alpha_2\frac{1}{2}\frac{1}{2})$	$P\begin{smallmatrix}Fm2m\\1\,1\,1\end{smallmatrix} : U\begin{smallmatrix}Pm2m\\1\,1\,1\end{smallmatrix}$	Petříček, Cisarova, de Boer, Zhou, Meetsma, Wiegers & van Smaalen (1993)
$[ZrA][A]_x$ (A = N, O, F)	$Abmm(00\gamma_1)0s0 : Pmcm(0\frac{1}{2}\gamma_2)$	$P\begin{smallmatrix}Abmm\\1\,s\,\bar{1}\end{smallmatrix} : B\begin{smallmatrix}Pmcm\\s\,1\,1\end{smallmatrix}$	Schmid & Withers (1995)

of 1D modulated structures but the satellite reflection intensities are comparable with those of main reflections, indicating that the modulation amplitudes are very large. In addition, the modulation wave is strongly unharmonic, giving up to fourth-order satellite reflections. In principle, the complete description of a rotational motion of a rigid body can be made by the rotation around the center of gravity, which is given by an orthogonal matrix. It is known that the 3 × 3 orthogonal matrix can be given by three parameters known as the Eulerian angles φ, θ and ψ. It is noted that the description is more complicated than that of the approximation mentioned above but it does not necessitate additional parameters. Therefore, we can consider a program where the translation vector and the Eulerian angles are refined as a function of the fourth coordinate. Such a program has not been written yet.

3.4. *Examples of modulated and composite crystals*

Since the first application of nD crystallography to γ-Na_2NO_3 by van Aalst, den Hollander, Peterse & de Wolff (1976), the 1D modulated crystals have been determined extensively on the basis of the superspace groups (Table 1). The application of the theory to 2D and 3D cases were given by Yamamoto (1982*a*,*c*, 1983*a*,*b*). The composite crystal structure of $[LaS]_x[CrS_2]$ was analyzed for the first time based on the superspace group by Kato (1990). The examples of the modulated-

structure analyses for 2D or 3D modulated crystals and those of composite crystals are, however, not many in number. They are listed in Tables 2 and 3. There are many other composite crystals to which such a theory has not been applied [see Table 1 in Yamamoto (1993*b*)].

4. Indexing of diffraction patterns of quasicrystals

A characteristic feature of quasicrystals is seen in the diffraction pattern, which consists of sharp diffraction spots with non-crystallographic symmetry. Such diffraction patterns cannot be indexed by three (reciprocal) vectors and three Miller indices. In the hypothetical 2D quasicrystals like the octagonal Penrose, Penrose and Stampfli tilings, we need four vectors and four integers. According to nD crystallography, this indicates that these can be described as crystals in 4D space. In this theory, the location of diffraction spots in the external space is regarded as the projection of the lattice points of the reciprocal lattice in nD space onto the external space and their intensity as Fourier spectra of a crystal in nD space. Such an interpretation is possible because the diffraction intensity is given by the Fourier spectra of the crystal. From the properties of the Fourier transformation, the diffraction pattern of an intersection of the structure is given by the projection of the structure factor along the internal (complementary, perpendicular) space, which is normal to the external space. This principle was applied to the interpretation of the diffraction patterns of incommensurate structures and enabled us to give their nD description as mentioned above. This is independent of the symmetry of the diffraction patterns and is applicable to quasicrystals. Therefore, if all the reflections can be assigned by using n reciprocal unit vectors, they are regarded as the reciprocal unit vectors in nD space.

4.1. *Polygonal quasicrystals*

As examples of fictitious polygonal quasicrystals, we first consider the octagonal Penrose, Penrose and Stampfli tilings, which are tilings in 2D space. These have diffraction patterns with octagonal, decagonal and dodecagonal symmetries, which can be regarded as the projection of reciprocal lattices in 4D space. Their diffraction patterns are shown in Figs. 2(*a*)–(*c*), which are calculated by the 4D description of these patterns as shown later. For these cases, four vectors $\mathbf{d}_i^{*e}$ ($i \leq 4$) are sufficient for indexing and each diffraction spot located at $\mathbf{h}$ is expressed as $\sum_{i=1}^{4} h_i \mathbf{d}_i^{*e}$ with Miller indices $h_1h_2h_3h_4$ (Figs. 9*a*–*c*). The diffraction pattern of the Penrose tiling (Fig. 2*b*) can be indexed by five vectors (arrows) $\mathbf{d}_i^{*e}$ ($i \leq 5$) written in the figure. These are regarded as the projection of the unit vectors of a lattice in 5D space onto the 2D external space. One of them is expressed by the integral linear combination of the other four because $\sum_{i=1}^{5} \mathbf{d}_i^{*e} = 0$. Therefore, there are infinitely many sets of Miller indices $h_1h_2h_3h_4h_5$, which give the same position: the indices $h_1'h_2'h_3'h_4'h_5'$ and $h_1h_2h_3h_4h_5$ give the same position in the external space if $h_i' = h_i + m$ with an integer m for all i. This means that the lattice points $\sum_{i=1}^{5} h_i' \mathbf{d}_i^*$ and $\sum_{i=1}^{5} h_i \mathbf{d}_i^*$ may be different in 5D space but they are projected onto the same position. These structure factors have to be summed in order to obtain the intensity of the Penrose tiling. Similarly, dodecagonal patterns can be indexed with six unit vectors (arrows) shown in Fig. 2(*c*) but only four of them $\mathbf{d}_i^{*e}$ ($i = 1, 2, 3, 4$) are independent. Two of them are expressed by integral linear combinations of the other two ($\mathbf{d}_5^{*e} = \mathbf{d}_3^{*e} - \mathbf{d}_1^{*e}$, $\mathbf{d}_6^{*e} = \mathbf{d}_4^{*e} - \mathbf{d}_2^{*e}$). Thus, without loss of generality, the four independent vectors $\mathbf{d}_i^{*e}$ ($i = 1, 2, 3, 4$) can be regarded as the projection of the unit vectors $\mathbf{d}_i^*$ in a 4D reciprocal lattice.

Since the diffraction pattern shows the noncrystallographic point symmetry in the present case, we can construct a 4×4 representation of the noncrystallographic point group based on the unit vectors $\mathbf{d}_i^*$. The octagonal group D_8 is generated by an eightfold rotation C_8 and a mirror σ (which interchanges $\mathbf{d}_1^*$ and $\mathbf{d}_4^*$ and $\mathbf{d}_2^*$ and

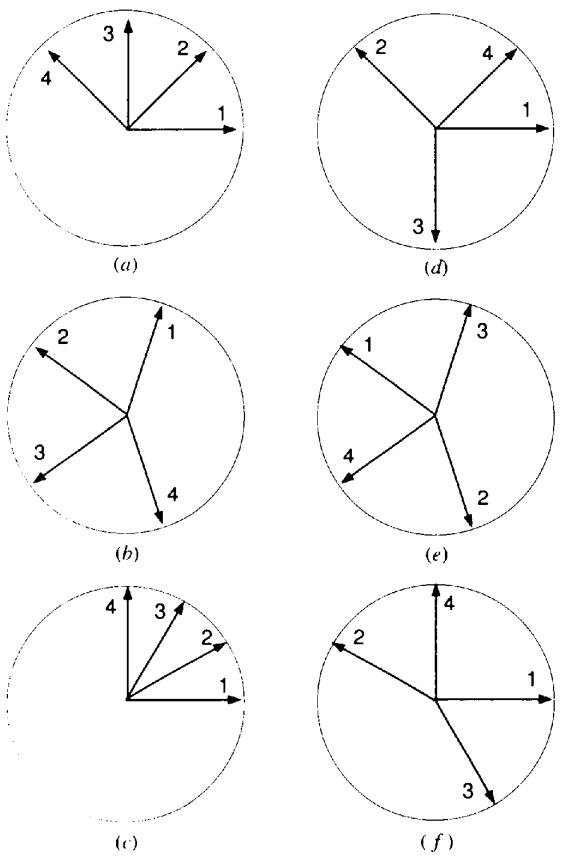

Fig. 9. The projection of the unit vectors of polygonal reciprocal lattices in 4D space. The external components of the unit vectors of (*a*) octagonal, (*b*) decagonal and (*c*) dodecagonal lattices and their corresponding internal space components, (*d*), (*e*) and (*f*).

$\mathbf{d}_3^*$), the representations of which are given by

$$R(C_8) = \begin{bmatrix} 0 & 1 & 0 & 0 \\ 0 & 0 & 1 & 0 \\ 0 & 0 & 0 & 1 \\ -1 & 0 & 0 & 0 \end{bmatrix}, \tag{11}$$

$$R(\sigma) = \begin{bmatrix} 0 & 0 & 0 & 1 \\ 0 & 0 & 1 & 0 \\ 0 & 1 & 0 & 0 \\ 1 & 0 & 0 & 0 \end{bmatrix}. \tag{12}$$

Similarly, the representations of n-fold rotations C_n ($n = 10$ and 12) for decagonal and dodecagonal groups $R(D_{10})$ and $R(D_{12})$ are

$$R(C_{10}) = \begin{bmatrix} 0 & 1 & 0 & 0 \\ 0 & 0 & 1 & 0 \\ 0 & 0 & 0 & 1 \\ -1 & -1 & -1 & -1 \end{bmatrix}, \tag{13}$$

$$R(C_{12}) = \begin{bmatrix} 0 & 1 & 0 & 0 \\ 0 & 0 & 1 & 0 \\ 0 & 0 & 0 & 1 \\ -1 & 0 & 1 & 0 \end{bmatrix}. \tag{14}$$

All elements of the group can be written as $C_n^i \sigma^j$ ($i = 0, 1, \ldots, n-1$, $j = 0, 1$) provided that $C_n^0 = \sigma^0$ is the identity operator E. The orders of D_8, D_{10} and D_{12} are 16, 20 and 24, respectively. The representation for the mirror, which interchanges $\mathbf{d}_1^*$ and $\mathbf{d}_4^*$ and $\mathbf{d}_2^*$ and $\mathbf{d}_3^*$, is the same as in the octagonal group.

These representations are reducible. In the dihedral group generated by the n-fold rotation and the mirror, there are $2 + m$ [$m = (n - 1)/2$] irreducible representations for n odd, two of which are 1D and the others are 2D. This is not relevant in the present case but we discuss this first for application to the pentagonal quasicrystals discussed later. The first 1D irreducible representation is the identity representation, where $R_1^1(C_n) = 1$ and $R_1^1(\sigma) = 1$. The other 1D representation is given by $R_2^1(C_n) = 1$ and $R_2^1(\sigma) = -1$. (The superscript stands for the dimension of the irreducible representation.) The 2D representations are given by

$$R_k^2(C_n) = \begin{bmatrix} c_k & -s_k \\ s_k & c_k \end{bmatrix} \quad (k = 1, 2, \ldots, m) \tag{15}$$

$$R_k^2(\sigma) = \begin{bmatrix} 0 & 1 \\ 1 & 0 \end{bmatrix} \quad (k = 1, 2, \ldots, m), \tag{16}$$

where c_k and s_k are $\cos(2\pi k/n)$ and $\sin(2\pi k/n)$. The representations for the other operations are obtained by the multiplication of these.

On the other hand, when n is even, there are four 1D representations, which are $(R_k^1(C_n), R_k^1(\sigma)) = (1, 1)$, $(1, -1)$, $(-1, 1)$ and $(-1, -1)$ for $k = 1$, 2, 3 and 4. The 2D representations are given by (15) and (16) with $m = (n - 2)/2$. From the characters of the 4×4 representations and the characters of D_8, D_{10} and D_{12} in Tables 4–6, they are reduced to two irreducible representations R_1^2 and R_3^2 for $n = 8$ and $n = 10$ and R_1^2 and R_5^2 for $n = 12$. If we use the orthogonal basis in the 2D external space, we have R_1^2 for all cases. From the projection-operator method or inspection, we can obtain the transformation matrix between the basis vectors of each irreducible representation and the unit vectors $\mathbf{d}_i^*$. The latter is based on the fact that the basis vectors of the different irreducible representations are orthogonal to each other. The unit vectors $\mathbf{d}_j^*$ ($j = 1$, 2, 3, 4) in the octagonal, decagonal and dodecagonal lattices are expressed in terms of the basis vectors of the corresponding irreducible representations $\mathbf{a}_i$ ($i \leq 4$) as follows, where $\mathbf{a}_i \cdot \mathbf{a}_j = \delta_{ij}$ owing to the orthogonality.

$$\mathbf{d}_j^* = (a^*/2)[c_{(j-1)}\mathbf{a}_1 + s_{(j-1)}\mathbf{a}_2] + (a^{*\prime}/2)[c_{3(j-1)}\mathbf{a}_3 + s_{3(j-1)}\mathbf{a}_4] \quad \text{(octagonal)} \tag{17}$$

$$\mathbf{d}_j^* = (a^*/5^{1/2})[c_{(j-1)}\mathbf{a}_1 + s_{(j-1)}\mathbf{a}_2 + (a^{*\prime}/5^{1/2})[c_{2(j-1)}\mathbf{a}_3 + s_{2(j-1)}\mathbf{a}_4] \quad \text{(decagonal)} \tag{18}$$

$$\mathbf{d}_j^* = (a^*/2^{1/2})[c_{(j-1)}\mathbf{a}_1 + s_{(j-1)}\mathbf{a}_2] + (a^{*\prime}/2^{1/2})[c_{5(j-1)}\mathbf{a}_3 + s_{5(j-1)}\mathbf{a}_4] \quad \text{(dodecagonal).} \tag{19}$$

Here, a^* and $a^{*\prime}$ are the lattice constants of the 4D reciprocal lattice in the external and internal spaces. Since the scaling in the internal space is physically meaningless, $a^{*\prime}$ is often taken to be equal to a^* (Fig. 9). It is easily checked that the $\mathbf{a}_i$ are the basis vectors of the irreducible representation mentioned above, since $M^{-1}RM$ becomes a $2 + 2$ block-diagonal matrix for any element of the group, where the matrix elements of M are defined by $\mathbf{d}_i^* = \sum_{j=1}^4 M_{ij}\mathbf{a}_j$. Several different definitions of the lattice constant a^* are possible but the factors $1/2$, $1/5^{1/2}$ and $1/2^{1/2}$ introduced in (17)–(19) are chosen so that the lattice constant a^* corresponds to that of the nD ($n = 4$, 5, 6) hypercubic lattice when $a^* = a^{*\prime}$.

The selection of the unit vectors $\mathbf{d}_i^*$ is not unique as in normal crystals. In order to avoid this, the reduced cell is used for the normal crystals. (Consider the monoclinic lattice for example.) This is, however, not applicable to quasicrystals because the scale in the internal space is physically meaningless, as mentioned above. As a result, there is no criterion that selects a particular set

Table 4. *Characters of irreducible representations of the octagonal group D_8*

$\alpha = C_8$, $\beta = \sigma'$. χ is the character of the representations with respect to the basis vectors of the 4D octagonal lattice.

	ε	2α	$2\alpha^2$	$2\alpha^3$	α^4	4β	$4\alpha\beta$
R_1^1	1	1	1	1	1	1	1
R_2^1	1	1	1	1	1	−1	−1
R_3^1	1	−1	1	−1	1	1	−1
R_4^1	1	−1	1	−1	1	−1	1
R_1^2	2	$2^{1/2}$	0	$-2^{1/2}$	−2	0	0
R_2^2	2	0	−2	0	2	0	0
R_3^2	2	$-2^{1/2}$	0	$2^{1/2}$	−2	0	0
χ	4	0	0	0	−4	0	0

of unit vectors among infinite sets of unit vectors spanning the same reciprocal lattice. These sets of vectors are related by the similarity transformation. Other unit vectors $\mathbf{d}_i^{*\prime}$ related by the similarity transformation are given by $\mathbf{d}_i^{*\prime} = \sum_{j=1}^{4} (\tilde{S})_{ij}^m \mathbf{d}_j^*$, with an integer m and the similarity transformation matrices

$$S = \begin{bmatrix} 1 & 1 & 0 & -1 \\ 1 & 1 & 1 & 0 \\ 0 & 1 & 1 & 1 \\ -1 & 0 & 1 & 1 \end{bmatrix} \quad \text{(octagonal)} \qquad (20)$$

$$S = \begin{bmatrix} 0 & 1 & 0 & -1 \\ 0 & 1 & 1 & -1 \\ -1 & 1 & 1 & 0 \\ -1 & 0 & 1 & 0 \end{bmatrix} \quad \text{(decagonal)} \qquad (21)$$

$$S = \begin{bmatrix} 1 & 0 & 0 & -1 \\ 1 & 1 & 0 & 0 \\ 0 & 1 & 1 & 1 \\ 0 & 0 & 1 & 1 \end{bmatrix} \quad \text{(dodecagonal)}, \qquad (22)$$

where the tilde means transposition. The new representations of the point group based on unit vectors $\mathbf{d}_i^{*\prime}$ are given by $\tilde{S}^m R \tilde{S}^{-m}$. The set of similarity transformations $\tilde{S}^m$ $(-\infty < m < \infty)$ constructs a group that leaves the matrix group generated by $R(C_n)$ and $R(\sigma)$ invariant. This set is called a normalizer. If it leaves each element in the matrix group invariant, it is called a centralizer. The matrix $\tilde{S}$ and its inverse matrix are generators of the centralizer and normalizer for the octagonal and decagonal cases and those of the normalizer for the dodecagonal one. The generators of the centralizer for the dodecagonal group are given by S^2 and its inverse matrix (Janssen, 1992). The normalizer and the centralizer are related to the self-similarity of quasiperiodic tilings and equivalence relations of space groups as shown later.

The new unit vectors $\mathbf{d}_i^{*\prime}$ have an external space component smaller by a factor τ^{-m} and an internal component larger by τ^n, where the similarity ratio τ is $1 + 2^{1/2}$, $(1 + 5^{1/2})/2$ or $(1 + 3^{1/2})/2^{1/2}$ for the octagonal, decagonal or dodecagonal lattice. The similarity transformation depends on lattice types (Bravais lattices) for 6D icosahedral lattices as shown below. It is, however, known that only the primitive lattice is present in the 4D octagonal, decagonal and dodecagonal lattices (Brown, Bülow, Neubüser, Wondratschek & Zassenhaus, 1978). For real polygonal quasicrystals in the 3D external space, we have to consider 5D lattices. It is known that the body-centered lattice exists in 5D octagonal lattices (Janssen, 1986; Rabson, Mermin, Rokhsar & Wright, 1991). The external and internal components of unit vectors in direct lattices can be expressed in a similar form for the octagonal case but have different forms for the others (see Fig. 10 and §5.2).

Table 5. *Characters of irreducible representations of the decagonal group D_{10}*

$\tau = (1 + 5^{1/2})/2$, $\alpha = C_{10}$, $\beta = \sigma'$. χ is the character of the representations with respect to the basis vectors of the 4D decagonal lattice

	ε	2α	$2\alpha^2$	$2\alpha^3$	$2\alpha^4$	α^5	5β	$5\alpha\beta$
R_1^1	1	1	1	1	1	1	1	1
R_2^1	1	1	1	1	1	1	−1	−1
R_3^1	1	−1	1	−1	1	−1	1	−1
R_4^1	1	−1	1	−1	1	−1	−1	1
R_1^2	2	τ	τ^{-1}	$-\tau^{-1}$	$-\tau$	−2	0	0
R_2^2	2	τ^{-1}	$-\tau$	$-\tau$	τ^{-1}	2	0	0
R_3^2	2	$-\tau^{-1}$	$-\tau$	τ	τ^{-1}	−2	0	0
R_4^2	2	$-\tau$	τ^{-1}	τ^{-1}	$-\tau$	2	0	0
χ	4	1	−1	1	−1	−4	0	0

Table 6. *Characters of irreducible representations of the dodecagonal group D_{12}*

$\alpha = C_{12}$, $\beta = \sigma'$. χ is the character of the representations with respect to the basis vectors of the 4D dodecagonal lattice.

	ε	2α	$2\alpha^2$	$2\alpha^3$	$2\alpha^4$	$2\alpha^5$	α^6	6β	$6\alpha\beta$
R_1^1	1	1	1	1	1	1	1	1	1
R_2^1	1	1	1	1	1	1	1	−1	−1
R_3^1	1	−1	1	−1	1	−1	1	1	−1
R_4^1	1	−1	1	−1	1	−1	1	−1	1
R_1^2	2	$3^{1/2}$	1	0	−1	$-3^{1/2}$	−2	0	0
R_2^2	2	1	−1	−2	−1	1	2	0	0
R_3^2	2	0	−2	0	2	0	−2	0	0
R_4^2	2	−1	−1	2	−1	−1	2	0	0
R_5^2	2	$-3^{1/2}$	1	0	−1	$3^{1/2}$	−2	0	0
χ	4	0	2	0	−2	0	−4	0	0

4.2. *Icosahedral quasicrystals*

The first quasicrystal found in the Al–Mn system showed icosahedral symmetry, which needs six unit

vectors to index the diffraction pattern. They are defined by Duneau & Katz (1985), Elser (1985) and Janssen (1986) as follows.

$$\begin{aligned}\mathbf{d}_1^* &= (a^*/2)\mathbf{a}_3 + (a^{*\prime}/2)\mathbf{a}_6,\\ \mathbf{d}_i^* &= (a^*/2)[(c_i\mathbf{a}_1 + s_i\mathbf{a}_2)s + c\mathbf{a}_3]\\ &\quad + (a^{*\prime}/2)[(c_{2i}\mathbf{a}_4 + s_{2i}\mathbf{a}_5)s - c\mathbf{a}_6]\\ &\quad (i = 2, 3, \ldots, 6),\end{aligned} \tag{23}$$

where $c_i = \cos(2\pi i/5)$, $s_i = \sin(2\pi i/5)$, $c = \cos\theta = 1/5^{1/2}$, $s = \sin\theta$, a^* is the lattice constant of the reciprocal lattice and $a^{*\prime}$ is that of the internal space (Fig. 11). The vectors $\mathbf{a}_1$, $\mathbf{a}_2$, $\mathbf{a}_3$ represent the unit vectors of the external space and $\mathbf{a}_4$, $\mathbf{a}_5$, $\mathbf{a}_6$ those of the internal space. The icosahedral group is generated by a fivefold rotation C_5, a threefold rotation C_3 around a fivefold and a threefold axis of the regular icosahedron (Fig. 12) and the inversion I. The external components of $\mathbf{d}_i^*$ are along six fivefold axes of the icosahedron. The 6D representation of the icosahedral point group is obtained by using $\mathbf{d}_i^{*e}$. The 6D representations of the generators are

$$R(C_5) = \begin{bmatrix}1&0&0&0&0&0\\0&0&1&0&0&0\\0&0&0&1&0&0\\0&0&0&0&1&0\\0&0&0&0&0&1\\0&1&0&0&0&0\end{bmatrix} \tag{24}$$

$$R(C_3) = \begin{bmatrix}0&0&0&0&0&1\\1&0&0&0&0&0\\0&0&0&0&1&0\\0&0&-1&0&0&0\\0&0&0&-1&0&0\\0&1&0&0&0&0\end{bmatrix}. \tag{25}$$

Here, C_5 is the fivefold rotation around $\mathbf{d}_1^*$ and C_3 the threefold rotation around $\mathbf{d}_1^* + \mathbf{d}_2^* + \mathbf{d}_6^*$ [Fig. 11]. All the elements of the group are given by $(C_5)^i(C_2)^j(C_2')^k(C_3)^l(I)^m$ with $0 \le i \le 4$, $0 \le j, k, m \le 1$, $0 \le l \le 2$, where $C_2 = C_3C_5$ and $C_2' = (C_3)^2C_5$ and the matrix elements of I are $-\delta_{ij}$ $(1 \le i, j \le 6)$.

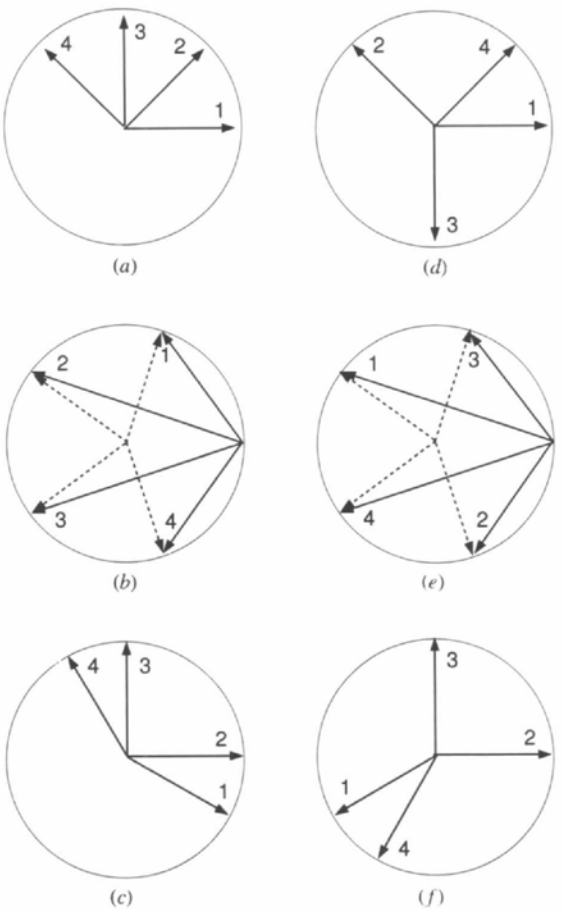

Fig. 10. The projection of the unit vectors of polygonal lattices in 4D space. The external components of the unit vectors of (*a*) octagonal, (*b*) decagonal and (*c*) dodecagonal lattices and their corresponding internal space components, (*d*), (*e*) and (*f*).

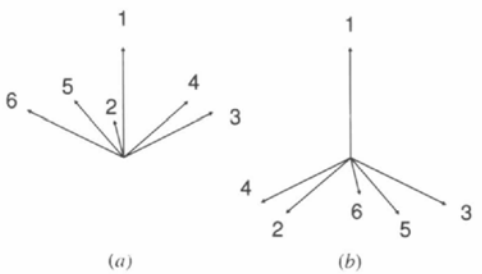

Fig. 11. The projection of unit vectors of the icosahedral lattice in 6D space into (*a*) the external and (*b*) the internal space. The unit vectors of the reciprocal lattice are parallel to the corresponding unit vectors shown here.

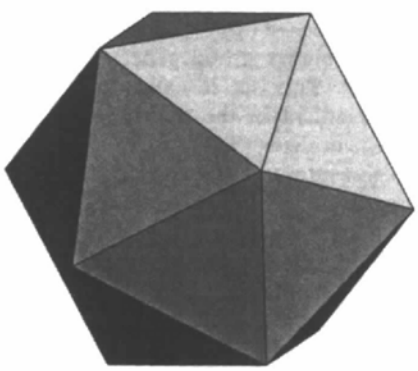

Fig. 12. The regular icosahedron. The fivefold (threefold) axis passes through the center of the icosahedron and a vertex (center of a triangle).

Table 7. *Characters of irreducible representations of the icosahedral group Y*

$\tau = (1 + 5^{1/2})/2$, $\alpha = C_5$, $\beta = C_3$. χ is the character of the representations with respect to the basis vectors of the 6D icosahedral lattice.

	ε	12α	$12\alpha^2$	20β	$15\alpha\beta$
R_1^1	1	1	1	1	1
R_1^3	3	$-\tau^{-1}$	τ	0	-1
R_2^3	3	τ	$-\tau^{-1}$	0	-1
R_1^4	4	-1	-1	1	0
R_1^5	5	0	0	-1	1
χ	6	1	1	0	-2

This representation is reducible as is clear from the character in Table 7 and reduced to two 3D representations, R_1^3 and R_2^3, the basis vectors of which are $(\mathbf{a}_1, \mathbf{a}_2, \mathbf{a}_3)$ and $(\mathbf{a}_4, \mathbf{a}_5, \mathbf{a}_6)$. The lattice spanned by $\mathbf{d}_i^*$ given above is called the primitive icosahedral lattice. This has the similarity transformation matrix $\tilde{S}^3$ with

$$S = \frac{1}{2}\begin{bmatrix} 1 & 1 & 1 & 1 & 1 & 1 \\ 1 & 1 & 1 & -1 & -1 & 1 \\ 1 & 1 & 1 & 1 & -1 & -1 \\ 1 & -1 & 1 & 1 & 1 & -1 \\ 1 & -1 & -1 & 1 & 1 & 1 \\ 1 & 1 & -1 & -1 & 1 & 1 \end{bmatrix}. \qquad (26)$$

The similarity ratio of $\tilde{S}$ is $\tau = (1+5^{1/2})/2$, so that the similarity ratio of the primitive lattice is $\tau^3 = 2 + 5^{1/2}$. There are two lattices with the similarity transformation matrix $\tilde{S}$. These are called the face-centered and body-centered icosahedral lattices. The former is seen in several icosahedral quasicrystals (Henley, 1988; Ishimasa, Fukano & Tsuchimori, 1988; Ebalard & Spaepen, 1989). Their reciprocal-lattice points are given by the vectors $\mathbf{h} = \sum_{i=1}^{6} h_i \mathbf{d}_i^*$ with h_i all even or all odd for the former and $\sum_{i=1}^{6} h_i$ even for the latter. The matrix S and its inverse matrix are the generators of the normalizer of the icosahedral point group for the face-centered and body-centered lattices and S^3 and its inverse are those for the primitive lattice (Elser, 1985; Levitov & Rhyner, 1988).

The projection of all lattice points of 4D polygonal lattices or 6D icosahedral lattices covers densely the 2D or 3D external space. Therefore, there is always another lattice point in the close vicinity of any reflection. However, the diffraction patterns of quasicrystals consist of discrete diffraction spots. This is because the diffraction intensities strongly depend on the internal components of their diffraction vectors (Elser, 1985) and a reflection having a diffraction vector with a large internal component cannot be observed in practice. This will be shown later. Thus, we can index all the reflections of polygonal or icosahedral quasicrystals by using four or six vectors. In real polygonal quasicrystals, there exists a period perpendicular to the 2D plane in the external space considered above. Then the diffraction pattern in the 3D external space consists of several equidistant diffraction planes like those in Fig. 2 stacked repeatedly along the normal to the plane with the distance $c^* = 1/c$, where c is the period (Fig. 25). Thus, we need five vectors $\mathbf{d}_i^*$ $(i = 1, 2, 3, 4)$ and $\mathbf{d}_5^* = c^*\mathbf{a}_5$, where $\mathbf{a}_5$ is the unit vector in the external space that is perpendicular to $\mathbf{a}_1$ and $\mathbf{a}_2$. This means that the polygonal quasicrystals discussed above are described as crystals in 5D space.

5. Polygonal tiling

The tiling was considered to be a key to understanding quasicrystal structures since the 3D Penrose tiling was shown to give a diffraction pattern similar to that of *i*-Al–Mn (Duneau & Katz, 1985). However, the point density of the 3D Penrose tiling that gives such a diffraction pattern is much smaller than that of *i*-Al–Mn (about 1/4). Therefore, several simple decorations of the 3D Penrose tiling were considered (Ishihara & Shingu, 1986). Such an approach was partially successful for *i*-Al–Cu–Li but for most cases the simple decorations do not explain the diffraction intensities. On the other hand, the high-resolution transmission-electron-microscope (HRTEM) images of decagonal quasicrystals clarified that the tiling gives the location of atom clusters (Hiraga, Lincoln & Sun, 1991; Hiraga, Sun, Lincoln & Matsuo, 1993). This seems to be true for all quasicrystals. Thus, the tilings are still important to determine quasicrystal structures and may play the role of the average structure for modulated structures, which is first determined in the structure analysis.

There are four methods to obtain a quasiperiodic tiling as mentioned previously. We treat three of them (DM, PM and SM) because these are shown to be equivalent for tiling problems. Another one (IDM) relies on the matching rules but there are many tilings without simple matching rules and this method cannot calculate the diffraction pattern, which is essential for structure determination by diffraction methods. The matching rules may however be important for the crystal growth of quasicrystals (Onoda, Steinhardt, DiVincenzo & Socolar, 1988) and several tilings derived from the former methods have simple matching rules. Some tilings given by the IDM have not been derived by other methods (Watanabe, Ito & Soma, 1987). The quasiperiodic tiling is space filling with primitive tiles. In contrast to periodic structures, it needs two or more tiles in order to obtain non-crystallographic symmetry.

5.1. *The dual method*

The dual method is applicable to polygonal tilings discussed in the previous section and more general polygonal tilings or icosahedral tilings. In this section, simple derivations of the octagonal Penrose, Penrose and Stampfli tilings in 2D space are described. For 2D tilings,

the use of complex numbers gives an elegant description because a 2D vector can be expressed by a complex number (de Bruijn, 1981; Beenker, 1982) but this is not employed here since its extension to the 3D tiling is impossible. The following derivations of tilings are essentially the same as those given by Beenker (1982), de Bruijn (1981) and Korepin, Gähler & Rhyner (1988).

(*a*) *Octagonal Penrose tiling*. This tiling with edge length a can be derived from the periodic 4-grid, which is given by

$$\mathbf{e}_i^* \cdot \mathbf{x} = n_i + \gamma_i \quad (i \leq 4) \tag{27}$$

with an integer n_i and the unit vectors in the external space

$$\mathbf{e}_{i+1}^* = a^*[\cos(2\pi i/8)\mathbf{a}_1 + \sin(2\pi i/8)\mathbf{a}_2], \tag{28}$$

where $\mathbf{a}_i$ ($i = 1, 2$) are the unit vectors of 2D external space and γ_i represents the phase shift of the parallel lines shown below. The vectors $\mathbf{x}$ fulfilling (27) construct the 4-grid, which is a set of parallel lines (grid lines) normal to the four directions specified by $\mathbf{e}_i^*$ ($i \leq 4$) (see Fig. 13*a*). It is noted that from (17) $\mathbf{e}_i^*$ ($i \leq 4$) are given by $2\mathbf{d}_i^{*e}$. Let $\mathbf{y}$ be a vector in an area enclosed by several lines. This is a triangle or a convex polygon in the present case. Let the point $\mathbf{y}$ be between the n_ith and $(n_i + 1)$th line along the ith direction $\mathbf{e}_i^*$. Then we can assign four integers, $n_i = \lfloor \mathbf{e}_i^* \cdot \mathbf{y} - \gamma_i \rfloor$, to the area where $\lfloor x \rfloor$ is the largest integer less than or equal to x. Plot a point at $\mathbf{r}_0 = \sum_{i=1}^4 n_i \mathbf{e}_i$, where $\mathbf{e}_i$ are the external components of the unit vectors of the 4D octagonal lattice $\mathbf{d}_i^e$ for any i [see (30)]. Join a line with the length $a = 1/a^*$. These procedures give the octagonal Penrose tiling with the edge length a (Fig. 13*b*). The transformation that transforms an area enclosed by grid lines into a point given above is called the dual transformation. This is also a transformation that transforms a point into an area. The same tiling can be obtained based on this principle. Consider the crosspoint $\mathbf{y}'$ with the n_ith and n_jth grid lines along the ith and jth directions and let the cross point be between the n_k and $n_k + 1$ grid line ($k \neq i$, $k \neq j$) for other directions. Then we assign four integers, $n_i = \lfloor \mathbf{e}_i^* \cdot \mathbf{y}' - \gamma_i \rfloor$ to the point and plot a rhombus with the corners at $\mathbf{r}_0$, $\mathbf{r}_0 + \mathbf{e}_i$, $\mathbf{r}_0 + \mathbf{e}_j$, $\mathbf{r}_0 + \mathbf{e}_i + \mathbf{e}_j$. These two algorithms work well when the grid has no singular grid points where more than two grid lines cross but the second one seems to be easier for programming. If the grid includes singular points, however, the latter algorithm does not work. For the singular point, we have to place a polygon, the shape of which depends on the singularity. In the present case, there are singular grid points along four directions parallel to $\mathbf{e}_i$ ($i \leq 4$) when $\gamma_i = 0$. We can shift the singular points to another place with non-zero γ_i. The octagonal Penrose tiling has a self-similarity with the similarity ratio of $1 + 2^{1/2}$ as shown by dotted lines in Fig. 13(*b*). It should be noted that this is equal to that of the octagonal lattice. The parallel lines given in Fig. 13(*a*) can be regarded as the intersection of 3D hyperplanes normal to four unit vectors of the 4D octagonal lattice or regarded as the unit-cell boundary at each lattice point of 4D space.

(*b*) *Penrose tiling*. The extension of the above theory to Penrose tiling is straightforward. [Historically, this was first obtained by de Bruijn (1981).] This uses the 5-grid instead of the 4-grid (Fig. 14*a*), which is given by

$$\mathbf{e}_i^* \cdot \mathbf{x} = n_i + \gamma_i \quad (i \leq 5), \tag{29}$$

where $\mathbf{e}_i^*$ ($1 \leq i \leq 4$) are given by $5\mathbf{d}_i^{*e}/2$ of (18) and $\mathbf{e}_5^* = -\sum_{i=1}^4 \mathbf{e}_i^*$. The dual transformation leads to the tiling consisting of the rhombi, the edge vectors of which are a pair of $\mathbf{d}_i^e$ ($i \leq 5$) in (31). Their edge length is $2a/5^{1/2}$. In this case, a different tiling with pentagonal symmetry is obtained for a different $\gamma = \sum_{i=1}^5 \gamma_i$ within $0 < \gamma < 1/2$ and decagonal tilings are obtained when $\gamma = 0$ or 0.5. The other values of γ lead to tilings locally isomorphic to some tilings with γ within this range. The local isomorphism is defined as follows. If any area of one tiling is completely overlapped by

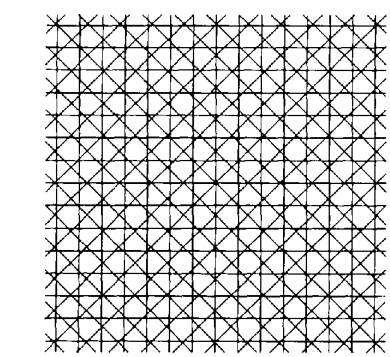

(*a*)

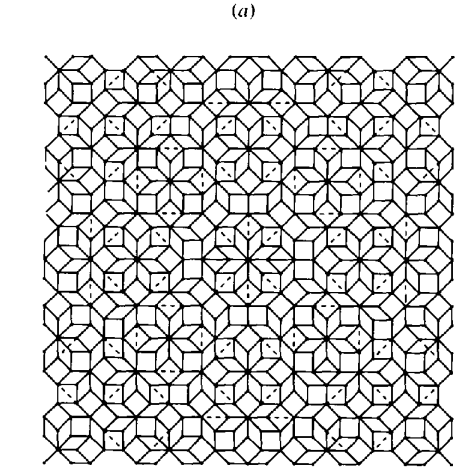

(*b*)

Fig. 13. (*a*) The 4-grid and (*b*) its dual pattern. The pattern plotted in dashed lines shows a self-similar pattern.

shifting and/or rotating on the other, these two are locally isomorphic. These tilings are called Penrose ($\gamma = 0$) and generalized Penrose tilings ($\gamma \neq 0$), two of which are shown in Figs. 14(*b*) and (*d*). When $\gamma_i = 0$ ($i \leq 5$), the singular grid points appear at the origin (Fig. 14*a*) and along five directions perpendicular to $\mathbf{e}_i^*$. These points can be shifted by choosing nonzero γ_i with $\sum_{i=1}^{5} \gamma_i = 0$. The similarity ratio of these tilings are $(1 + 5^{1/2})/2$ and its square as denoted by dotted lines in Figs. 14(*b*) and (*d*). They correspond to the similarity ratios of the 4D and 5D decagonal lattices. Note that the decoration of large tiles are the same for all cases and independent of the local environment in Fig. 14(*b*), while it depends on the local environment in Fig. 14(*d*).

The derivation of the tiling is related with the 5D decagonal lattice. The parallel lines given by (29) can be regarded as the intersection of 4D hyperplanes normal to five unit vectors of the 5D decagonal lattice with the 2D external space similarly to the octagonal Penrose tiling.

(*c*) *Stampfli tiling*. This is obtained from a modified DM (Korepin, Gähler & Rhyner, 1988). In this case, the grid is not a set of parallel lines but the double honeycomb net (Fig. 15*a*), in which a hexagon is located at the lattice points of double hexagonal lattice, one of which is rotated by 30° from the other. One hexagonal (reciprocal) lattice is spanned by $\mathbf{e}_i^*$ ($i = 1, 3$) and the other by $\mathbf{e}_i^*$ ($i = 2, 4$), where $\mathbf{e}_i^*$ are given by $3^{1/2}\mathbf{d}_i^{*e}$ of (19). This is an extension of the DM mentioned above. Another extension of the DM has been made by Socolar, Steinhardt & Levine (1985) as shown below. We call this the generalized dual method according to Socolar *et al.*, though the former is called the generalized grid projection method by Korepin, Gähler & Rhyner (1988). In this method, each area enclosed by lines of two honeycomb nets is also a convex polygon. When such an area belongs to the hexagons centered at $n_1\mathbf{e}_1 + n_3\mathbf{e}_3$ and $n_2\mathbf{e}_2 + n_4\mathbf{e}_4$, we plot a point at $\mathbf{r} = \sum_{i=1}^{4} n_i\mathbf{e}_i$, where $\mathbf{e}_i = \mathbf{d}_i^e$. The vectors $\mathbf{d}_i^e$ are the unit vectors of the 4D dodecagonal lattice in the direct space which is given in (34). The Stampfli tiling is obtained by joining points with a distance $2a/6^{1/2}$ (Fig. 15*b*). The double honeycomb net appearing in the present case is not related to the unit-cell boundaries in 4D space but the union of boundaries of Voronoi cells of two hexagonal lattices orthogonal to each other (Korepin *et al.*, 1988). As a result, the tiling consists of a rhombus, a square and a triangle, in contrast to the tilings given above. Such an extension has also been made for

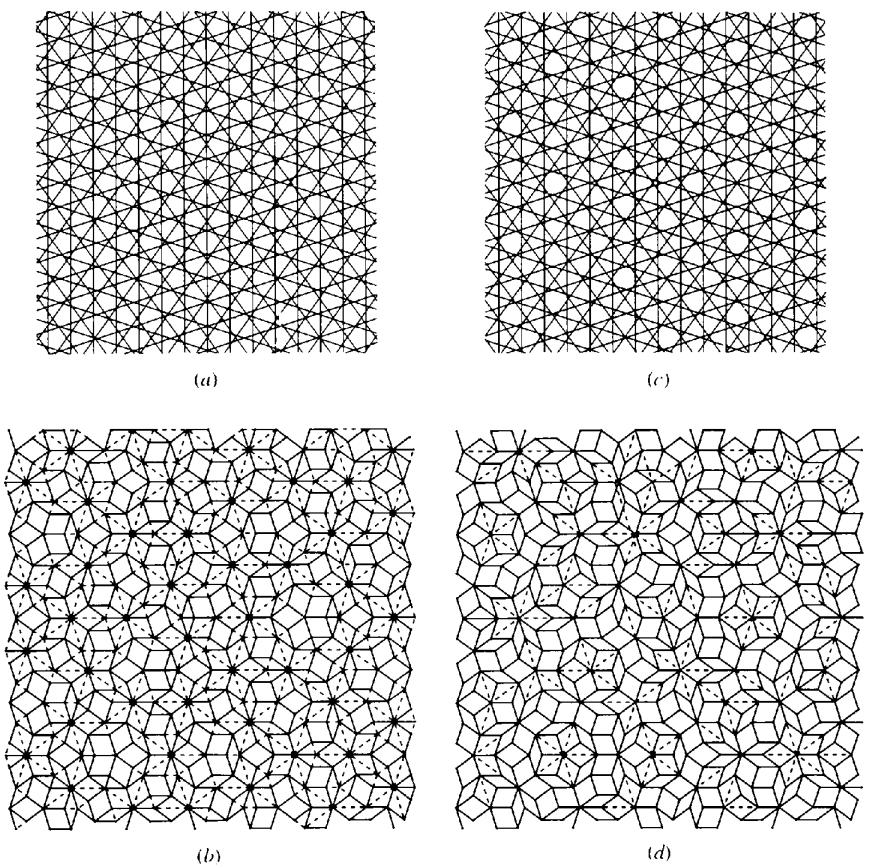

Fig. 14. (*a*) The 5-grid with $\gamma = 0$ and (*b*) its dual pattern. The corresponding patterns in the case of $\gamma = 0.1$ are shown in (*c*) and (*d*).

the icosahedral tiling, where boundaries of the Voronoi and the Delaunay cells of the face-centered icosahedral lattice in 6D space are taken (see §6).

5.2. *The projection and section methods*

The equivalence of the DM and PM was first shown by de Bruijn (1981) for the Penrose tiling and given for general quasiperiodic tilings consisting of rhombi by Gähler & Rhyner (1986). Several important tilings obtained from the generalized dual method (GDM) are also given by the SM or the PM. However, the general proof of equivalence is not known in this case. The difference between the PM and the SM is mainly in the concept. The former gives a point in the external space by the projection of an nD lattice point when the unit cell belonging to that lattice point intersects the external space. On the other hand, the latter uses the occupation domain at each lattice point extended along the internal space which is the projection of the unit cell (Bak, 1986; Janssen, 1986). Then the same point is obtained as an intersection of the occupation domain with the external space. This method provides a systematic treatment of all quasiperiodic structures including quasicrystals, modulated crystals and composite crystals because the latter two are usually treated as an intersection of an nD crystal with the 3D external space as mentioned in §4. Another difference is rather terminological. The PM is used for the tiling, which is often derived from a lattice in a dimension higher than the necessary dimension, while the SM is used for general quasiperiodic structures which are obtained from any kind of occupation domains but in space with the minimal dimension. Therefore, these two methods are almost equivalent for tiling problems. In the calculations of diffraction patterns or the point density, the latter has to be used.

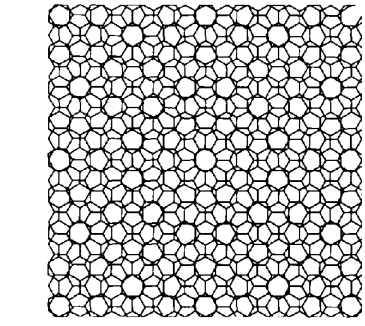

(*a*)

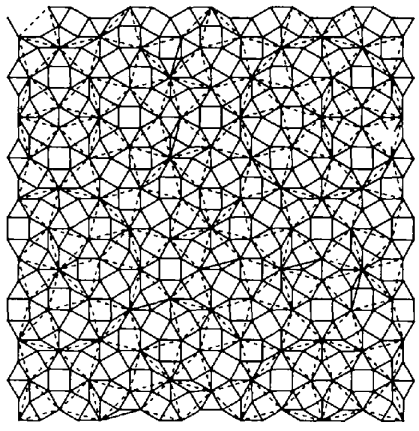

(*b*)

Fig. 15. (*a*) The double honeycomb net and (*b*) its dual pattern (Stampfli tiling).

One of the merits of the SM is that it gives an elegant way of giving diffraction patterns (Duneau & Katz, 1985; Katz & Duneau, 1986). In the PM, we need only a projection of the unit cell of an nD lattice onto the $(n-2)$D internal space for polygonal tilings and the $(n-3)$D internal space for icosahedral tilings. This is called a window. In the SM, the intersection of the projected unit cell with the minimal internal space has to be known. This is called an occupation domain (acceptance domain, atom surface). The window and the occupation domain are the same for the octagonal Penrose tiling but different for the Penrose tiling. The former is derived from 4D crystals as shown below and its internal space is 2D, which is equal to the minimal dimension given in the previous section. On the other hand, the Penrose tiling is obtained from 5D space (5D description) by the PM. Then the internal space is 3D but the minimal dimension is 2, which corresponds to a 4D description of the same structure (Janssen, 1986; Ishihara & Yamamoto, 1988).

The unit vectors of the n-gonal ($n = 8, 10, 12$) lattices are expressed in terms of their external and internal space components. In the following, c_j and s_j represent $\cos(2\pi j/n)$ and $\sin(2\pi j/n)$.

(*a*) *Octagonal Penrose tiling.* This is obtained from the 4D octagonal lattice, the unit vectors of which are reciprocal to (17) and given by

$$\mathbf{d}_{j+1} = a[c_j\mathbf{a}_1 + s_j\mathbf{a}_2] + a'[c_{3j}\mathbf{a}_3 + s_{3j}\mathbf{a}_4] \quad (0 \le j \le 3). \tag{30}$$

In the PM, a lattice point $\mathbf{n} = \sum_{i=1}^{4} n_i\mathbf{d}_i$ is plotted when the unit cell at $\mathbf{n}$ intersects the external space. Consider the 2D external space passing through the point $\mathbf{g} = \sum_{i=1}^{4} \gamma_i\mathbf{d}_i$. Then, the internal component of $\mathbf{n} - \mathbf{g}$, which is $\sum_{i=1}^{4} (n_i - \gamma_i)\mathbf{d}_i^i$, is in the polytope (polygon) that is the projection of the unit cell at $\mathbf{n}$ onto the internal space. Thus, we have to know the projection of the unit cell of the 4D octagonal lattice onto the 2D internal space. This can be done by projecting each corner of the unit cell onto the internal space and joining the outermost points. This is the regular octagon shown in Fig. 16(*a*). Thus, the window or the occupation domain of this case is the regular octagon. It is convenient to consider the body center of the unit

cell, which is located at $\mathbf{n}_c = \sum_{i=1}^{4}(n_i + 1/2)\mathbf{d}_i$. Then the same condition can be expressed as follows. When the internal component of $-\mathbf{n}_c + \mathbf{g}$ is in the octagon centered at the origin, $\mathbf{n}$ is projected onto the external space. The point appears at the external component of $\mathbf{n}$. In the SM, the point is regarded as the intersection of the occupation domain, which is located at each lattice point of the 4D lattice and extends to the internal space, with the external space as shown in Fig. 5(*c*).

(*b*) *Penrose tiling*. The difference between the PM and the SM becomes clear in this case. This is obtained from the 5D decagonal lattice in the former, which has unit vectors.

$$\mathbf{d}_j = (2a/5^{1/2})[c_j\mathbf{a}_1 + s_j\mathbf{a}_2] + (2a'/5^{1/2}) \times [c_{2j}\mathbf{a}_3 + s_{2j}\mathbf{a}_4] + a'\mathbf{a}_5 \qquad (1 \le j \le 5), \quad (31)$$

where $\mathbf{a}_1$ and $\mathbf{a}_2$ are the unit vectors of the external space and $\mathbf{a}_3$, $\mathbf{a}_4$ and $\mathbf{a}_5$ are those of the internal space. Let the 2D external space pass through the point $\mathbf{g} = \sum_{i=1}^{5}\gamma_i\mathbf{d}_i$ and the center of the unit cell be $\mathbf{n}_c = \sum_{i=1}^{5}(n_i + 1/2)\mathbf{d}_i$. The window is the rhombic icosahedron with the edge length of a' (Fig. 17). If the internal component of $-\mathbf{n}_c + \mathbf{g}$ is in the rhombic icosahedron centered at the origin, the lattice point $\mathbf{n} = \sum_{i=1}^{5} n_i\mathbf{d}_i$ is projected onto the external space.

In contrast to the PM, the SM uses the 4D decagonal lattice, since this is enough to index the diffraction patterns as shown in §4. The unit vectors are reciprocal to (18) and are given by (Janssen, 1986; Pavlovitch & Kléman, 1987; Yamamoto & Ishihara, 1988)

$$\mathbf{d}'_j = (2a/5^{1/2})[(c_j - 1)\mathbf{a}_1 + s_j\mathbf{a}_2] + (2a'/5^{1/2}) \times [(c_{2j} - 1)\mathbf{a}_3 + s_{2j}\mathbf{a}_4] \qquad (1 \le j \le 4). \quad (32)$$

The 4D space is a 4D hyperplane of the 5D space discussed above, which is normal to $\mathbf{a}_5$ and passes through the origin of the 5D space. The vectors $\mathbf{d}'_i = \mathbf{d}_i - \mathbf{d}_5$ $(1 \le i \le 4)$ span the 4D lattice since these have no $\mathbf{a}_5$ components. The vectors $\mathbf{d}'_5 = \sum_{i=1}^{5}\mathbf{d}_i$ and $\mathbf{d}'_i$ $(i \le 4)$ span the sublattice of the 5D decagonal lattice. The determinant of the transformation matrix T shown below is 5, so that there are five lattice points of the original lattice in the unit cell of the sublattice. The transformation matrix is given by

$$T = \begin{bmatrix} 1 & 0 & 0 & 0 & -1 \\ 0 & 1 & 0 & 0 & -1 \\ 0 & 0 & 1 & 0 & -1 \\ 0 & 0 & 0 & 1 & -1 \\ 1 & 1 & 1 & 1 & 1 \end{bmatrix}. \quad (33)$$

The windows located at these five points intersect with the 4D hyperplane at different positions. Their 4D coordinates with respect to $\mathbf{d}'_i$ $(i \le 4)$ are $(i, i, i, i)/5$ $(i = 0, 1, 2, 3, 4)$. The intersections of the windows at these points are the occupation domains. They are shown in Fig. 18 for the cases $\gamma = 0$ and 0.1. These are the occupation domains for the SM. Therefore, in the SM we use five occupation domains placed at $(i, i, i, i)/5$ $(i = 0, 1, 2, 3, 4)$, one of which reduces to a point for $\gamma = 0$. In this method, we consider five points in the unit cell at $\mathbf{n} = \sum_{j=1}^{4} n_j\mathbf{d}'_j$, that is $\mathbf{n} + \mathbf{x}_i$ $(i = 0, 1, \ldots, 4)$, where $\mathbf{x}_i = \sum_{j=1}^{4}(i/5)\,\mathbf{d}'_j$. If the internal component of $-\mathbf{n} - \mathbf{x}_i$ is in the ith occupation domain,

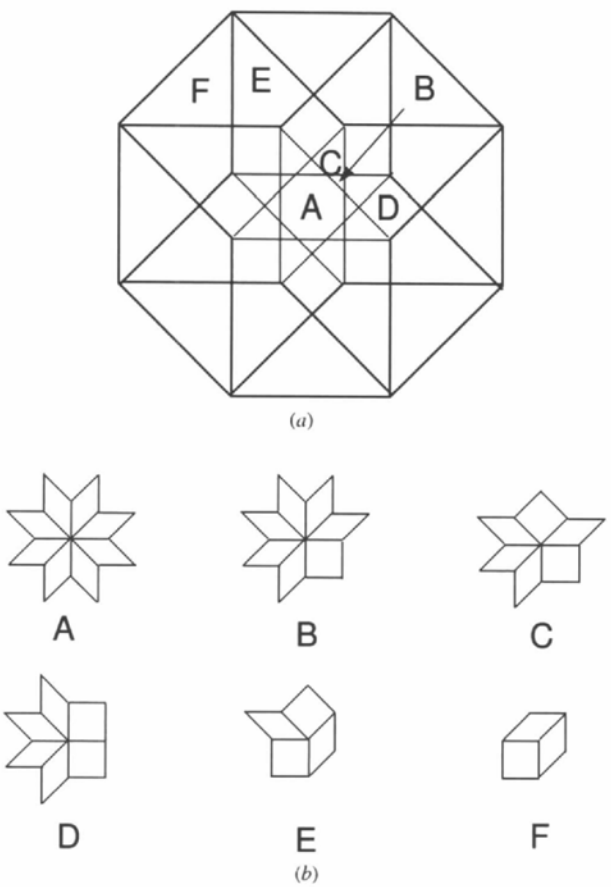

Fig. 16. (*a*) The occupation domain of the octagonal Penrose pattern. The points generated by the subdomains *A*–*F* have different local environments as shown in (*b*).

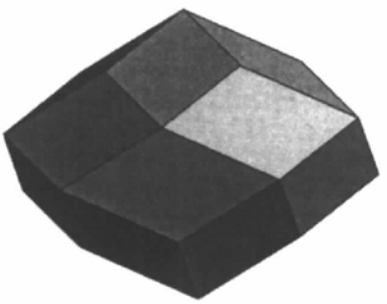

Fig. 17. The rhombic icosahedron appearing as the window of the Penrose pattern.

the occupation domain intersects the external space. Then, we plot its external component. In this case, the effect of γ mentioned above is reflected in the shape of the occupation domains.

(*c*) *Stampfli tiling*. This is obtained from the 4D dodecagonal lattice with the unit vectors

$$\begin{aligned}\mathbf{d}_{j+1} &= (2a/6^{1/2})[c_{(j-1)}\mathbf{a}_1 + s_{(j-1)}\mathbf{a}_2] + (2a'/6^{1/2}) \\ &\quad \times [c_{5(j-1)}\mathbf{a}_3 + s_{5(j-1)}\mathbf{a}_4] \qquad (j = 0, 1) \\ \mathbf{d}_{j+1} &= (2a/6^{1/2})[c_{(j+1)}\mathbf{a}_1 + s_{(j+1)}\mathbf{a}_2] + (2a'/6^{1/2}) \\ &\quad \times [c_{5(j+1)}\mathbf{a}_3 + s_{5(j+1)}\mathbf{a}_4] \qquad (j = 2, 3).\end{aligned} \tag{34}$$

As stated above, the occupation domain or window of this tiling does not come from the unit cell but from the union of the projection of Voronoi cells of the two hexagonal lattices. This is the dodecagonal star which is the union of two hexagons rotated by 30° around the common center (see Fig. 19). In this case, the space used is minimal, so that the difference between the PM and the SM is not essential. The methods used for the octagonal Penrose tiling are applicable.

(*d*) *Other polygonal tilings*. The pentagonal Penrose tiling is obtained from one decagonal occupation domain at the origin (Niizeki, 1991). The occupation domain is a decagon which is the projection of the Voronoi cell of the 4D decagonal lattice (Fig. 18*c*). Another decagonal tiling (binary tiling) is obtained from three occupation domains at $\pm(1, 1, 1, 1)/5$ and $(0, 0, 0, 0)$, where the pentagonal rhombic stars and a decagon are situated (Zobetz, 1992) (see Fig. 20). The dodecagonal Penrose tiling consists of three rhombi with equal edge length or a skinny rhombus, a triangle and a square (Ishihara, Nishitani & Shingu, 1987). This is obtained from the 6D dodecagonal lattice or from a direct extension of the 5D case given above (Socolar, 1989). Its occupation domains in 4D representations consist of four triangles and four squashed hexagons with threefold symmetry. They are at the special positions $(0, 1, 0, 2)/3$ and $(1, 1, 2, 2)/3$ with the site symmetry $3m$ and other equivalent positions.

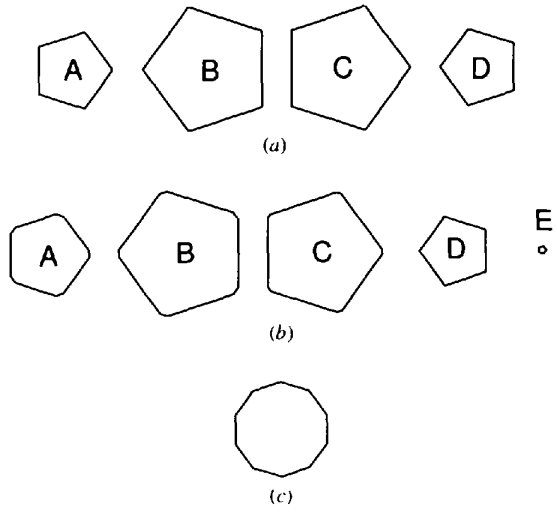

Fig. 18. The occupation domains of Penrose patterns. The rhombic and pentagonal Penrose patterns are obtained from occupation domains in (*a*) and (*c*), while the generalized Penrose pattern with $\gamma = 0.1$ is given by (*b*). The domains *A*–*E* are located at $(i, i, i, i)/5$ ($i = 1, 2, \ldots, 5$) of the 4D decagonal lattice.

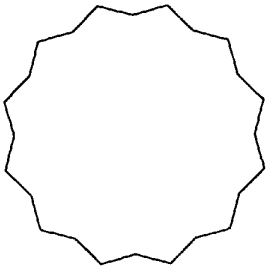

Fig. 19. The occupation domain of the Stampfli pattern. This is a union of two hexagons.

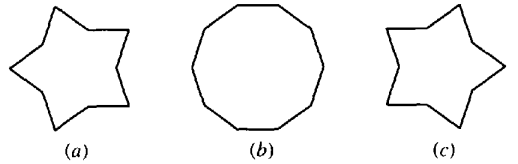

Fig. 20. The occupation domains of the binary tiling. The domains in (*a*), (*b*) and (*c*) are located at $-(1, 1, 1, 1)/5$, $(0, 0, 0, 0)$ and $(1, 1, 1, 1)/5$ in the 4D decagonal lattice.

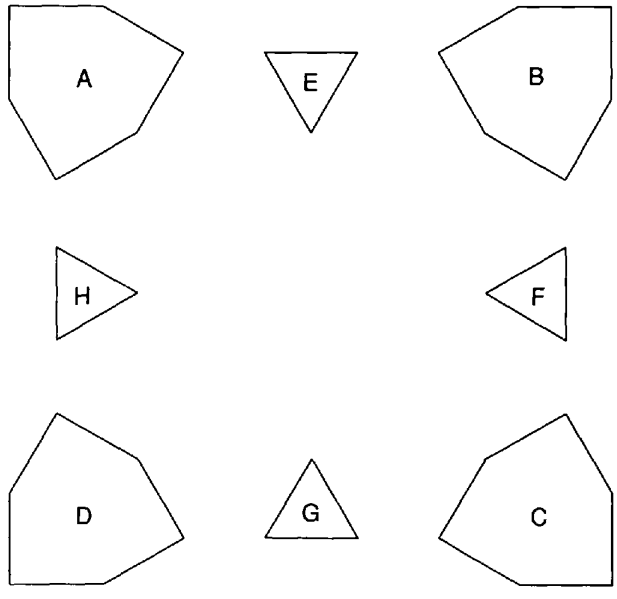

Fig. 21. The occupation domains of the dodecagonal Penrose pattern. The domains *A* and *E* are independent. The others are related to these by symmetry operations.

Four triangles or hexagons are related to the fourfold rotation (Fig. 21). Another extension to generalized 2D polygonal tilings has been made by Whittaker & Whittaker (1988) using the PM. They are tilings with n-fold ($n \geq 7$) symmetry and obtained from nD n-gonal lattices. Because of the equivalence of the PM and the DM, this is also obtained from the corresponding n-grid by the DM. In order to obtain such tilings, the DM seems to be easier than the SM. The occupation domains of typical tilings are given in Tables 13 and 14.

6. Icosahedral tiling

The 3D quasiperiodic tilings can be obtained by a method similar to that described above. This uses a grid that consists of equidistant 2D planes normal to several directions. In order to obtain the tiling with icosahedral symmetry (icosahedral tiling), we use six vectors $\mathbf{e}_i^*$ ($i \leq 6$) that point to six corners of the regular icosahedron (Figs. 11*a* and 12).

6.1. *The dual method*

The derivation of two typical icosahedral tilings by the DM is discussed in the following.

(*a*) *Three-dimensional Penrose tiling.* This is derived from the 3D 6-grid

$$\mathbf{e}_i^* \cdot \mathbf{x} = n_i + \gamma_i \quad (i \leq 6) \tag{35}$$

by a similar method. The vectors $\mathbf{e}_i^*$ are 3D and are given by $2\mathbf{d}_i^{*e}$ of (23). In this case, the grid is a set of equidistant 2D planes normal to $\mathbf{e}_i^*$ ($i \leq 6$). There are 3D areas (polyhedra) enclosed by planes. Let the vector $\mathbf{y}$ be in the polyhedron that is between n_ith and n_{i+1}th planes for the ith direction. Then we assign six integers $n_i = \lfloor \mathbf{e}_i^* \cdot \mathbf{y} - \gamma_i \rfloor$ ($i \leq 6$) to the area. We plot a point at $\mathbf{r}_0 = \sum_{i=1}^{6} n_i \mathbf{e}_i$ and join points with the distance $a = |\mathbf{e}_i|$, where $\mathbf{e}_i = \mathbf{d}_i^e$, which are the external part of the unit vectors of the 6D icosahedral lattice [see (37)]. In the second algorithm, we assign $n_i = \lfloor \mathbf{e}_i^* \cdot \mathbf{y}' - \gamma_i \rfloor$ ($i \leq 6$) to the cross points $\mathbf{y}'$ of three grid planes normal to $\mathbf{e}_i^*$, $\mathbf{e}_j^*$, $\mathbf{e}_k^*$ ($i \neq j \neq k$) and draw a rhombohedron spanned by $\mathbf{e}_i$, $\mathbf{e}_j$ and $\mathbf{e}_k$ at $\mathbf{r}_0$. This tiling consists of rhombohedra spanned by $\mathbf{e}_i$, $\mathbf{e}_j$, $\mathbf{e}_k$ ($i \neq j \neq k$), which are classified into two shapes shown in Figs. 23(*a*) and (*b*). It is known that more than three grid planes intersect at a point. Such a point is called a singular (grid) point. If we choose $\gamma_i = 0$ for all i, the grid includes singular points at the origin and along a fivefold axis, where six and five planes intersect. Since they appear only on these lines, we can shift these points to other places by selecting nonzero γ_i. Any γ_i leads to tilings locally isomorphic to each other. The projections of the tilings along the fivefold and twofold axes are shown in Fig. 22. Note that Fig. 22(*a*) is the pentagonal Penrose tiling. As shown by Kramer & Neri (1984), this is a special case among tilings obtained from the 12-grid or double 6-grid. It is known that this has the similarity ratio of $2 + 5^{1/2}$ (Ogawa, 1985), which is equal to that of the 6D primitive icosahedral lattice.

(*b*) *Socolar tiling.* Another important 3D icosahedral tiling has been derived by the GDM (Socolar, Steinhardt & Levine, 1985), where a quasiperiodic grid is used instead of the periodic grid described above. This was shown to have the similarity ratio of $\tau = (1 + 5^{1/2})/2$, which suggests that the tiling is related to the face-centered or body-centered icosahedral lattice. It was shown recently that this is the face-centered icosahedral lattice (Danzer, 1989; Danzer & Talis, 1993; Kramer, Papadopolos, Schlottmann & Zeidler, 1994). The generalized icosahedral tilings are obtained by

$$\mathbf{e}_i^* \cdot \mathbf{x} = n_i + \alpha + \tau^{-1} \lfloor n_i \tau^{-1} + \beta \rfloor \quad (i \leq 6) \tag{36}$$

and the dual transformation given in (*a*). When $\alpha = \tau^{-1}$, $\beta = -1/2$, the tiling has a similarity ratio of τ and

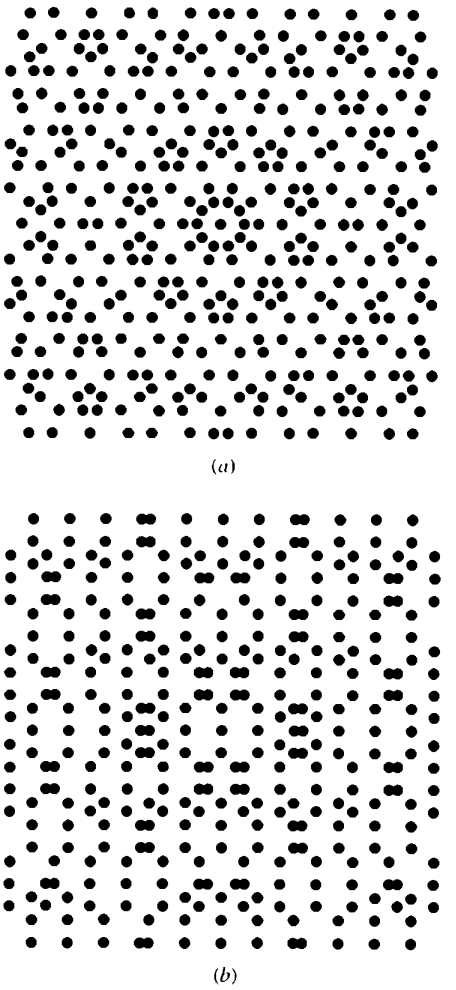

Fig. 22. The projections of the 3D Penrose pattern along (*a*) fivefold and (*b*) twofold axes. The former is the pentagonal Penrose pattern.

is called the Socolar tiling. In this case, there are many singular grid points distributed in 3D space in contrast to 3D Penrose tiling. The singular points are classified into three cases, sixfold, fivefold and fourfold singular points, where six, five and four grid planes may intersect. In this case, the second algorithm of the dual transformation has to be modified. If the point is the sixfold, the fivefold or the fourfold singular point, we have to place a rhombic triacontahedron, rhombic icosahedron or rhombic dodecahedron instead of a rhombohedron (Fig. 23). It is known that only the acute rhombohedron (Fig. 23*a*) is obtained from the non-singular point. Thus the Socolar tiling consists of these four primitive tiles.

Since the corresponding SM had not been known for the GDM, its diffraction pattern could not be calculated, but this problem was solved recently as shown later.

6.2. *The projection and section methods*

The same tilings are obtained by the projection method or the section method.

(*a*) *Three-dimensional Penrose tiling*. This is obtained by the PM or the SM from 6D space because the minimal dimension of icosahedral quasiperiodic tilings is 6 (Duneau & Katz, 1985; Katz & Duneau, 1986). The window or the occupation domain is obtained from the projection of the unit cell in the 6D icosahedral lattice onto the 3D internal space. The unit vectors in the direct space are

$$\begin{aligned}\mathbf{d}_1 &= a\mathbf{a}_3 + a'\mathbf{a}_6,\\ \mathbf{d}_i &= a[(c_i\mathbf{a}_1 + s_i\mathbf{a}_2)s + c\mathbf{a}_3]\\ &\quad + a'[(c_{2i}\mathbf{a}_4 + s_{2i}\mathbf{a}_5)s - c\mathbf{a}_6] \quad (i = 2, 3, \ldots, 6).\end{aligned} \tag{37}$$

The occupation domain is the triacontahedron with the edge length a' (Fig. 23*c*) and each edge is parallel to one of $\mathbf{d}_i^i$ ($i \leq 6$). The 3D Penrose tiling consists of two rhombohedra with the edge length a. An acute rhombohedron has edges parallel to $\mathbf{d}_1$, $\mathbf{d}_2$ and $\mathbf{d}_3$ (Fig. 23*a*) while an obtuse one has edges parallel to $\mathbf{d}_4$, $-\mathbf{d}_5$ and $\mathbf{d}_6$ (Fig. 23*b*). A part of the 3D Penrose tiling can be constructed from four primitive polyhedra, the dodecahedral star, rhombic triacontahedron, rhombic icosahedron and obtuse rhombohedron (Ogawa, 1985; Audier & Guyot, 1988) (see Fig. 23). We call this a framework structure. This is obtained from a complicated occupation domain (Yamamoto, Sato, Kato, Tsai & Masumoto, 1994).

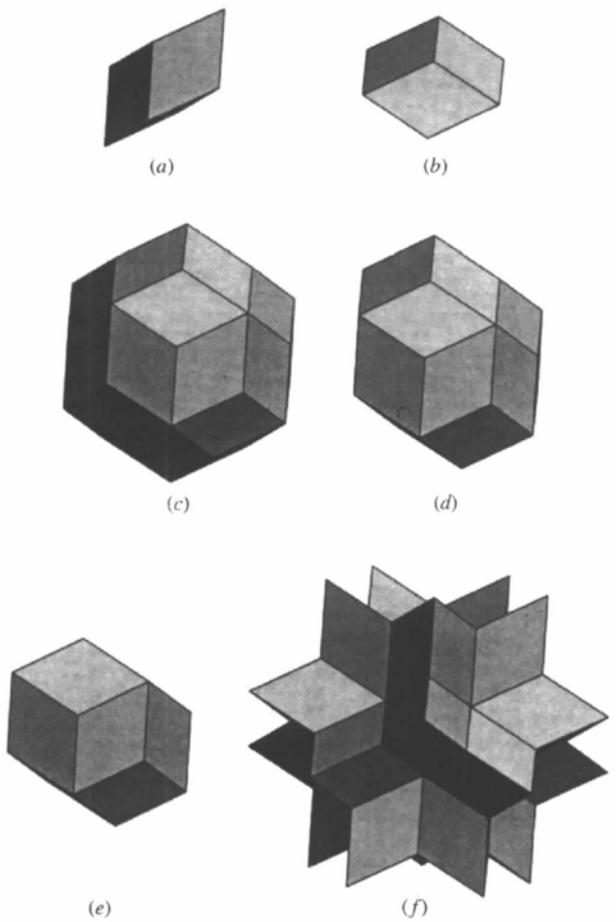

Fig. 23. The occupation domains appearing in icosahedral quasicrystals. (*a*) Acute rhombohedron. (*b*) Obtuse rhombohedron. (*c*) Rhombic triacontahedron. (*d*) Rhombic icosahedron. (*e*) Rhombic dodecahedron. (*f*) Dodecahedral star.

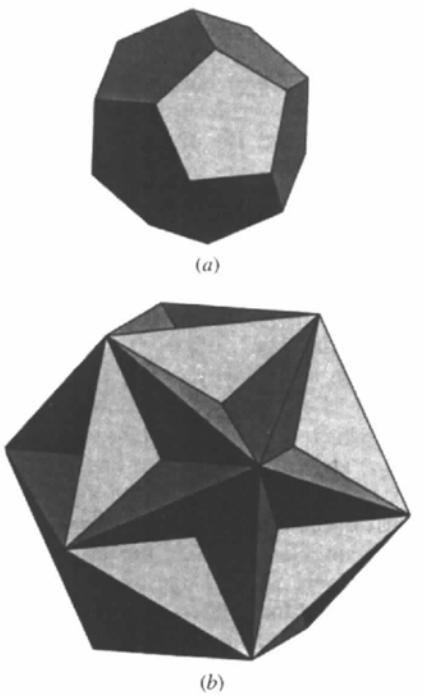

Fig. 24. Two independent occupation domains of the Socolar tiling. (*a*) and (*b*) are located at (1, 1, 1, 1, 1, 1)/4 and (3, 1, 1, 1, 1, 1)/4 and the positions equivalent to them by the centering translations of the face-centered icosahedral lattice in 6D space.

(*b*) *Socolar tiling*. This tiling consists of four primitive polyhedra as mentioned in §6.1. The Socolar tiling can be divided into acute and obtuse rhombohedra, since the primitive polyhedra can be divided into them. However, any division cannot have the symmetry of the primitive polyhedra. In order to divide them into several pieces holding such a symmetry, we have to use octahedra (or tetrahedra) instead of rhombohedra. The 3D tiling (Danzer tiling) with icosahedral symmetry was proposed by Danzer (1989), which consists of four octahedra (or tetrahedra). It was shown recently that part of the Danzer tiling gives the Socolar tiling (Roth, 1993; Danzer & Talis, 1993). Its occupation domains are given by Kramer, Papadopolos, Schlottmann & Zeidler, 1994). The tiling has the face-centered icosahedral lattice, which is spanned by $\mathbf{d}'_i = \sum_{j=1}^{6} S_{ij}\mathbf{d}_j$ with

$$S = \begin{bmatrix} 0 & 2 & 0 & 0 & 0 & 0 \\ 0 & 0 & 2 & 0 & 0 & 0 \\ 2 & 0 & 0 & 0 & 0 & 0 \\ 1 & -1 & 1 & -1 & -1 & 1 \\ 1 & 1 & -1 & 1 & -1 & -1 \\ -1 & 1 & 1 & 1 & 1 & 1 \end{bmatrix}. \qquad (38)$$

The determinant of S is 32. The lattice is equivalent to a sublattice of the primitive icosahedral lattice consisting of lattice points with even (or odd) parity. In the following, the vector is represented with respect to $\mathbf{d}_i$. There are two occupation domains placed at $(1, 1, 1, 1, 1, 1)/2$ and $(3, 1, 1, 1, 1, 1)/2$. These are neither the projection of the unit cell nor that of the Voronoi cell but are related to the Delaunay cell (Kramer, Papadopolos, Schlottmann & Zeidler, 1994). The first one is a regular dodecahedron with a corner vector $(-1, 1, -1, -1, 1, 1)/2$ and 19 other corners obtained from it by the symmetry operation of the icosahedral group. The second one is obtained from the regular icosahedron with a corner vector $(1, 1, 1, 1, 1, 1)/2$ and another 11 corners equivalent to it by subtracting a tetrahedron sharing a triangle (Fig. 24). A radius on the threefold axis is $-(1, 1, 1, 1, -1, 1)/2$ (Table 14).

(*c*) *Generalized icosahedral tilings*. As seen in §5, there is an infinite number of generalized tilings obtained from nD ($n = 8, 10, 12$) spaces. The corresponding tilings with icosahedral symmetry are also possible. These consist of two rhombohedra as in the 3D Penrose tiling. In contrast to it, however, there exist two tiles of the same shape having face-to-face contact with each other. They are obtained from 12D space by the DM or the SM (Yamamoto, 1995).

7. Symmetry of quasicrystals

According to the nD crystallography introduced by de Wolff (1974) and formulated by Janner & Janssen (1977, 1979), the symmetry reflected in diffraction patterns is that of the nD crystals. If the crystal has a (hyper-) glide plane or a (hyper-) screw axis, it causes a systematic extinction of reflections. This is observed in several decagonal quasicrystals and is related to the non-primitive translation in a symmetry operator of nD space, which leaves the nD crystal unchanged. The rotational symmetry is obtained from the point group of the diffraction pattern, while the non-primitive translation is obtained from the extinction rules. In this section, we discuss how this is taken into account in the model construction for polygonal quasicrystals.

Real polygonal quasicrystals have a period parallel to the n-fold ($n = 8, 10, 12$) axis. Therefore, we have to add one dimension for this direction and consider 5D crystals. Let the unit vectors of this 5D lattice be $\mathbf{d}_i$ ($i \leq 5$), the first four of which are given by (30), (32) or (34) and $\mathbf{d}_5 = c\mathbf{a}_5$. Their reciprocal vectors $\mathbf{d}_i^*$ are given by (17), (18) or (19) and $\mathbf{d}_5^* = c^*\mathbf{a}_5$ ($c^* = 1/c$). In §5, the 2D tilings were considered. A real quasicrystal structure may not be the repeated stacking of such tilings. The first point to be considered is the systematic absence of reflections if any. Such an absence of reflections in a plane including the n-fold axis was first observed in the electron diffraction patterns of decagonal Al–Mn and Al–Fe (*d*-Al–Mn, *d*-Al–Fe) (Fung, Yang, Zhou, Zhan & Shen, 1986; Yamamoto & Ishihara, 1988). We consider the diffraction patterns of *d*-Al–Pd–Mn in Fig. 25. (*d*-Al–Mn also shows similar patterns.) It is seen in Fig. 25(*b*) that reflections with h_5 odd are absent. The reflection condition can be written as $h_5 = 2n$ for $h_1, h_2, \bar{h}_2, \bar{h}_1, h_5$. This means that there exists a (hyper-) glide plane $\{\sigma'|\mathbf{t}\}$, the rotation matrix of which is given by

$$R(\sigma') = \begin{bmatrix} 0 & 0 & 0 & -1 & 0 \\ 0 & 0 & -1 & 0 & 0 \\ 0 & -1 & 0 & 0 & 0 \\ -1 & 0 & 0 & 0 & 0 \\ 0 & 0 & 0 & 0 & 1 \end{bmatrix} \quad \text{(decagonal)} \qquad (39)$$

and the non-primitive translation $\mathbf{t}(\sigma') = \mathbf{d}_5/2 = c\mathbf{a}_5/2$. This suggests that there exist two groups of occupation domains that are related by the glide plane. Note that the coordinates are transformed by the rotation with the same matrix $R(\sigma')$. Therefore, if an occupation domain is at $(x_1, x_2, x_3, x_4, x_5)$, another one must be at $(-x_4, -x_3, -x_2, -x_1, x_5 + 1/2)$. The latter occupation domain is obtained from the former by σ'. In order to consider this transformation, the action of the rotation operator in the internal space has to be known because the occupation domain extends only in the internal space. This is given by the reduced matrix R, which is given by $M'^{-1}RM'$. The matrix M' is a 5×5 matrix,

$$M' = \begin{bmatrix} M & 0 \\ 0 & 1 \end{bmatrix}, \qquad (40)$$

where M is the 4×4 matrix given in §4. The reduced matrix is a $2+2+1$ block-diagonal matrix and the second 2×2 matrix transforms the occupation domain. As shown in §§5 and 6, the occupation domains of typical tilings are polygons, most of which are convex but is a polygon with concave parts for the Stampfli tiling. Let a corner be $a_3\mathbf{a}_3 + a_4\mathbf{a}_4$. Then this is transformed into $a'_3\mathbf{a}_3 + a'_4\mathbf{a}_4$, where $a'_j = \sum_{k=3}^{4}(M^{-1}RM)_{jk}a_k$ $(j = 3, 4)$. The second 2×2 part of $M^{-1}R(\sigma')M$ is given by

$$\begin{bmatrix} -1 & 0 \\ 0 & 1 \end{bmatrix}, \tag{41}$$

which transforms a_3 into $-a_3$ and a_4 into itself. Note that σ' transforms the occupation domain A of the Penrose tiling into D and B into C in Fig. 18(a). Thus, in order to obtain the extinction rule mentioned above, if A (B) is at $(x_1, x_2, x_3, x_4, x_5)$, D (C) must be at $(-x_4, -x_3, -x_2, -x_1, x_5+1/2)$ (Yamamoto & Ishihara, 1988).

As a group including the glide plane, we consider the 5D space group $P10_5/mmc$, which is generated by a tenfold screw axis, the glide plane and the inversion. The rotation matrix of the tenfold rotation is given by

$$R(C_{10}) = \begin{bmatrix} 0 & 0 & 0 & -1 & 0 \\ 1 & 1 & 1 & 1 & 0 \\ -1 & 0 & 0 & 0 & 0 \\ 0 & -1 & 0 & 0 & 0 \\ 0 & 0 & 0 & 0 & 1 \end{bmatrix}. \tag{42}$$

The matrix representation of the inversion is $R(I)_{ij} = -\delta_{ij}$ $(i \leq 5)$ and that of σ' is in (39). The non-primitive translation of C_{10} is $\mathbf{t}(C_{10}) = \mathbf{d}_5/2$. The space group $P10_5/mmc$ is generated by $\{C_{10}|\mathbf{t}(C_{10})\}$, $\{\sigma'|\mathbf{t}(\sigma')\}$, $\{I|0\}$ and lattice translation $\{E|\mathbf{d}_i\}$ $(i = 1, 2, 3, 4)$. In particular, the tenfold screw axis and the inversion cause the mirror plane perpendicular to $\mathbf{a}_5$ at $z = 1/4$.

In many cases, the occupation domains are located at the special position of the space group. They are invariant under the site-symmetry group, which is a subgroup of the point group. The site symmetry restricts the shape of the occupation domain, since the shape has to be invariant under the site-symmetry group. Consider the A, B, C, D domains of the Penrose tiling in Fig. 18(a), which are located at $(i, i, i, i, 5z)/5$ $(i \leq 4)$, the site symmetries of which are D_5. The site-symmetry groups are generated by $\{C_5|i\mathbf{d}_4\}$ $(1 \leq i \leq 5)$ and $\{\sigma|0\}$, where the rotation matrix of σ is

$$R(\sigma) = \begin{bmatrix} 0 & 0 & 0 & 1 & 0 \\ 0 & 0 & 1 & 0 & 0 \\ 0 & 1 & 0 & 0 & 0 \\ 1 & 0 & 0 & 0 & 0 \\ 0 & 0 & 0 & 0 & 1 \end{bmatrix} \quad \text{(decagonal)}. \tag{43}$$

The point group can be divided into cosets by using the site-symmetry group and the coset representa-

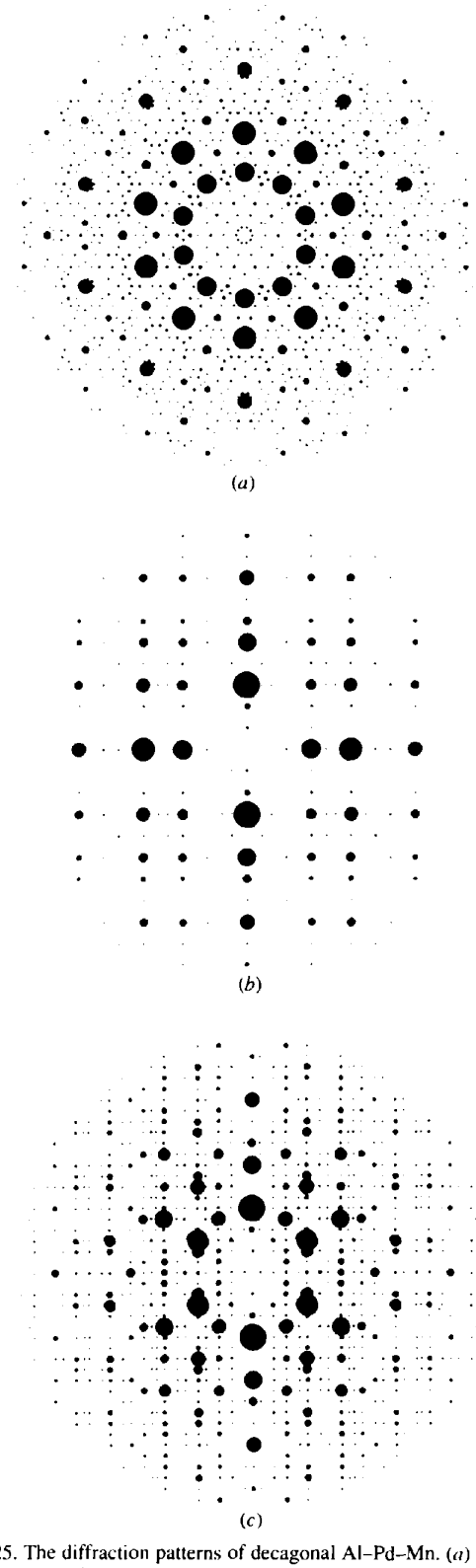

Fig. 25. The diffraction patterns of decagonal Al–Pd–Mn. (a) The zero layer normal to the tenfold axis. The planes (b) between the axes and (c) along the axes are denoted by dotted and solid lines in Fig. 26(b). The tenfold axis is vertical in (b) and (c).

Table 8. *Octagonal space groups in 5D space with highest symmetries*

There exist the primitive (denoted by P in the prefix) and body-centered (I) lattices. The latter gives the reflection condition for general reflections, $\sum_{i=1}^{5} h_i = 2n$ for $h_1h_2h_3h_4h_5$. The order of the point group $8/mmm$ is 32.

Space group	Special reflection condition
$P8/mmm$	No condition
$P8/mbm$	$h_2 = 2n$ for $h_1h_2h_10h_5$
$P8/mcc$	$h_5 = 2n$ for $h_1h_2h_10h_5$
	$h_5 = 2n$ for $h_1h_2h_2h_1h_5$
$P8/mnc$	$h_2 + h_5 = 2n$ for $h_1h_2h_10h_5$
	$h_5 = 2n$ for $h_1h_2h_2h_1h_5$
$P8/nmm$	$\sum_{i=1}^{4} h_i = 2n$ for $h_1h_2h_3h_40$
$P8/nbm$	$h_2 = 2n$ for $h_1h_2h_10h_5$
	$\sum_{i=1}^{4} h_i = 2n$ for $h_1h_2h_3h_40$
$P8/ncc$	$h_5 = 2n$ for $h_1h_2h_10h_5$
	$h_5 = 2n$ for $h_1h_2h_2h_1h_5$
	$\sum_{i=1}^{4} h_i = 2n$ for $h_1h_2h_3h_40$
$P8/nnc$	$h_2 + h_5 = 2n$ for $h_1h_2h_10h_5$
	$h_5 = 2n$ for $h_1h_2h_2h_1h_5$
	$\sum_{i=1}^{4} h_i = 2n$ for $h_1h_2h_3h_40$
$P8_4/mmc$	$h_5 = 2n$ for $h_1h_2h_2h_1h_5$
$P8_4/mbc$	$h_5 = 2n$ for $h_1h_2h_2h_1h_5$
	$h_2 = 2n$ for $h_1h_2h_10h_5$
$P8_4/mcm$	$h_5 = 2n$ for $h_1h_2h_10h_5$
$P8_4/mnm$	$h_2 + h_5 = 2n$ for $h_1h_2h_10h_5$
$P8_4/nmc$	$h_5 = 2n$ for $h_1h_2h_2h_1h_5$
	$\sum_{i=1}^{4} h_i = 2n$ for $h_1h_2h_3h_40$
$P8_4/nbc$	$h_5 = 2n$ for $h_1h_2h_2h_1h_5$
	$h_2 = 2n$ for $h_1h_2h_10h_5$
	$\sum_{i=1}^{4} h_i = 2n$ for $h_1h_2h_3h_40$
$P8_4/ncm$	$h_5 = 2n$ for $h_1h_2h_10h_5$
	$\sum_{i=1}^{4} h_i = 2n$ for $h_1h_2h_3h_40$
$P8_4/nnm$	$h_2 + h_5 = 2n$ for $h_1h_2h_10h_5$
	$\sum_{i=1}^{4} h_i = 2n$ for $h_1h_2h_3h_40$
$I8/mmm$	No condition
$I8/mmc$	$h_5 = 2n$ for $h_1h_2h_2h_1h_5$
$I8_2/ndm$	$2h_2 + h_5 = 4n$ for $h_1h_2h_10h_5$
	$\sum_{i=1}^{4} h_i = 2n$ for $h_1h_2h_3h_40$
$I8_2/ndc$	$2h_2 + h_5 = 4n$ for $h_1h_2h_10h_5$
	$h_5 = 2n$ for $h_1h_2h_2h_1h_5$
	$\sum_{i=1}^{4} h_i = 2n$ for $h_1h_2h_3h_40$

tives give equivalent positions. In the present case, $D_{10h} = D_5 + C_{2z}D_5 + \sigma_z D_5 + ID_5$. Therefore, $\{E|0\}$, $\{C_{2z}|\mathbf{d}_5/2\}$, $\{\sigma_z|\mathbf{d}_5/2\}$ and $\{I|0\}$ lead to the equivalent positions $(i,i,i,i,5z)/5$, $-(i,i,i,i,5(1/2 - z))/5$, $(i,i,i,i,5(1/2 - z))/5$ and $-(i,i,i,i,5z)/5$.

8. Space groups of quasicrystals

The space groups for polygonal and icosahedral quasicrystals have been given (Gähler & Rhyner, 1986; Gähler, 1990; Janssen, 1986; Rokhsar, Wright & Mermin, 1988; Levitov & Rhyner, 1988; Rabson, Mermin, Rokhsar & Wright, 1991). There are 90 octagonal, 34 decagonal, 33 dodecagonal and 11 icosahedral non-equivalent space groups. The equivalence relation is the same as the direct extension of the equivalence relation in 3D space into nD space.* Space groups with highest symmetries and their reflection conditions are shown in Tables 8, 9 and 10. The primitive and body-centered lattices are present in 5D octagonal lattices, while only the primitive lattice exists for 5D decagonal and dodecagonal lattices. The body-centered lattice has an additional lattice point at $\sum_{i=1}^{5} \mathbf{d}_i/2$ in a unit cell. The 6D icosahedral lattices have three lattice types: primitive, face-centered and body-centered lattices. There exist 32 centering translations in the face-centered lattice, which are $(0,0,0,0,0,0)$, $(1,1,0,0,0,0)/2$, $(1,0,1,0,0,0)/2$ *etc.*, while those of the body-centered lattice are $(0,0,0,0,0,0)$ and $(1,1,1,1,1,1)/2$ with respect to the unit vectors given in (37).

Table 9. *Decagonal space groups in 5D space with highest symmetries*

There exists only the primitive lattice in this case. The order of the point group $10/mmm$ is 40.

Space group	Special reflection condition
$P10/mmm$	No condition
$P10/mcc$	$h_5 = 2n$ for $h_1h_2h_2h_1h_5$
	$h_5 = 2n$ for $h_1h_2\bar{h}_2\bar{h}_1h_5$
$P10_5/mmc$	$h_5 = 2n$ for $h_1h_2h_2\bar{h}_1h_5$
$P10_5/mcm$	$h_5 = 2n$ for $h_1h_2h_2h_1h_5$

Table 10. *Dodecagonal space groups in 5D space with highest symmetries*

Note that $P12_6/mmc$, which has the reflection condition $h_5 = 2n$ for $h_1h_2h_2h_1h_5$, is equivalent to $P12_6/mcm$ because of the normalizer as given in the text. The order of the point group $12/mmm$ is 48.

Space group	Special reflection condition
$P12/mmm$	No condition
$P12_6/mcm$	$h_5 = 2n$ for $h_1h_2h_10h_5$
$P12/mcc$	$h_5 = 2n$ for $h_1h_2h_10h_5$
	$h_5 = 2n$ for $h_1h_2h_2h_1h_5$

An important point related to the equivalence, which is specific to space groups of quasicrystals, is the similarity transformation discussed in §4. This gives a different setting of the unit vectors. The space groups transformed to each other by the change of the unit vectors are equivalent. International symbols of the space groups (Hermann–Mauguin symbols) in Tables 8 to 11 consist of symbols of the lattice type (primitive, body-centered *etc.*) and the generators of space groups that give the essential extinction rules. The lattice type can be determined easily by the extinction rules for general reflections. In order to find a space group, we have to know the point group first, which is given by the rotational symmetry of diffraction patterns. The

* Note that the equivalence relation used in space groups of modulated structures is different from it and the space groups classified by the former are called superspace groups. It gives a finer classification than that used in the classification of space groups of quasicrystals.

non-primitive translations can be determined from the extinction rules. Therefore, it is convenient to consider the extinction rules derived from the screw axes or glide planes corresponding to the generators in the symbol of the space group. In the dihedral groups with the highest symmetry, they are the n-fold axis (n = 8, 10 or 12), the mirror plane perpendicular to it and two mirror planes including the axis and two other axes (denoted as '*along*' and '*between*' in Fig. 26). The rotational parts of the latter two are denoted as σ and σ'. Their matrix representations in the decagonal lattice are given by (39) and (43). That of σ' is common for the octagonal and dodecagonal lattices and given by

$$R(\sigma') = \begin{bmatrix} 0 & 0 & 0 & 1 & 0 \\ 0 & 0 & 1 & 0 & 0 \\ 0 & 1 & 0 & 0 & 0 \\ 1 & 0 & 0 & 0 & 0 \\ 0 & 0 & 0 & 0 & 1 \end{bmatrix} \quad \text{(octagonal, dodecagonal)} \tag{44}$$

while the matrix of σ is different. The matrix representations of σ for the octagonal and dodecagonal cases are

$$R(\sigma) = \begin{bmatrix} 0 & 0 & 1 & 0 & 0 \\ 0 & 1 & 0 & 0 & 0 \\ 1 & 0 & 0 & 0 & 0 \\ 0 & 0 & 0 & -1 & 0 \\ 0 & 0 & 0 & 0 & 1 \end{bmatrix} \quad \text{(octagonal)} \tag{45}$$

$$R(\sigma) = \begin{bmatrix} 0 & 0 & 1 & 0 & 0 \\ 0 & 1 & 0 & 0 & 0 \\ 1 & 0 & 0 & 0 & 0 \\ 0 & 1 & 0 & -1 & 0 \\ 0 & 0 & 0 & 0 & 1 \end{bmatrix} \quad \text{(dodecagonal)}. \tag{46}$$

There are no tables of the symmetry operators for quasicrystals but they can be calculated from the symbol of the space group as shown below. The generators of these space groups are given by $\{C_n|\mathbf{t}(C_n)\}$ (n = 8, 10, 12), $\{\sigma|\mathbf{t}(\sigma)\}$, $\{I|0\}$ and lattice translation $\{E|\mathbf{d}_i\}$ ($i \leq 5$) for polygonal quasicrystals and $\{C_5|\mathbf{t}(C_5)\}$, $\{C_3|\mathbf{t}(C_3)\}$, $\{I|0\}$ and lattice translation $\{E|\mathbf{d}_i\}$ ($i \leq 6$) for icosahedral ones. $R(C_8)$ and $R(C_{12})$ are (4 + 1) block-diagonal matrices with (11) and (14) for the first 4 × 4 part and 1 for the second, while $R(C_5)$ and $R(C_3)$ for the icosahedral case are in (24) and (25). The corresponding non-primitive translation can be obtained from the reflection conditions (extinction rules) in Tables 8–11. This is zero for all generators in symmorphic space groups like $P8/mmm$, $P10/mmm$ and $Pm\bar{3}\bar{5}$.

An example of the calculation of non-primitive translations is shown for the octagonal case. In order to obtain them for non-symmorphic space groups, it should be noted that σ' is given by $C_8\sigma$ and the last two letters in a space-group symbol represent $\{\sigma|\mathbf{t}(\sigma)\}$ and $\{\sigma'|\mathbf{t}(\sigma')\}$. From $\{C_8|\mathbf{t}(C_8)\}\{\sigma|\mathbf{t}(\sigma)\} = \{C_8\sigma|C_8\mathbf{t}(\sigma) + \mathbf{t}(C_8)\}$, $\mathbf{t}(\sigma')$ should be $C_8\mathbf{t}(\sigma)+\mathbf{t}(C_8)$. The non-primitive translations can be divided into two parts. One is intrinsic, which is independent of the choice of the origin, and the other is non-intrinsic. The first part is responsible

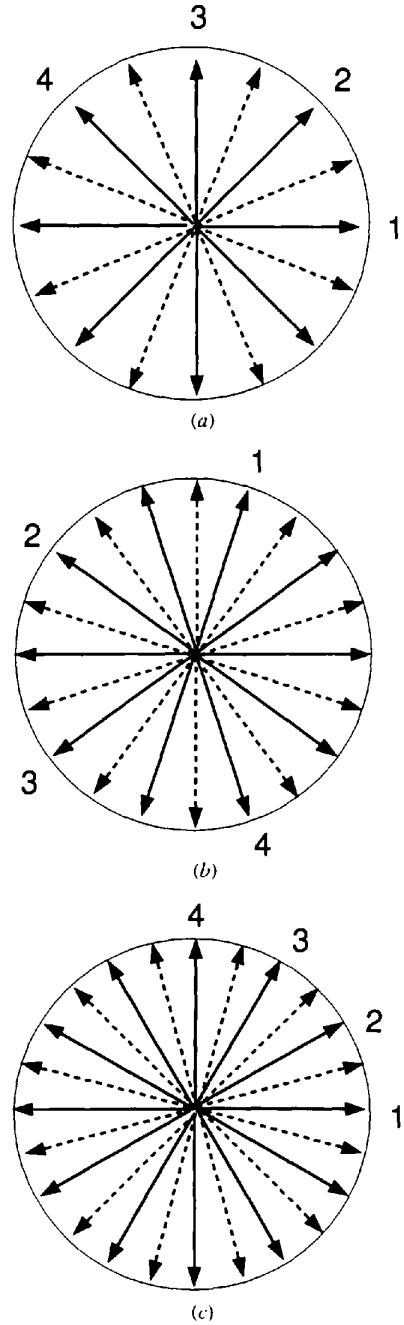

Fig. 26. The location of glide planes of (*a*) octagonal, (*b*) decagonal and (*c*) dodecagonal lattices. The solid lines are *along* the unit vectors, while the dotted lines are *between* the vectors. The numbers stand for the independent vectors.

Table 11. *Icosahedral space groups in 6D space*

The primitive, body-centered and face-centered lattices are denoted by P, I and F in the prefix. The body-centered lattice gives the reflection condition $\sum_{i=1}^{6} h_i = 2n$ for $h_1h_2h_3h_4h_5h_6$ while for the face-centered lattice h_i $(1 \leq i \leq 6)$ are all even or all odd for $h_1h_2h_3h_4h_5h_6$. The space groups $P235_m$, $I235_m$, $F235_m$ $(m = 2, 3, 4)$ are equivalent to $P235_1$, $I235_1$, $F235_1$ because of the presence of the normalizer given in the text. The orders of the point groups 235 and $m\bar{3}\bar{5}$ are 60 and 120.

Space group	Special reflection condition
$P235$	No condition
$P235_1$	$h_1 = 5n$ for $h_1h_2h_2h_2h_2h_2$
$I235$	No condition
$I235_1$	$h_1 + 5h_2 = 10n$ for $h_1h_2h_2h_2h_2h_2$
$F235$	No condition
$F235_1$	$h_1 + 5h_2 = 10n$ for $h_1h_2h_2h_2h_2h_2$
$Pm\bar{3}\bar{5}$	No condition
$Pn\bar{3}\bar{5}$	$h_5 - h_6 = 2n$ for $h_1h_2\bar{h}_1\bar{h}_2h_5h_6$
$Im\bar{3}\bar{5}$	No condition
$Fm\bar{3}\bar{5}$	No condition
$Fn\bar{3}\bar{5}$	$h_5 - h_6 = 4n$ for $h_1h_2\bar{h}_1\bar{h}_2h_5h_6$

Table 12. *Non-primitive translations for the generators of icosahedral space groups*

Space group	$\mathbf{t}(C_5)$	$\mathbf{t}(C_3)$
$P235_1$	$[\mathbf{d}_1 - \mathbf{d}_3 + \mathbf{d}_5]/5$	0
$I235_1$	$[\mathbf{d}_1 - \mathbf{d}_3 + 6\mathbf{d}_5]/10$	0
$F235_1$	$[\mathbf{d}_1 - \mathbf{d}_3 + 6\mathbf{d}_5]/10$	0
$Pn\bar{3}\bar{5}$	$[\mathbf{d}_5 + \mathbf{d}_6]/2$	0
$Fn\bar{3}\bar{5}$	$[\mathbf{d}_5 - \mathbf{d}_6]/4$	0

for the extinction rules and is known from the symbol. In the following, the origin is assumed to be at the inversion center. The non-intrinsic part of the non-primitive translation $\mathbf{t}(C_8)$ can be determined from the mirror plane or the glide plane that is normal to the n-fold axis. The rotational part is represented by σ_z in the following. Since $(C_8)^4$ is the twofold rotation C_2, $\sigma_z = I(C_8)^4$. Therefore,

$$\mathbf{t}(\sigma_z) = -\sum_{i=0}^{3} (C_8)^i \mathbf{t}(C_8). \tag{47}$$

This fixes the non-intrinsic part of $\mathbf{t}(C_8)$. For example, consider $P8_4/nbc$. Then, the extinction rules for $h_1h_2h_3h_40$ imply that the intrinsic part of $\mathbf{t}(\sigma_z)$ is $\sum_{i=1}^{4} \mathbf{d}_i/2$. This is consistent with $\mathbf{t}(C_8) = (\mathbf{d}_1 + \mathbf{d}_5)/2$ and $\mathbf{t}(C_2) = \sum_{i=1}^{4} \mathbf{d}_i/2$ shows that the non-intrinsic part of $\mathbf{t}(\sigma_z)$ is zero. On the other hand, the intrinsic part of $\mathbf{t}(\sigma)$ is $\mathbf{d}_2/2$. This leads to $\mathbf{t}(\sigma') = (\mathbf{d}_1 + \mathbf{d}_4, + \mathbf{d}_5)/2$, which means the c-glide plane. Thus, $P8_4/nbc$ is generated by $\{C_8|[\mathbf{d}_1 + \mathbf{d}_5]/2\}$, $\{\sigma|\mathbf{d}_2/2\}$, $\{I|0\}$ and lattice translations. Similar calculations can be made for the dodecagonal space groups but for the decagonal case the relation $\sigma' = C_2\sigma$ has to be used instead of $\sigma' = C_n\sigma$ $(n = 8, 12)$. For the non-symmorphic icosahedral space groups, the non-primitive translations of generators are shown in Table 12.

So far, the polygonal quasicrystals with non-symmorphic space groups are found but all icosahedral quasicrystals have primitive or face-centered symmorphic space groups. Many decagonal quasicrystals are centrosymmetric but d-Al–Ni–Fe shows pentagonal $P\bar{1}0m2$, which is a noncentrosymmetric subgroup of $P10/mmm$ (Saito, Tanaka, Tsai, Inoue & Masumoto, 1992).

9. Morphology of quasicrystals

The observation of growth morphology is possible for stable quasicrystals. It is known that the morphology of normal crystals is explained by several laws. Well known rules are the law of rational indices, the law of Bravais–Friedel (see Janssen & Janner, 1987). The application of such laws was attempted for an incommensurately modulated structure (Dam & Janner, 1985)

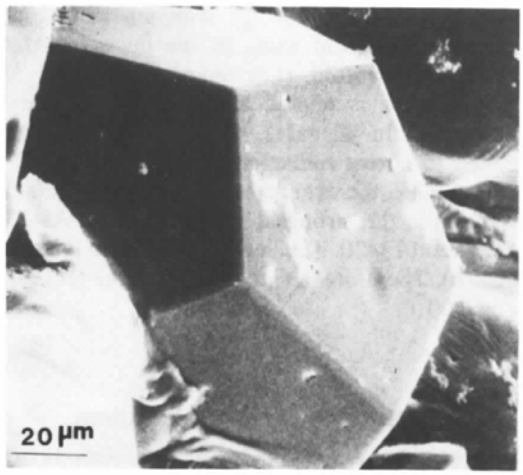

(*a*)

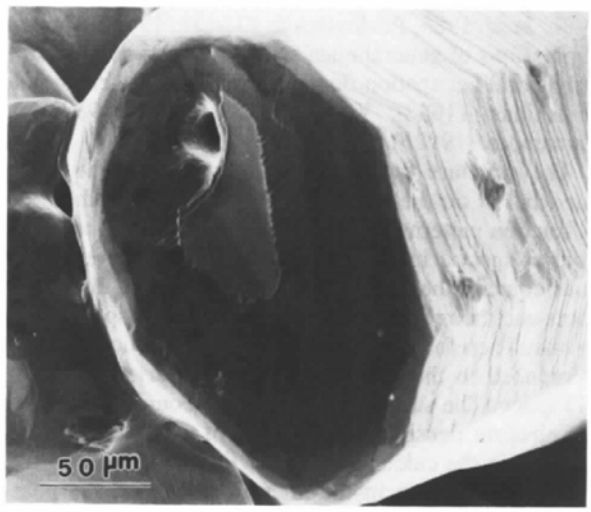

(*b*)

Fig. 27. The growth morphology of (*a*) *i*-Al-Cu-Fe and (*b*) *d*-Al–Ni–Co. (Courtesy of A. P. Tsai.)

and all faces of calaverite are shown to have small integral Miller indices. However, the importance of the dense lattice plane asserted by the Bravais–Friedel law has not been confirmed. In modulated structures and quasicrystals, some lattice planes are not periodic. In particular, in icosahedral quasicrystals, all lattice planes are not periodic. Therefore, the direct application of the Bravais–Friedel law is impossible. However, the law of rational indices can be applicable the same as in the modulated structure. Two examples are shown in Fig. 27 (Tsai, Inoue & Masumoto, 1987, 1989). The first found stable icosahedral quasicrystal Al–Cu–Li shows a triacontahedral morphology, indicating that the faces are indexable as 110000 *etc.*, which is perpendicular to the twofold axes (Dubost, Lang, Tanaka, Stainfort & Audier, 1986). On the other hand, that of face-centered icosahedral Al–Cu–Fe is dodecahedral (Fig. 27*a*). This has faces with indices 100000 *etc.* that are perpendicular to the fivefold axes. Decagonal Al–Ni–Co (Fig. 27*b*) has decagonal-columnar shape with ten faces that are normal to the twofold axes. In the decagonal lattice, there are two twofold axes along 10000 and $10\bar{1}0$ but which index is related to the prism face has not been clarified. In all cases, the crystal faces seem to be related to strong reflections. In fact, in *i*-Al–Cu–Li and *i*-Al–Cu–Fe, the strongest reflections are 110000 and 100000, while the strongest reflections of *d*-Al–Ni–Co are 00002 and 13420. The latter is parallel to the twofold axes $10\bar{1}0$. Therefore, a face parallel to the tenfold axis may be $10\bar{1}0$.

10. Structure-factor calculations

The structure-factor calculations of quasiperiodic tilings have been performed by several people (Duneau & Katz, 1985; Kalugin, Kitayev & Levitov, 1985*a*,*b*; Elser, 1986; Jarić, 1986; Pavlovitch & Kléman, 1987). Analytic expressions of general quasicrystals having polygonal or polyhedral occupation domains are given by Yamamoto & Ishihara (1988), Yamamoto & Hiraga (1988) and Yamamoto (1992*b*).

The structure factors of quasicrystals can be calculated based on the section method. In this method, the diffraction patterns are regarded as the projection of the Fourier spectra in nD space onto the external space. In quasicrystals, the correspondence between the diffraction spots and the reciprocal-lattice points in nD space is one to one. Therefore, the calculation of the structure factor is reduced to the calculation of the Fourier spectra in nD space. The structure factor is the Fourier integral of the electron density in a unit cell of nD space. This is reduced to the calculation of the Fourier integral of the occupation domain in the internal space and the phase factor related to the location of the domain. It is usually assumed that the occupation domains of quasicrystals are polygonal for polygonal quasicrystals and polyhedral for icosahedral quasicrystals, since this is the case for those of quasiperiodic tilings. They are divided into triangles or tetrahedra, the Fourier integrals of which are given analytically. Thus, we obtain the analytical expression for the structure factor. In a rough approximation, a polygon or a polyhedron can be approximated by a circle or a sphere. In fact, for the pentagonal Penrose tiling or Stampfli tiling and 3D Penrose tiling, this is a good approximation (see Figs. 18*c*, 19 and 23*c*). In such cases, the structure factor can easily be calculated. In all cases, it has the following form:

$$F(\mathbf{h}) = \sum_{\mu} \sum_{\{R|\mathbf{t}\}^{\mu}} f^{\mu}(\mathbf{h}^e) p^{\mu} \exp[-B^{\mu}(h^e)^2/4] \times \exp[2\pi i \mathbf{h} \cdot (R\mathbf{r}^{\mu} + \mathbf{t})] F_0^{\mu}(R^{-1}\mathbf{h}), \quad (48)$$

where the position, temperature factor and occupancy of the μth independent occupation domain are represented by $\mathbf{r}^{\mu}$, B^{μ} and p^{μ}. $F_0^{\mu}(\mathbf{h})$ and $f^{\mu}(\mathbf{h}^e)$ are the Fourier integral and atomic scattering factor of the μth occupation domain. The sum of $\{R|\mathbf{t}\}^{\mu}$ runs over the symmetry operators of the space group which create new occupation domains in a unit cell from the independent ones. If the occupation domain is a circle with a radius r, its Fourier integral is

$$F_0^{\mu}(\mathbf{h}) = 2V J_1(q_0)/q_0 \quad (49)$$

with $V = \pi r^2$ and $q_0 = 2\pi h^i r$, where J_1 is the Bessel function of first order. Similarly, the Fourier integral of a sphere with radius r is given by

$$F_0^{\mu}(\mathbf{h}) = 3V[\sin(q_0) - q_0 \cos(q_0)]/(q_0)^3 \quad (50)$$

with $V = 4\pi r^3/3$.

For polygonal or polyhedral domains, which are decomposed into several triangles or tetrahedra, $F_0^{\mu}(\mathbf{h})$ is calculated by using the site symmetry from their independent parts. Since the Fourier integral is linear, F_0^{μ} is given by the summation of Fourier integrals of triangles or tetrahedra. Provided that the occupation domain consists of ν independent triangles or tetrahedra, it is given by

$$F_0^{\mu}(\mathbf{h}) = \sum_{i=1}^{\nu} \sum_{R'} F_{0i}^{\mu}(R'^{-1}\mathbf{h}), \quad (51)$$

where R' is the rotational part of the site-symmetry operator, which runs over all site-symmetry operators. The Fourier integral of a triangle defined by the vector $\mathbf{e}_1$ and $\mathbf{e}_2$ (see Fig. 28*a*) is given by (Jarić, 1986; Ishihara & Yamamoto, 1988)

$$F_{0i}(\mathbf{h}) = V\{q_1[\exp(iq_2) - 1] - q_2[\exp(iq_1) - 1]\}/q_1 q_2 (q_1 - q_2), \quad (52)$$

where $V = |\mathbf{e}_1 \times \mathbf{e}_2|$, $q_j = 2\pi \mathbf{e}_j \cdot \mathbf{h}^i$ ($j = 1, 2$), $\mathbf{e}_j$ are edge vectors of a triangle constructing the polygon.* The Fourier integral of the tetrahedron defined by $\mathbf{e}_1$, $\mathbf{e}_2$ and $\mathbf{e}_3$ (Fig. 28*b*) is given by (Yamamoto, 1992*b*)

$$F_{0_t}(\mathbf{h}) = -iV[q_2q_3q_4 \exp(iq_1) + q_3q_1q_5 \exp(iq_2) + q_1q_2q_6 \exp(iq_3) + q_4q_5q_6]/(q_1q_2q_3q_4q_5q_6), \quad (53)$$

where $q_j = 2\pi \mathbf{h}^i \cdot \mathbf{e}_j$ ($j = 1, 2, 3$), $q_4 = q_2 - q_3$, $q_5 = q_3 - q_1$, $q_6 = q_1 - q_2$ and $V = \mathbf{e}_1 \cdot [\mathbf{e}_2 \times \mathbf{e}_3]$ is the volume of the rhombohedron with the edge vectors $\mathbf{e}_1$, $\mathbf{e}_2$ and $\mathbf{e}_3$. Note that (49) and (52) [(50) and (53)] give the area (volume) of the circle and the triangle (the sphere and the tetrahedron) in the small h^i limit as expected.

In the above consideration, it is assumed that the shape of the occupation domain is known. One of the difficult problems of the structure determinations is to determine its size and shape. The occupation domain with any shape can be approximated by a deformed circle or sphere (Elcoro, Pérez-Mato & Madariaga, 1994). The deviation from the circle or sphere can be expressed in terms of trigonometric functions or spherical harmonics. The Fourier integral of such an occupation domain cannot be given analytically and has to be calculated numerically. In this method, however, we can refine the size and shape of the occupation domain under the constraint of the site symmetry. It is also possible to refine the size and shape of polygonal and polyhedral occupation domains by changing the length of the edge vectors. If their independent part consists of several triangles or tetrahedra, the directions of some edge vectors can also be changed. Such a refinement has been made in the analysis of decagonal quasicrystals (Steurer, Haibach, Zhang, Kek & Lück, 1993).

A characteristic feature of the cluster model discussed later is that there exist many occupation domains with the same shape so that their Fourier integral is common to many equivalent and non-equivalent sites and can be calculated only once for each $\mathbf{h}$. Furthermore, if the domain has a full (decagonal *etc.* or icosahedral) point symmetry, $F_0^\mu(\mathrm{R}^{-1}\mathbf{h}) = F_0^\mu(\mathbf{h})$. The use of these relations decreases the calculation time very much.

* It should be noted that q_j depends only on the internal-space component of $\mathbf{h}$ because $\mathbf{e}_j$ is a vector in the internal space. Consequently, $F_0(\mathbf{h})$ also depends only on the internal-space component of $\mathbf{h}$.

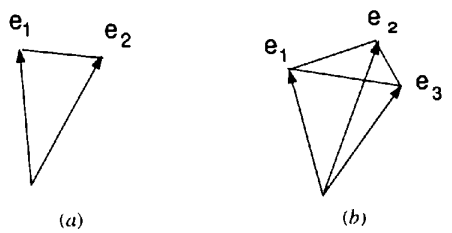

Fig. 28. Primitive domains of (*a*) polygonal and (*b*) icosahedral quasicrystals.

As mentioned in §§5 and 6, typical quasiperiodic tilings like the octagonal Penrose, Stampfli and 3D Penrose tilings have an occupation domain at the origin. Such an occupation domain may be approximated by a circle or a sphere with the same area or volume. Then their structure factors are proportional to (49) or (50). It is noted that they decrease with increasing the internal component of the diffraction vector, h^i, because of the presence of q_0 in the denominator. On the other hand, they agree with V in the small h^i limit. This means that only reflections with small h^i are observable in practice. This is the reason why the diffraction spots are observed although the projection of the lattice points cover everywhere the 2D or 3D external space. In a general tiling with several occupation domains in the unit cell, the structure factor is the summation of F_0^μ multiplied by a phase factor depending on the location of the occupation domains. The decrease of each F_0^μ with increasing h^i will give a similar tendency in the diffraction intensity.

11. Point density and frequency of subpatterns

The density of quasicrystals is a fundamental quantity and has to be explained by their models. The density calculations are based on the fact that the occupation domain at some lattice point $\mathbf{n}$ intersects the external space at a point and the set of all possible cross points covers the occupation domain homogeneously (Elser, 1986). Therefore, the point density of such points is proportional to the volume (or area) of the occupation domain in the internal space. The factor is given by the inverse of the unit-cell volume in nD ($n = 4, 5, 6$) space. Let the unit vectors of the lattice be $\mathbf{d}_i = \sum_{j=1}^{n} Q_{ij}\mathbf{a}_j$ ($Q_{ij} = M_{ij}^{-1}$). Then the unit-cell volume is given by $\det|Q_{ij}|$ and the point density by $\rho = V^i/\det|Q_{ij}|$ when the sum of the volume (area) of the occupation domain is V^i. It is simple to calculate the unit-cell volume of the hypercubic lattice. In 4D octagonal and 6D icosahedral lattices defined by (30) and (37), the hypercubic lattice is obtained when $a = a'$. Then the volume is $2a^4$ for the former, while the occupation domain of the octagonal Penrose tiling is the octagon with the edge length a, the area of which is $2a^2 \operatorname{cotan}(\pi/8)$. Therefore, the point density of the octagonal Penrose tiling is $\rho = \operatorname{cotan}(\pi/8)/a^2$. The result is independent of the value of a'. For the hypercubic lattice in 6D space, the cell volume is $8a^6$ provided that $a = a'$. The volume of the triacontahedral occupation domain for the 3D Penrose tiling can be given by the sum of the volume of the ten acute and ten obtuse rhombohedra and is $8a^3[\sin(2\pi/5) + \sin(4\pi/5)]$. The point density is $\rho = [\sin(2\pi/5) + \sin(4\pi/5)]/a^3$ (Elser, 1986). The point density of the Penrose tiling with an edge length of $2a/5^{1/2}$ is given by $\rho = [\sin(2\pi/5) + \sin(4\pi/5)]/a^2$ (Yamamoto & Ishihara, 1988).

In some cases, it is important to know the classification of the local environment around a specified point and its frequency. For example, this is necessary to know the physical properties and to model quasicrystals. The latter is reduced to the frequency of the set of points (an atom cluster) appearing in the external space. This means that the occupation domains of neighboring atoms intersect the external space when that of the specified atoms intersects it. This is possible only when the occupation domains of neighboring atoms and the specified atom have a common part when they are projected onto the internal space (see Fig. 5*c*). Let the occupation domain of the jth atom of a cluster centered at $\mathbf{r}_j$ be $V(\mathbf{r}_j)$. Then $\bigcup_i V(\mathbf{r}_j^i) \neq \emptyset$ is proportional to the frequency of the atom cluster. For example, the frequency of the 12–fold vertices of the 3D Penrose tiling, from which 12 edges go out, is obtained from $V(0)\bigcup[\bigcup_{i=1}^{12} V(\mathbf{d}_j^i)]$, where $\mathbf{d}_{6+i} = -\mathbf{d}_i$, $V(0)$ is the rhombic triacontahedron with edge length a' (Fig. 23*c*). The common part $V(0)[\bigcup_{i=1}^{12} V(\mathbf{d}_j^i)]$ is also the rhombic triacontahedron but with the edge length of $\tau^{-2}a'$, so that the frequency of the 12-fold vertices is smaller than that of all the vertices by a factor τ^{-6} (Elser, 1986). In the octagonal Penrose tiling, there exist threefold to eightfold vertices, which come from the area shown in Fig. 16 (Beenker, 1982). In this case, if vertices appear at $\mathbf{d}_j^e$ and $\mathbf{d}_{j+1}^e$ (or $\mathbf{d}_j^e$ and $\mathbf{d}_{j+2}^e$), an additional vertex appears at $\mathbf{d}_j^e + \mathbf{d}_{j+1}^e$ ($\mathbf{d}_j^i + \mathbf{d}_{j+2}^i$) because $|\mathbf{d}_j^i + \mathbf{d}_{j+1}^i| < |\mathbf{d}_j^i|$ ($|\mathbf{d}_j^i + \mathbf{d}_{j+2}^i| < |\mathbf{d}_j^i|$), forming a rhombus (square) together with the vertex of the cluster center. The frequency of each vertex is proportional to the area of its occupation domain. Such a classification has been made for the Penrose, generalized Penrose and 3D Penrose tilings (de Bruijn, 1981; Pavlovitch & Kléman, 1987; Zobetz & Preisinger, 1990; Henley, 1986).

12. Description of quasicrystal structures

Quasicrystal structures have to be described by a finite number of parameters. The essential parameters are the position, the size and the shape of the occupation domains, and the temperature factor. In quasicrystals, an atom site may be occupied partially by several atoms statistically. Then we need, in addition, occupation probabilities of each site by constituent atoms. When the occupation domain is polygonal or polyhedral, we can specify its shape and size with the independent triangles or tetrahedra and the site symmetry (Yamamoto, 1992*b*). The shape of the occupation domain is restricted by the site symmetry. Its symmetry should be equal to or higher than the site symmetry. For example, the occupation domain at the special point with full rotational symmetry can be expressed by only a small number of independent triangles or tetrahedra because of the high site symmetry. The octagonal Penrose, pentagonal Penrose, Stampfli and 3D Penrose tilings are obtained from the octagon, decagon, dodecagonal star and triacontahedron, which can be formed from one triangle or tetrahedron by the site-symmetry operations (Figs. 16*a*, 18*c*, 19 and 23*c*). Thus, they are specified by two or three radial vectors from the center of the occupation domain, which are listed in Table 13. In order to specify the shape of occupation domains, we can use the internal components of the unit vectors in the minimal dimension. It is however convenient to use the vectors $\mathbf{e}_j^i = (2a'/5^{1/2})[c_{2j}\mathbf{a}_3 + s_{2j}\mathbf{a}_4]$ ($j \leq 5$) for the decagonal and $\mathbf{e}_j^i = (2a'/6^{1/2})[c_{5(j-1)}\mathbf{a}_3 + s_{5(j-1)}\mathbf{a}_4]$ ($j \leq 6$) for the dodecagonal tilings (Figs. 10*e* and *f*). They are related to the internal-space components of 5D and 6D representations of the tilings. These are also related to the internal components of the unit vectors in 4D space by

Table 13. *The occupation domains of typical tilings with one occupation domain*

The shape of the occupation domain can be specified by the vectors pointing to the corners of a triangle or tetrahedron and the site symmetry. The vectors are represented with respect to the vectors $\mathbf{e}_j^i$, which are the internal component of $\mathbf{d}_j^i$ for the Beenker and 3D Penrose tilings, $\mathbf{e}_j^i = (2a'/5^{1/2})[c_{2j}\mathbf{a}_3 + s_{2j}\mathbf{a}_4]$ ($j \leq 5$) for the pentagonal Penrose tiling, $\mathbf{e}_j^i = (2a'/6^{1/2})[c_{5j}\mathbf{a}_3 + s_{5j}\mathbf{a}_4]$ ($j \leq 6$) for the Stampfli tiling, where $c_j = \cos(2\pi j/n)$ and $s_j = \sin(2\pi j/n)$, n is 10 and 12 for the pentagonal Penrose and the Stampfli tilings.

Tiling	Symmetry	Corner vector	Site symmetry
Octagonal	*p*8*mm*	$(1,\bar{1},0,1)/2$	8*mm*
Penrose		$(1,\bar{1},\bar{1},1)/2$	
Pentagonal	*p*10*mm*	$(1,0,\bar{1},0,0)$	10*mm*
Penrose		$(1,1,\bar{1},0,\bar{1})/2$	
Stampfli	*p*12*mm*	$(1,0,0,0,0,0)$	12*mm*
		$(1,0,0,0,0,1)/3^{1/2}$	
3D Penrose	$Pm\bar{3}\bar{5}$	$(1,\bar{1},\bar{1},1,\bar{1},\bar{1})/2$	$m\bar{3}\bar{5}$
		$(1,1,\bar{1},\bar{1},\bar{1},\bar{1})/2$	
		$(1,0,\bar{1},\bar{1},0,\bar{1})/2$	

$$\begin{bmatrix}\mathbf{d}_1^i\\ \mathbf{d}_2^i\\ \mathbf{d}_3^i\\ \mathbf{d}_4^i\end{bmatrix} = \begin{bmatrix}1&0&0&0&-1\\ 0&1&0&0&-1\\ 0&0&1&0&-1\\ 0&0&0&1&-1\end{bmatrix}\begin{bmatrix}\mathbf{e}_1^i\\ \mathbf{e}_2^i\\ \mathbf{e}_3^i\\ \mathbf{e}_4^i\\ \mathbf{e}_5^i\end{bmatrix} \quad \text{(decagonal)} \tag{54}$$

$$\begin{bmatrix}\mathbf{d}_1^i\\ \mathbf{d}_2^i\\ \mathbf{d}_3^i\\ \mathbf{d}_4^i\end{bmatrix} = \begin{bmatrix}1&0&0&0&-1&0\\ 0&1&0&0&0&-1\\ 0&0&1&0&1&0\\ 0&0&0&1&0&1\end{bmatrix}\begin{bmatrix}\mathbf{e}_1^i\\ \mathbf{e}_2^i\\ \mathbf{e}_3^i\\ \mathbf{e}_4^i\\ \mathbf{e}_5^i\\ \mathbf{e}_6^i\end{bmatrix} \quad \text{(dodecagonal).} \tag{55}$$

Table 14. *The occupation domains of typical tilings with several occupation domains*

These have two independent occupation domains located at the special positions. The corner vectors of their independent part are shown. The notation for the corner vector is the same as in Table 12, while the position of the center of the occupation domains is given by the 4D and 6D coordinates for polyhedral and icosahedral tilings. Note that the Socolar tiling has a face-centered lattice with a doubled lattice constant.

Tiling	Symmetry	Corner vector	Site symmetry	Position
Penrose	$p10mm$	(1,0,0,0,0)	$5m$	(1,1,1,1)/5
		(1,0,0,1,0)/2		
		(1,0,0,1,0)	$5m$	(2,2,2,2)/5
		(1,2,0,1,0)/2		
Binary	$p10mm$	(1,0,0,0,0)	$10mm$	(0,0,0,0)
		(1,0,0,0,$\bar{1}$)/2		
		(0,0,0,0,$\bar{1}$)	$5m$	(1,1,1,1)/5
		(0,0,$\bar{1}$,0,$\bar{1}$)		
Dodecagonal Penrose	$p12mm$	(0,$\bar{1}$,0,1,0,2)/3	$3m$	(0,1,0,2)/3
		(0,1,0,2,0,1)/6		
		(2,$\bar{1}$,1,1,$\bar{1}$,2)/3	$3m$	(1,1,2,2)/3
		($\bar{1}$,$\bar{1}$,$\bar{2}$,1,$\bar{1}$,2)/3		
Socolar	$Fm\bar{3}\bar{5}$	($\bar{1}$,1,$\bar{1}$,$\bar{1}$,1,1)/4	$m\bar{3}\bar{5}$	(1,1,1,1,1,1)/4
		($\bar{1}$,0,0,0,1,0)/4		
		($\bar{5}$,1,1,1,1,1)/20		
		($\bar{1}$,1,1,1,1,1)/4	$m\bar{3}\bar{5}$	(3,1,1,1,1,1)/4
		($\bar{1}$,1,0,1,1,0)/4		
		($\bar{1}$,1,$\bar{1}$,$\bar{1}$,1,1)/4		

For the octagonal and icosahedral tilings, $\mathbf{e}_j^i \equiv \mathbf{d}_j^i$. Tables 13 and 14 use the coordinates with respect to $\mathbf{e}_j^i$ (Figs. 10*d–f* and 11*b*).

Other quasiperiodic tilings have several occupation domains. In the Penrose, binary and dodecagonal Penrose tilings, their number is 4, 3 and 8 but two of them are independent for all the cases (Figs. 18*a*, 20 and 21). The tiling obtained by Niizeki is derived from the occupation domains *A*, *B*, *C* and *D* in Fig. 21 (Niizeki, 1989). For the icosahedral Socolar tiling, two occupation domains exist (Fig. 24). Their location and the corner vectors are listed in Table 14 together with the site symmetry. Except for the generalized Penrose tilings, which are obtained from the n-gonal lattice ($n = 8$, 10, 12) in nD space (the octagonal, decagonal, dodecagonal Penrose tilings and 3D Penrose tiling *etc.*), the shape of the occupation domain is not related to the projection of the unit cell, so that we can obtain many tilings by tailoring the occupation domains. In particular, the occupation domains for the cluster models have a complicated shape as shown in §16.

13. Phason in quasicrystals

The linear shear strain in quasicrystals gives prominent effects in the diffraction pattern and leads to a variety of structures. They can be classified into two categories. One is the phonon strain and the other the phason strain. The former leaves the external space passing through the origin invariant, while the latter leaves the internal space unchanged. In Figs. 29(*b*) and (*c*), these two are shown for the Fibonacci lattice (1D analog of the quasicrystal), where the primitive tiles are reduced into short (*S*) and long (*L*) bars in the external space (horizontal line) and the occupation domain is a vertical bar. The phonon strain changes the size of the short and long tiles, keeping the arrangement of the tiles, while the phason strain changes the arrangement of the tiles, keeping the size of the tiles. The diffraction patterns corresponding to the distorted lattices under the phonon and phason strains are shown in Fig. 30. In the nD crystallography, the observed diffraction patterns are regarded as the projection of the reciprocal lattice onto the external space (horizontal line) along the internal space (vertical line). The phonon distortion does not change the position of the diffraction spots but the intensity, while the position is displaced under the phason strain, keeping the intensity unchanged. The displacement from the position of the undistorted lattice is proportional to the internal component of the diffraction vector. It should be noted that, under an appropriate phason distortion, we get a periodic structure (Fig. 31*a*). Then, an infinite number of reciprocal-lattice points is projected onto the same point in the external space (Fig. 31*b*). This is the crystalline approximant. Therefore, the structure factor for the crystalline approximant is obtained by summing up structure factors of the reciprocal-lattice points which are projected onto the same position. In this case, the symmetry of the Fibonacci lattice is oblique before and after the phason distortion and is unchanged. On the other hand, the phason distortion lowers the symmetry of polygonal or icosahedral quasicrystals and a variety of phason distortions can be considered (Ishii, 1989; Wang, Quin, Lu, Feng & Xu, 1994).*

* Exactly speaking, the structure under the phonon strain in Fig. 29(*b*) is different from a normal structure under the shear strain as in Fig. 7(*c*). In this case, only the lattice is deformed by the strain keeping the occupation domain unchanged.

For simplicity, we neglect the phonon distortion with respect to the n-fold ($n = 8, 10, 12$) axis along the periodic direction for polygonal quasicrystals. Then the unit vectors of the distorted lattice are given by

$$\mathbf{d}'_i = \sum_{j=1}^{m} Q_{ij}\mathbf{a}'_j = \sum_{j=1}^{m} (QT^{e/i})_{ij}\mathbf{a}_j, \qquad (56)$$

where $m = 4$ and 6 for polygonal and icosahedral quasicrystals and Q_{ij} are defined by (30), (32), (34) and (37). T^e and T^i are the strain tensors for the linear phonon and linear phason strains, which have following forms:

$$T^e = \begin{bmatrix} I_d & 0 \\ U^e & I_d \end{bmatrix} \qquad (57)$$

$$T^i = \begin{bmatrix} I_d & U^i \\ 0 & I_d \end{bmatrix}, \qquad (58)$$

where I_d is the $d \times d$ unit matrix, U^e and U^i are general $d \times d$ matrices and $U^i = -\tilde{U}^e$, $d = 2$ for polygonal and $d = 3$ for icosahedral quasicrystals. An appropriate combination of the phonon and phason strains can give a rotation (Kramer, 1987; Torres, Pastor, Jimenez & Fayos, 1989; Soma & Watanabe, 1992). We now discuss the phason strain in more detail.

13.1. *Quasiperiodic tilings under phason strain*

In real quasicrystals, the phason strain always reduces the symmetry, which can be crystallographic or non-crystallographic. The SM can calculate their diffraction patterns (Elser & Henley, 1985; Wang & Kuo, 1988; Yamamoto, 1992*b*). The phason strain shifts the position of diffraction spots. The unit vectors in the reciprocal lattice under the phason strain are given by

$$\mathbf{d}^{*\prime}_i = \sum_{i=1}^{n} (MT^e)_{ij}\mathbf{a}_j. \qquad (59)$$

The diffraction vector $\mathbf{h}$ with Miller indices h_i ($i \le n$) under the phason strain is given by $\mathbf{h} = \sum_{i=1}^{n} h_i \mathbf{d}^{*\prime}_i$. The tiling under the phason strain is obtained easily from the SM. The effect of the phason strain appears in the location of the occupation domains and their shape. In the previous section, it is shown that the occupation domain can be specified by the coordinates with respect to the internal components of the unit vectors. As shown in §5, the occupation domains of typical tilings like the octagonal, decagonal and dodecagonal Penrose tilings are related to the projection of the unit cell of the nD space ($n = 4, 5, 6$) onto the internal space. Equations (57) and (59) indicate that the internal components of the unit vectors change according to the phason distortion with their external components left invariant. As a result, the shape of the occupation domain slightly changes. In order to obtain a tiling with the same tiles without gap or overlap, we have to use the projection of the new cell as the occupation domain. After that, we can obtain the quasiperiodic tilings under phason strain in a similar way. For example, if the internal component of

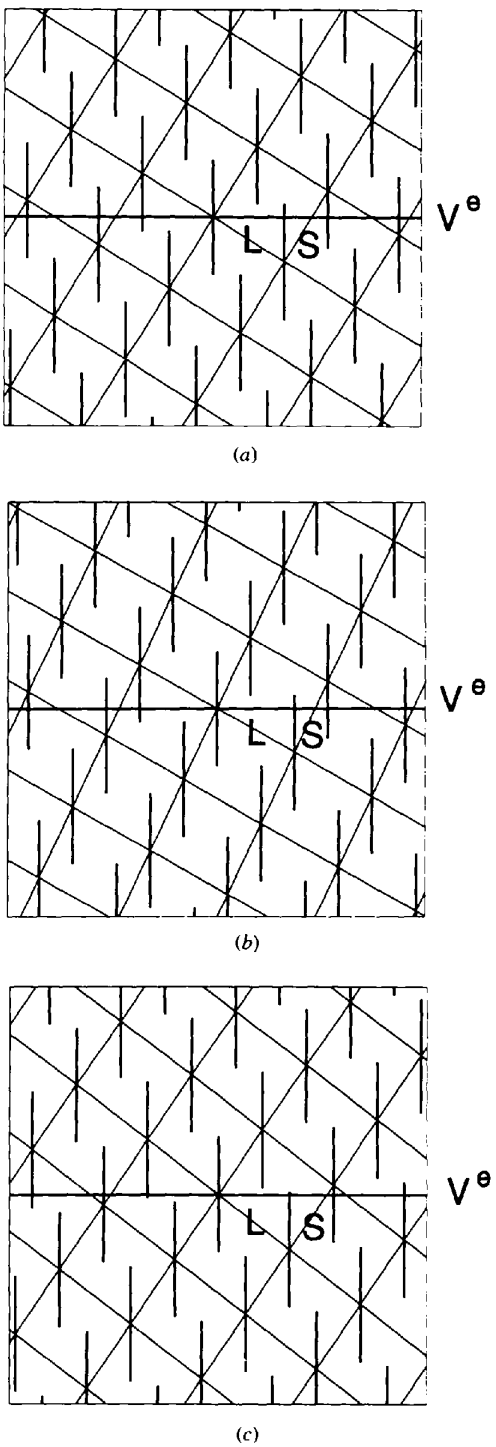

Fig. 29. 1D quasicrystals under (*a*) no strain, (*b*) phonon strain and (*c*) phason strain.

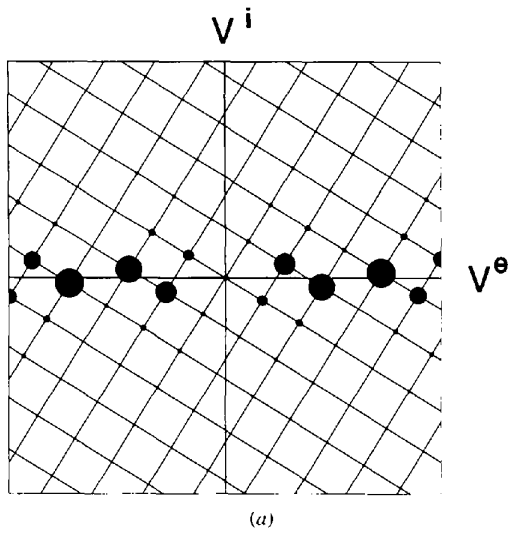

(a)

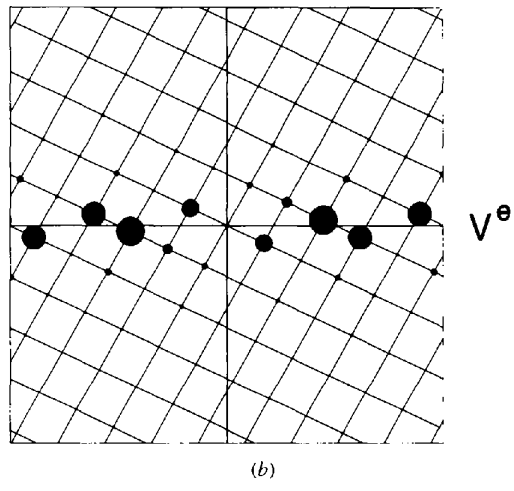

(b)

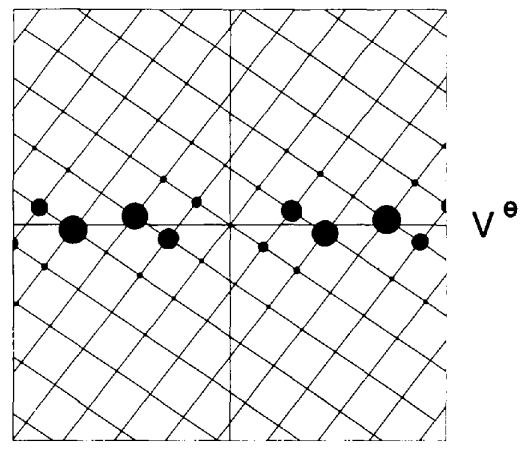

(c)

Fig. 30. The diffraction patterns corresponding to the structures in Fig. 29.

$-\mathbf{n}' = \sum_{j=1}^{4} n_j \mathbf{d}'_j$ is in the new occupation domain, its external component is plotted.

For the description of distorted quasiperiodic tilings, it should be noted that the site symmetry is reduced by the phason strain. Therefore, the independent part of the occupation domain is larger than that of the original one.

13.2. *Polygonal quasicrystals under phason strain*

For octagonal (dodecagonal) quasicrystals, $U^i_{11} = -U^i_{22}$ and $U^i_{12} = U^i_{21}$ ($U^i_{11} = U^i_{22}$ and $U^i_{21} = -U^i_{12}$) lead to the tetragonal distortion. Then the diffraction pattern shows the tetragonal symmetry although the number of unit vectors necessary for the indexing is still five (four for 2D tilings) in general. Therefore, the symmetry is crystallographic but the diffraction pattern is similar neither to that of usual crystals nor to that of modulated structures. In the latter, prominent so-called main reflections are found but there exist no such reflections in the distorted quasicrystals under the phason strain. Therefore, these should be called

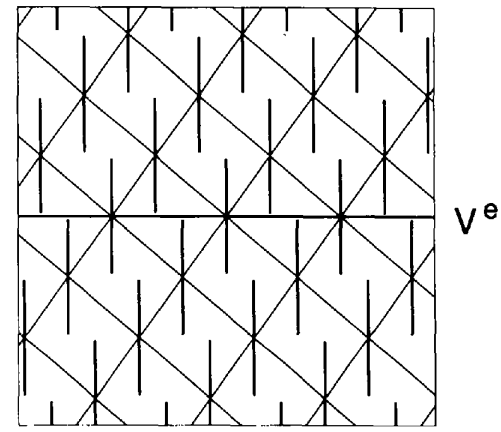

(a)

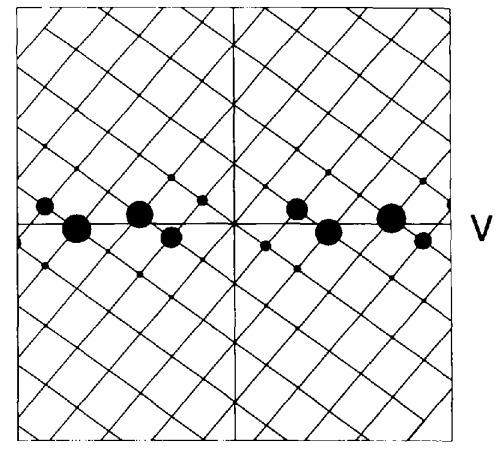

(b)

Fig. 31. (*a*) A periodic structure under the phason strain and (*b*) its diffraction pattern.

tetragonal quasicrystals. An example is shown in Figs. 32(*a*) and (*b*) for a distorted octagonal Penrose tiling. Similarly, the hexagonal quasicrystals are possible for dodecagonal cases when $U^i_{11} = -U^i_{22}$ and $U^i_{12} = U^i_{21}$. When $|U^i_{11}| \neq |U^i_{22}|$, orthorhombic quasicrystals are realized in general (including decagonal cases) while $|U^i_{12}| \neq |U^i_{21}|$ causes monoclinic distortion.

13.3. *Icosahedral quasicrystals under phason strain*

It is convenient to use two sets of unit vectors of the external and internal spaces. Pentagonal, cubic and trigonal quasicrystals can be derived in the icosahedral quasicrystals, as shown by Ishii (1989) (see also Mai, Tao, Zeng & Zhang, 1988). For the pentagonal quasicrystals, $\mathbf{a}_i$ given by (37) is convenient but another unit-vector set is more appropriate for the latter two although both sets can express all possible distortions. This is because two axes $\mathbf{a}_3$ and $\mathbf{a}_6$ are parallel to the fivefold axis in (37). Then, non-zero $U^i_{11} = U^i_{22}$ and U^i_{33} give the pentagonal quasicrystals. In order to treat the latter two cases, it is convenient to take unit vectors parallel to the twofold axes (Yamamoto, 1992*b*), which are defined by

$$\begin{bmatrix} \mathbf{d}_1 \\ \mathbf{d}_2 \\ \mathbf{d}_3 \\ \mathbf{d}_4 \\ \mathbf{d}_5 \\ \mathbf{d}_6 \end{bmatrix} = \frac{a}{(2+\tau)^{1/2}} \times \begin{bmatrix} 1 & \tau & 0 & \tau & -1 & 0 \\ \tau & 0 & 1 & -1 & 0 & \tau \\ \tau & 0 & -1 & -1 & 0 & -\tau \\ 0 & 1 & -\tau & 0 & \tau & 1 \\ -1 & \tau & 0 & -\tau & -1 & 0 \\ 0 & 1 & \tau & 0 & \tau & -1 \end{bmatrix} \begin{bmatrix} \mathbf{a}^c_1 \\ \mathbf{a}^c_2 \\ \mathbf{a}^c_3 \\ \mathbf{a}^c_4 \\ \mathbf{a}^c_5 \\ \mathbf{a}^c_6 \end{bmatrix}. \tag{60}$$

The phason strain matrix T^{ic} is defined by (57) when $\mathbf{a}_i$ is replaced with $\mathbf{a}^c_i$ in (56). Then, $U^{ic}_{11} = U^{ic}_{22} = U^{ic}_{33}$ gives cubic quasicrystals and $U^{ic}_{12} = U^{ic}_{23} = U^{ic}_{31}$ and $U^{ic}_{13} = U^{ic}_{21} = U^{ic}_{32}$ lead to trigonal quasicrystals.

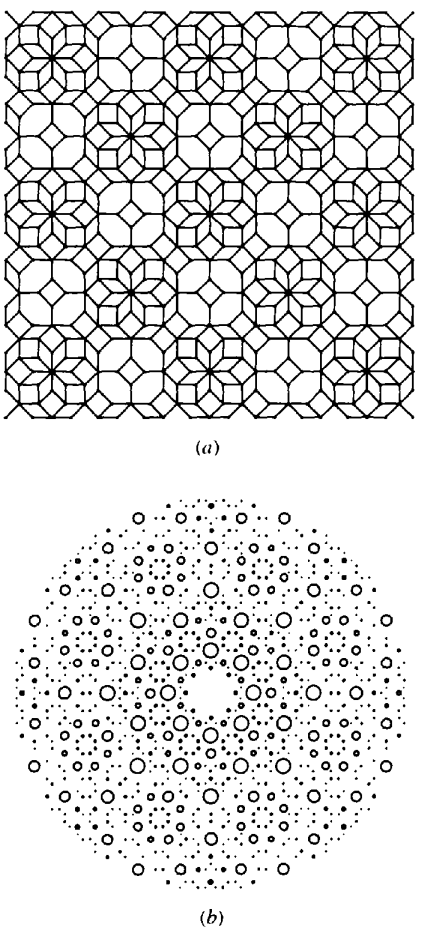

(*a*)

(*b*)

Fig. 32. (*a*) A periodic tetragonal pattern obtained from the octagonal Penrose pattern under the phason strain and (*b*) its diffraction pattern.

13.4. *Crystalline approximants*

The crystalline approximants are obtained when three linearly independent lattice points are in the external space passing through the origin. In polygonal cases, the fifth axis is always in the external space, so that it is enough to consider two vectors perpendicular to it. The crystalline approximants are important for understanding quasicrystal structures so that we discuss several cases in more detail.

The coordinates z_i with respect to $\mathbf{a}_i$ of the lattice vector $\sum_{j=1}^{n} n'_j \mathbf{d}'_j$ are given by

$$z'_i = \sum_{j=1}^{n} (\tilde{T}^i \tilde{Q})_{ij} n'_j. \tag{61}$$

From the condition under which the internal-axis components are zero, we can obtain the strength of the phason strain. In the polygonal (icosahedral) quasicrystals, there are four (nine) internal components of two (three) independent vectors that should be zero. This determines the four (nine) matrix elements of U^i. It should be noted that the strength depends on the lattice constant a' of the internal space. Since this is arbitrary, the strength has no physical meaning. Usually, a' is set equal to a but, even in this case, we cannot compare the values in coordinate systems with different a directly because of the similarity transformation. In order to compare the strength of the phason strain, we have to use the same coordinate system with the same lattice constant a and a'. For example, in the so-called (1, 1) cubic approximant as in the R phase of Al–Cu–Li or α phase of Al–Mn, the external space passes through the origin and $(1, 1, 1, 0, \bar{1}, 0)'$,

$(1,0,0,1,1,1)'$ and $(0,1,\bar{1},\bar{1},0,1)'$, where the prime means the coordinates with respect to the deformed unit vectors $\mathbf{d}'_i$. Therefore, if they are unit vectors in the crystalline approximant, their internal components are zero. Then, from $z'_i = 0$ $(i = 4, 5, 6)$ in (61), we have $U^i_{11} = U^i_{22} = U^i_{33} = -\tau^{-3}$ provided that $a = a' \simeq 4.8$ or 5.0 Å. In the trigonal approximant of i-Al–Cu–Fe, $(2,1,1,1,1,1)'$, $(1,2,1,\bar{1},\bar{1},1)'$, $(1,1,\bar{1},\bar{1},1,2)'$ of the face-centered icosahedral lattice are in the external space, forming a rhombohedral approximant. Similar calculations lead to the phason strain for this case:

$$U^i = \begin{bmatrix} \alpha & \gamma & \beta \\ \beta & \alpha & \gamma \\ \gamma & \beta & \alpha \end{bmatrix}, \tag{62}$$

where $\alpha = -\tau^{-8}/2$, $\beta = \tau^{-5}(1 + \tau^{-2})/2$ and $\gamma = -\tau^{-1}\beta$. The unit cell of the approximant is the acute rhombohedron with the edge length $2\tau^3 a$ ($a \simeq 4.8$ Å). In this case, their face centers are translationally equivalent to the origin because the approximant is related to a face-centered icosahedral quasicrystal. Thus, unit vectors of the primitive (rhombohedral) cell are given by $(a_R + b_R)/2$, $(b_R + c_R)/2$ and $(a_R + c_R)/2$, where a_R, b_R and c_R are $(2,1,1,1,1,1)'$, $(1,2,1,\bar{1},\bar{1},1)'$ and $(1,1,\bar{1},\bar{1},1,2)'$. (Note that they are in the external space.)

The distortion of the lattice shifts the position of the reflections in the external space according to (59). The diffraction patterns of R-Al–Cu–Li are shown in Fig. 33. In crystalline approximants, an infinite number of reflections in nD space is projected at the same position in the external space as mentioned above. Thus, the structure factor of the approximant can be calculated by the summation of the structure factors of the overlapped reflections of the quasicrystal. In Fig. 33, these overlapped reflections are plotted independently. The inverse relation was used to calculate the phases of reflections of the quasicrystals from the known approximant phases (Jarić & Quin, 1990).

The above argument determines the lattice of the crystalline approximant but there exists an ambiguity for the structure. We can obtain different crystalline approximant structure with different symmetries by choosing the external space passing through the different positions in nD space. (Even in quasicrystals, the different external spaces lead to different structures but they are locally isomorphic and their diffraction patterns and macroscopic physical properties are the same.) The symmetry of the crystalline approximant is generally represented by the subgroup of the space group of quasicrystals. The situation is similar to that of locked-in phases of modulated structures, where their space group is a subgroup of the superspace group of the incommensurate structure and it depends on the choice of the external space (Yamamoto & Nakazawa, 1982). For example, if it is desired to obtain the centrosymmetric structure, the external space passing through the inversion center in the nD space has to be chosen. Several examples of approximants of the pentagonal Penrose tiling were shown by Niizeki (1991). It should be noted that the approximant may have a lower symmetry than that of the unit cell depending on the choice of the external space. An example is shown in Fig. 34, which is obtained from the Penrose tiling by introducing the phason strain with $U^i_{11} = -\tau^{-6}$ and $U^i_{22} = -\tau^{-5}$. This has a rectangular cell but the structure has only one mirror plane through the origin. This is obtained from the external space passing through $(1,1,1,1)/5$.

Under the phason strain giving crystalline approximants, the external space passes only discrete points of the occupation domain. If the external space passes near or in particular at the boundary of the occupation domain, a slight or infinitesimal change in the shape of the occupation domain causes different structures.

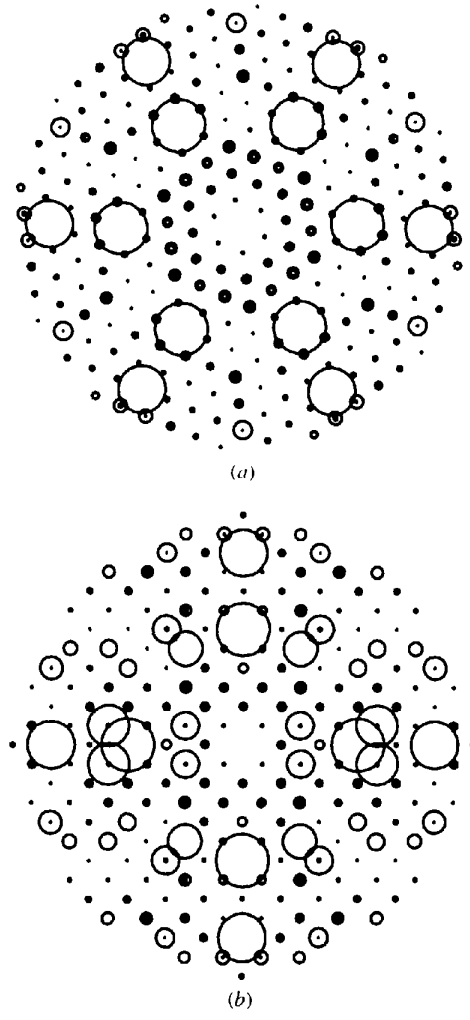

Fig. 33. The diffraction patterns of R-Al–Cu–Li along (a) a threefold axis and (b) a twofold axis. They are obtained from a 6D model of i-Al–Cu–Li by introducing the phason strain.

13.5. *Random phason*

In contrast to the linear phason strain, the random phason strain is the random shift of the occupation domains along the internal space, which depends on the external component of the position of occupation domains. This is a long-range fluctuation of the occupation domains, which is longer than the shortest interatomic distance and shorter than the coherence length of X-rays (several μm). On the stability of quasicrystals, the random tiling model asserts that they are stabilized by entropy effects that are caused by the presence of the random phason (Henley, 1987; Widom, Deng & Henley, 1989; Strandburg, Tang & Jarić, 1989). On the other hand, they may be stable energetically (Onoda, Steinhardt, DiVincenzo & Socolar, 1988). These two stabilization mechanisms have not been established yet. In any case, quasicrystals seem to include random phason strain, but this may or may not be essential for stabilization. Since conventional diffraction experiments observe the average periodic structures in nD space, the random phason strain obscures the boundary of the occupation domain and it is reflected in the phason temperature factor (Kalugin, Kitayev & Levitov, 1985*a*,*b*). If the fluctuation along the internal space is given by a Gaussian function, the occupation domain observed by the experiment is the convolution of the Gaussian function and the ideal occupation domain. Its Fourier integral adds a factor $\exp[-B'^{\mu}(h^{\perp})^2/4]$ in (48), where B'^{μ} is the phason temperature factor. Thus, the factor $\exp[-B^{\mu}(h^{\perp})^2/4]$ in (48) has to be replaced by $\exp[-B^{\mu}(h^{\perp})^2/4 - B'^{\mu}(h^{\parallel})^2/4]$. The anisotropic phason temperature factor is expected theoretically when the quasicrystal transforms into a crystalline approximant by the instability for a phason distortion (Jarić & Nelson, 1988).

14. Structure determination methods

There are several methods of the structure determination of quasicrystals. All the methods are based on the nD description of quasicrystal structures. Several classical methods are also applicable to quasicrystals. The Patterson method can draw Patterson maps in the nD space, from which we can derive the location of the occupation domains. The contrast variation method determines the partial structure factor by using several samples that have the same structure but consist of atoms with different scattering amplitudes. This can be achieved by neutron scattering with several samples by isomorphous replacement of isotopes or the anomalous-dispersion effects of X-rays using the absorption edge of constituent atoms. Then, the Patterson map gives the initial model of quasicrystal structures. The direct method gives the phases of observed reflections. On the other hand, in the trial-and-error method, an initial model has to be obtained from the investigation of quasiperiodic tilings and their decorations and/or electron microscopy. In particular, for polyhedral quasicrystals, electron microscopy gives important information for modeling. All methods have several drawbacks, so that they are complementary to each other.

14.1. *Patterson method*

The Patterson map of quasicrystals can easily be obtained from the Fourier transformation of the observed intensities which are indexed by nD Miller indices.

$$P(\mathbf{r}) = (1/V)\sum_{\mathbf{h}} |F_{\rm obs}(\mathbf{h})|^2 \exp(-2\pi i \mathbf{h}\cdot\mathbf{r}), \quad (63)$$

where V is the volume of the unit cell and $\mathbf{r}$ and $\mathbf{h}$ are the nD positional and reciprocal-lattice vectors. This

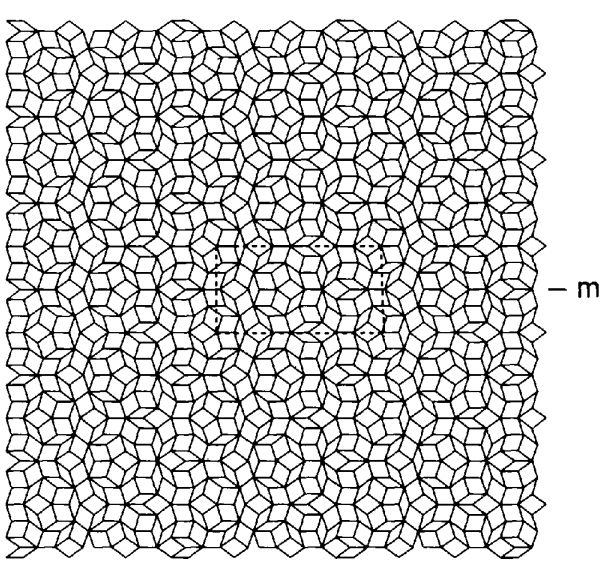

Fig. 34. A periodic pattern with a mirror plane and a rectangular lattice. The unit cell is shown as dotted lines.

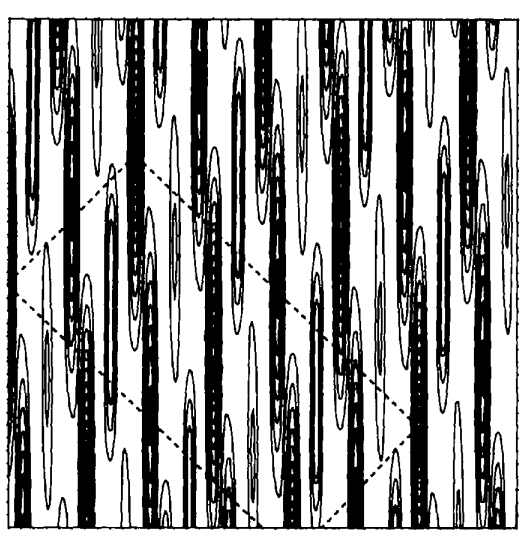

Fig. 35. The Patterson map of *i*-Al–Pd–Mn. Periods along two fivefold directions are shown by dotted lines. Short and long periods correspond to (100000) and (011111).

was applied to the analyses of *i*-Al–Cu–Fe (Gratias, Cahn & Mozer, 1988*a*,*b*) and *d*-Al–Mn (Steurer, 1989). Examples of the Patterson maps for *i*-Al–Pd–Mn having the face-centered icosahedral lattice are shown in Fig. 35 (Yamamoto, 1995). This is a self-convolution product of the density $\rho(\mathbf{r})$ in nD space:

$$P(\mathbf{r}) = (1/N) \int \rho(\mathbf{x})\rho(\mathbf{r} + \mathbf{x})\, d\mathbf{x}. \quad (64)$$

Therefore, the deduction of the electron density $\rho(\mathbf{r})$ is not an easy task but we can infer the location of large occupation domains and their rough size. From Fig. 35, we can consider that possible positions of the occupation domains are at $(0,0,0,0,0,0)$, $(1,0,0,0,0,0)/2$, $(1,1,1,1,1,1)/4$ and $(3,1,1,1,1,1)/4$ of the face-centered icosahedral lattice. The deviation of the occupation domain from the isotropic occupation domain (sphere) was observed in *i*-Al–Cu–Fe by Cornier-Quiquandon, Quivy, Lefebvre, Elkaim, Heger, Katz & Gratias (1991). It is, however, not easy to consider the distribution of constituent atoms. For this purpose, the contrast variation method explained below is efficient.

14.2. *Contrast variation method*

This can be used with either neutron scattering or anomalous X-ray diffraction to separate partial structure factors from the total structure factor. Let the change of neutron scattering lengths or atomic scattering factors be possible. The diffraction intensity of a binary alloy is given by

$$I(\mathbf{h}') = |b_A(\mathbf{h}')F_A(\mathbf{h}') + b_B(\mathbf{h}')F_B(\mathbf{h}')|^2, \quad (65)$$

where $b_{A/B}(\mathbf{h}')$ is the neutron scattering length or X-ray scattering factor at the diffraction vector $\mathbf{h}'$ for an A/B atom and $F_{A/B}$ is the corresponding normalized partial structure factor. The right-hand side of (65) becomes

$$b_A^2|F_A|^2 + b_B^2|F_B|^2 + 2b_A b_B|F_A||F_B|\cos\Delta\varphi_{AB}, \quad (66)$$

where $\Delta\varphi_{AB}$ is the phase difference between F_A and F_B. There are three unknown variables, $|F_A|$, $|F_B|$ and $\Delta\varphi_{AB}$ in the above expression. Thus, if we use three different sets of b_A and b_B, they are determined. $|F_A|$ or $|F_B|$ gives the partial Patterson map, which is a self-convolution product of the density function for one element. This makes the interpretation of the map much easier than that of the usual Patterson map. This was applied to the structure analyses of *i*-Al–Cu–Li and *i*-Al–Mn by neutron scattering (Janot, de Boissieu, Dubois & Pannetier, 1989; Janot, Pannetier, Dubois & Boissieu, 1989). Similarly, in the ternary alloys, six unknown quantities, $|F_A|$, $|F_B|$, $|F_C|$, $\Delta\varphi_{AB}$, $\Delta\varphi_{BC}$ and $\Delta\varphi_{AC}$ can be determined by six samples.

14.3. *Direct method*

The direct method has been applied to *i*-Al–Cu–Li by Fu, Li & Fan (1993) to check its efficiency in the quasicrystal structure determination. The quasicrystal is a crystal in nD space but the electron density is extended along the internal space since the occupation domain is parallel to the internal space. This is essentially different from a normal crystal and its direct extension to nD space, where the atom is spherically symmetric in nD space. The difference can be removed if we assume the occupation domains for all the atoms in nD space are the same and have the point symmetry of the lattice. Then, from (48), the structure factor is given by

$$F(\mathbf{h}) = F_0(\mathbf{h})\hat{F}(\mathbf{h}), \quad (67)$$

where

$$\hat{F}(\mathbf{h}) = \sum_\mu \sum_{\{R|\mathbf{t}\}^\mu} f^\mu(\mathbf{h}')p^\mu \exp[-B^\mu(h')^2/4] \times \exp[2\pi i\mathbf{h}\cdot(R\mathbf{r}^\mu + \mathbf{t})]. \quad (68)$$

Since the atomic scattering factors $f^\mu(\mathbf{h}')$ extend only over the external space and the δ function along the internal space, $\hat{F}(\mathbf{h})$ is quite similar to that of the usual structure factor. Thus, the usual direct-method phasing by the random starting tangent refinement procedure can be applied to $|\hat{F}(\mathbf{h})| = |F(\mathbf{h})|/|F_0(\mathbf{h})|$ (Yao, 1981). As the common occupation domain $F_0(\mathbf{h})$, the spherically symmetric occupation domain with an appropriate radius is employed. It was estimated from the origin peak in the Patterson map in nD space, which is spread in the internal space (Fu, Li & Fan, 1993). The radius used is nearly equal to that of the sphere with the volume of the rhombic triacontahedron for the 3D Penrose tiling. The direct-method phasing process gave peaks at the origin, edge center and body center in the 6D icosahedral lattice as expected. The next step is to calculate $F(\mathbf{h})$ with (67) since $\hat{F}(\mathbf{h})$ is now obtained and the factor $F_0(\mathbf{h})$ is given by (50). Finally, the electron density $\rho(\mathbf{r})$ in 6D space is obtained by the inverse Fourier transformation of the structure factor $F(\mathbf{h})$:

$$\rho(\mathbf{r}) = (1/V)\sum_{\mathbf{h}} F(\mathbf{h})\exp(-2\pi\mathbf{h}\cdot\mathbf{r}). \quad (69)$$

Thus, we can obtain the information of the occupation domain. In real quasicrystals as in *i*-Al–Cu–Li, the sizes of the occupation domains at the origin, edge center and body center are different and, in particular, the occupation domain at the edge center has no icosahedral symmetry. Therefore, the use of the common occupation domain with spherical symmetry is a rough approximation. Nevertheless, the procedure worked well. It seems to be insensitive to the choice of the common occupation domain. A similar procedure is expected to be applicable to the polygonal quasicrystals with the use of a circular

occupation domain instead of a spherical one for all atoms.

14.4. *Trial-and-error method*

The trial-and-error method is based on structure-factor calculations and the least-squares method. This is essentially the refinement method. Therefore, we need an initial model obtained from theoretical considerations or the methods mentioned above. We discuss the theoretical methods in the following. The basic model is the quasiperiodic tiling. Duneau & Katz (1985) showed that the 3D Penrose tiling gives the diffraction patterns similar to those of the first found quasicrystal *i*-Al–Mn and Yamamoto & Ishihara (1988) clarified that the diffraction patterns of *d*-Al–Mn are also similar to those of the 2D Penrose tiling and gave a possible model explaining the diffraction intensity and the extinction rules due to the space group $P10_5/mmc$. These models however gave too low point densities. In order to obtain a realistic density, decoration of the quasiperiodic tilings is necessary, which is the subject of the next section. The first realistic models of icosahedral and decagonal quasicrystals were derived for *i*-Al–Mn and *d*-Al–Co–Ni (Yamamoto & Hiraga, 1988; Yamamoto, Kato, Shibuya & Takeuchi, 1990) by the trial-and-error method. The models are based on the theoretical consideration of crystalline approximants and the relation between the approximants and quasicrystal structures under a linear phason strain. The structure models were constructed so as to give the crystalline approximants of α-Al–Mn and $Al_{13}Fe_4$. In both cases, the atom clusters are considered from the analogy of the crystalline approximants. They are observed in many quasicrystals and seem to be important building units for all quasicrystals. Thus, the structure model is not so simple in contrast to the first success of the quasiperiodic tiling.

15. Decoration of quasiperiodic tilings

So far, we have discussed general problems of quasicrystals and quasiperiodic tilings as the simplest models of quasicrystal structures. Simple tilings discussed in §§5 and 6 do not, however, give real quasicrystal structures but their vertices appear as the center of the cluster. The success of the 3D Penrose tiling for icosahedral quasicrystals was only qualitative (Yamamoto & Hiraga, 1988). It could not explain the density of the real quasicrystal. Therefore, in the next approximation, the density has to be explained. This can be done by considering the decoration of quasiperiodic tilings. A simple structure obtained from the 3D Penrose tiling was successful for *i*-Al–Cu–Li, where the edge-center atom and two atoms on the body diagonal of the acute rhombohedron (two body-diagonal positions) were introduced (Shen, Poon, Dmowski, Egami & Shiflet, 1987). As an example of such a decoration, we start with simple decorations of the octagonal Penrose tiling since this is the simplest case. As shown in §§5 and 12, the octagonal Penrose tiling is obtained from the octagonal occupation domain with the edge length a'. When the occupation domains at the lattice points $\mathbf{r}$ and $\mathbf{r}+\mathbf{d}_j$ intersect the external space, atoms appear at $\mathbf{r}^e$ and $\mathbf{r}^e+\mathbf{d}_j^e$. Then the external space intersects the union of their occupation domains: $V(\mathbf{r}^i)\bigcup V(\mathbf{r}^i+\mathbf{d}_j^i)$. The edge-center atom at $\mathbf{r}^e+\mathbf{d}_j^e/2$ is obtained from the union of the two occupation domains at $\mathbf{r}+\mathbf{d}_j/2$. This is a squashed hexagon with the edge length a' (Fig. 36*a*). Similarly, the face center position of the rhombus (square) with edges $\mathbf{d}_1^e$ and $\mathbf{d}_2^e$ ($\mathbf{d}_1^e$ and $\mathbf{d}_3^e$) is obtained from the union $V(\mathbf{r}^i)\bigcup V(\mathbf{r}^i+\mathbf{d}_1^i)\bigcup V(\mathbf{r}^i+\mathbf{d}_2^i)\bigcup V(\mathbf{r}^i+\mathbf{d}_1^i+\mathbf{d}_2^i)$ at $\mathbf{r}+(\mathbf{d}_1+\mathbf{d}_2)/2$. These are a rhombus with an angle $\pi/4$ and a square with the edge length a' (Figs. 36*b*,*c*). The tiling with atoms at all edge and face centers is shown in Fig. 37.

Similar calculations can be made for the 3D Penrose tiling. From the crystalline approximants of *i*-Al–Cu–Li, it is expected that atoms are situated at the edge-center and two body-diagonal positions of the acute rhombohedron, which divide the diagonal into $\tau^{-2}:\tau^{-3}:\tau^{-2}$ (Henley & Elser, 1986). From a similar consideration, the edge-center position is given by the occupation domain at the edge center $\mathbf{d}_j/2$, which is a union of two triacontahedral occupation domains at the origin and $\mathbf{d}_j^i$.

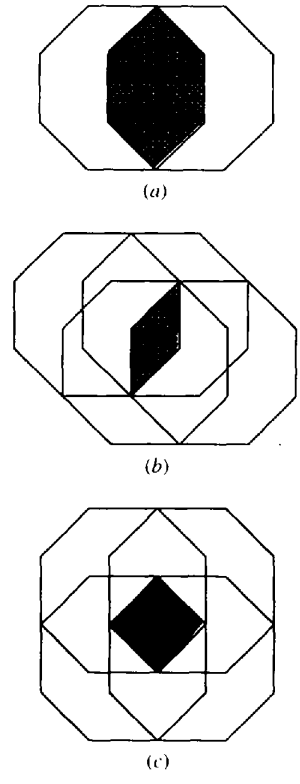

Fig. 36. The occupation domains for (*a*) edge centers, and face centers of (*b*) rhombi and (*c*) squares.

Its shape is given by the rhombic icosahedron with edge length a' (Fig. 23*d*). The occupation domain related to the diagonal two positions is the same in shape as that of the body-center position of the acute rhombohedron but is shifted. The union of the eight triacontahedra at $\mathbf{r}^i$, $\mathbf{r}^i + \mathbf{d}^i_j$ ($j = 1, 2, 3$), $\mathbf{r}^i + \mathbf{d}^i_j + \mathbf{d}^i_k$ [$(j, k) = (1, 2)$, $(2, 3)$, $(3, 1)$] and $\mathbf{r}^i + \mathbf{d}^i_1 + \mathbf{d}^i_2 + \mathbf{d}^i_3$ is the acute rhombohedron (Fig. 23*a*). [This agrees with the union of four rhombic triacontahedra at $\mathbf{r}^i$ and $\mathbf{r}^i + \mathbf{d}^i_j$ ($j = 1, 2, 3$).]

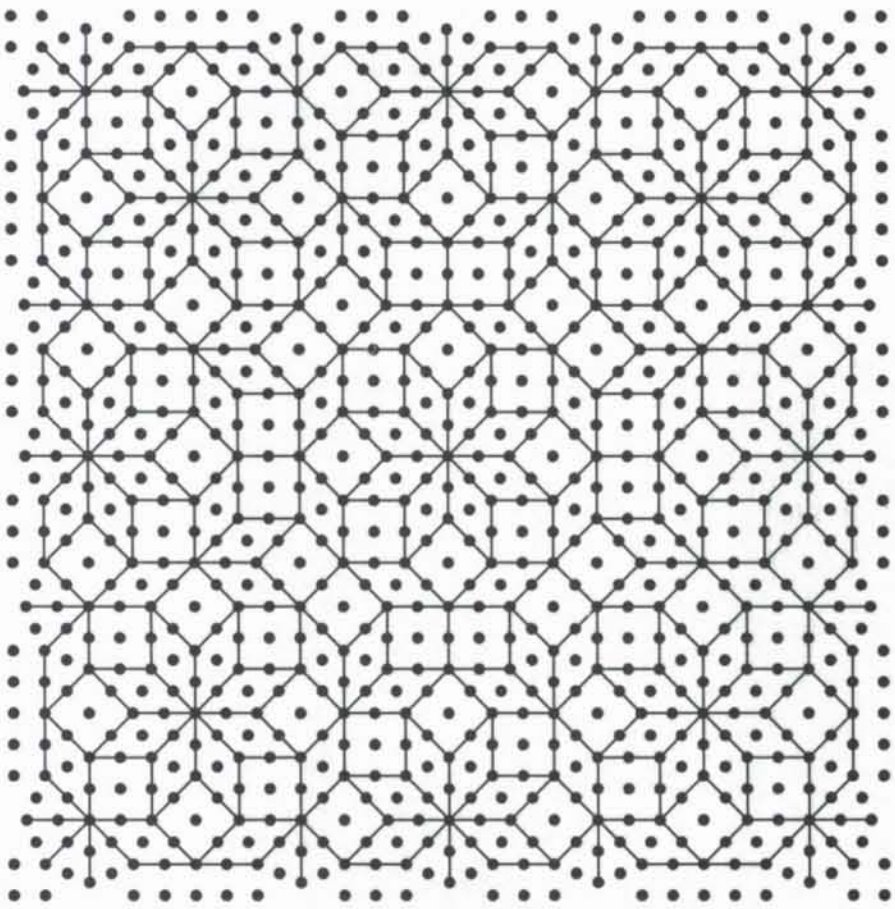

Fig. 37. The octagonal pattern decorated with edge-center and face-center atoms.

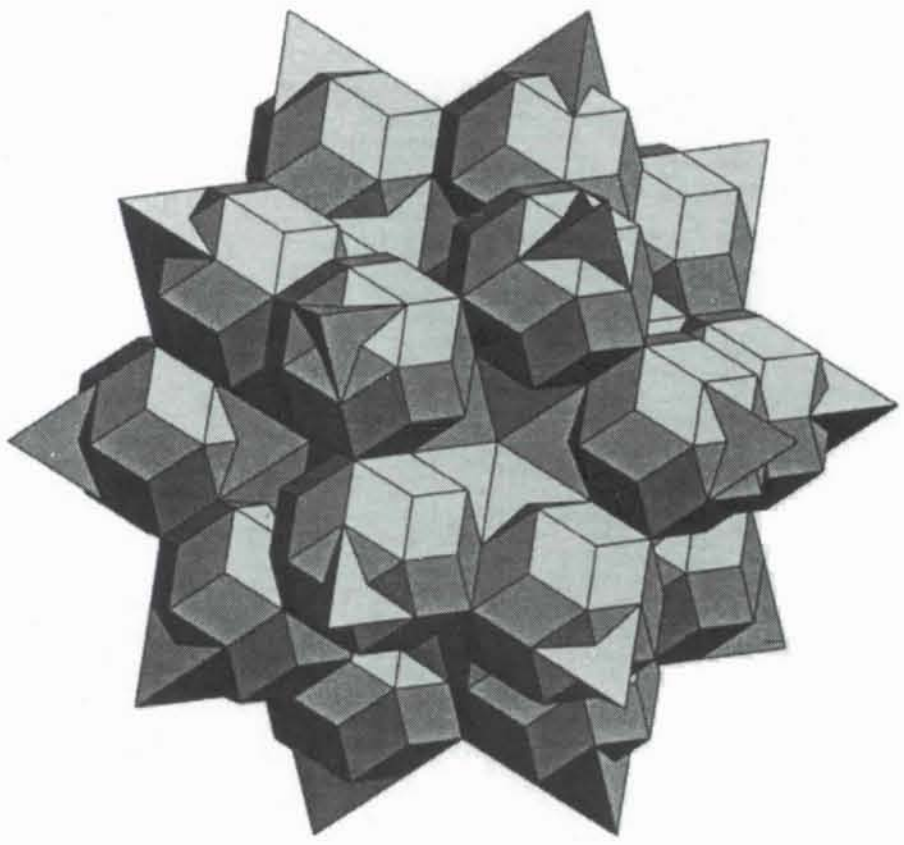

Fig. 38. The occupation domain of a cluster model of Li in *i*-Al–Cu–Li at the body center of the icosahedral lattice.

If this is located at the body center $\mathbf{r} + \sum_{j=1}^{3} \mathbf{d}_j/2$, an atom appears at the body center of the acute rhombohedron $\mathbf{r}^e + \sum_{j=1}^{3} \mathbf{d}^e_j/2$. In order to obtain atoms at the two body-diagonal positions, the occupation domain has to be shifted by $\pm\tau^{-3} \sum_{j=1}^{3} \mathbf{d}^e_j/2$ along the external space. When all the body-diagonal positions with 20 different orientations are considered, the resulting occupation domains construct a dodecahedral star shown in Fig. 23(*f*) (Yamamoto, 1990). In *i*-Al–Cu–Li, the vertex and edge-center positions are occupied mainly by Al and Cu statistically, and the two body-diagonal positions by Li. This was the first success of simple decoration models for quasicrystals (Elswijk, de Hosson, van Smaalen & de Boer, 1988). A detailed analysis gave a slightly different model, which is the cluster model discussed below.

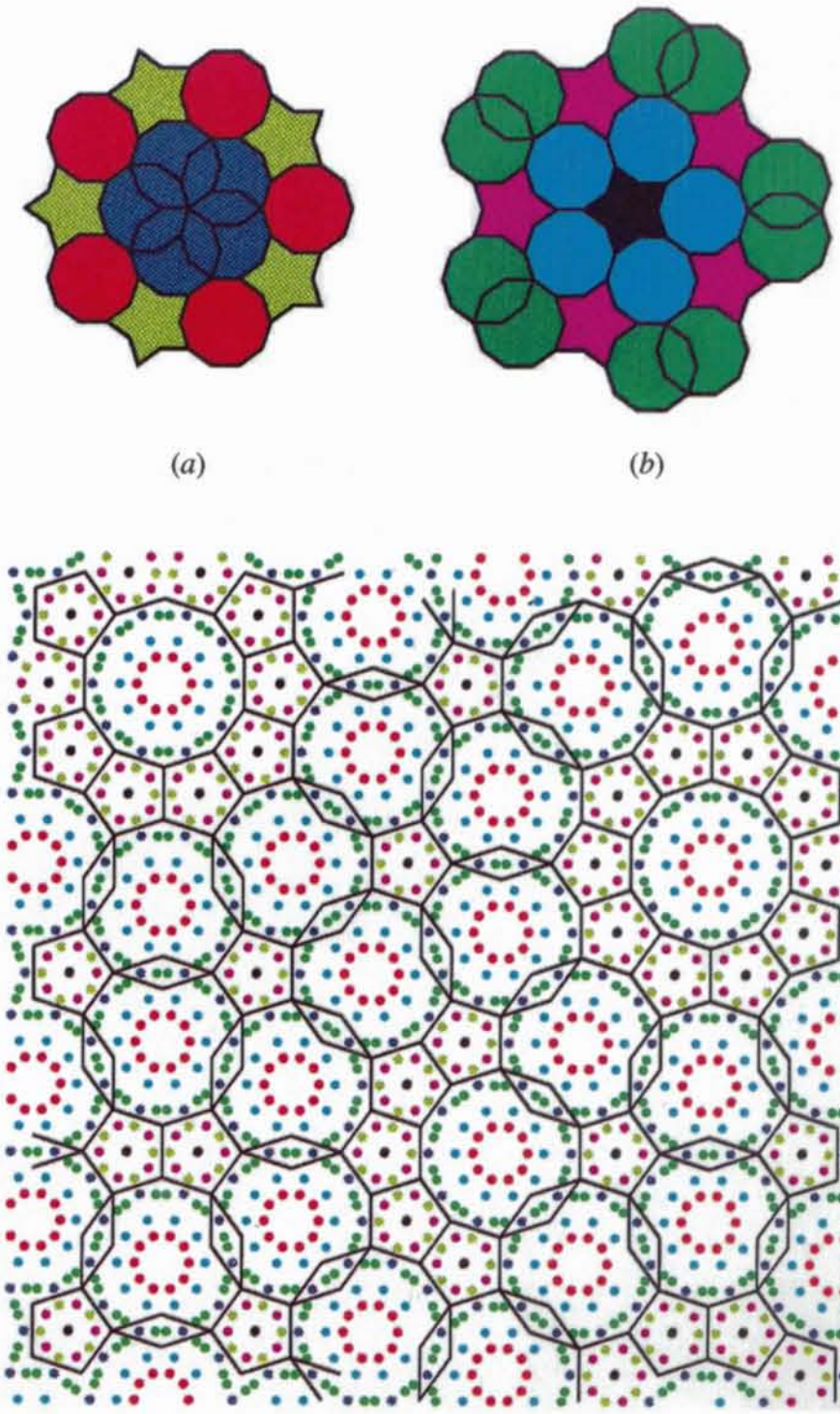

(*a*) (*b*)

(*c*)

Fig. 39. (*a*), (*b*) The occupation domains of (*c*) the Burkov model for *d*-Al–Cu–Co. The domains (*a*) and (*b*) are located at $(1, 1, 1, 1, 5z)/5$ and $(2, 2, 2, 2, 5z)/5$ in the 5D decagonal lattice. The atoms derived from small occupation domains in (*a*) and (*b*) are represented by the same color in (*c*).

16. Cluster models of quasicrystals

Cluster models for quasicrystals are inferred from the structure of crystalline approximants, which consists of atom clusters with high symmetries. In fact, the diffraction intensity distribution of the approximant of *i*-Al–Mn was shown to be similar to that of the *i*-Al–Mn quasicrystal (Elser & Henley, 1985). Clearer evidence is obtained from high-resolution electron microscopy for polyhedral quasicrystals. Several clusters were observed in decagonal phases (Hiraga, 1995). The symmetry of the atom cluster is closely related to that of quasicrystals. For the first quasicrystal found, *i*-Al–Mn, the corresponding approximant is α-Al–Mn–Si, which consists of icosahedral clusters $(Al/Si)_{42}Mn_{12}$. In the decagonal quasicrystals *d*-Al–Ni–Co and *d*-Al–Mn (*d*-Al–Pd–Mn), $Al_{11}Co_4$ ($Al_{13}Fe_4$) and Al_3Mn may be good approximants (Li, Shi, Ma, Ma & Kuo, 1995; Brack, 1955; Hiraga, Kaneko, Matsuo & Hashimoto, 1993). They have atom clusters with decagonal symmetry. A typical case is shown in Fig. 40 (Hiraga & Sun, 1993).

In the cluster model, we consider first the location of the cluster center. For the earliest found icosahedral quasicrystals *i*-Al–Cu–Li and *i*-Al–Mn, it was assumed that they are located at the 12-fold vertices of the 3D Penrose tiling (Yamamoto & Hiraga, 1988; Yamamoto, 1992*b*). We consider a cluster model of *i*-Al–Cu–Li. From the argument in the previous section, the occupation domain of the cluster center is the common part of 13 rhombic triacontahedra located at the origin and 12 vertices on the fivefold axes, which is the rhombic triacontahedron with the edge length $\tau^{-2}a'$. The frequency of the cluster center is proportional to a small triacontahedron, which is smaller than that of

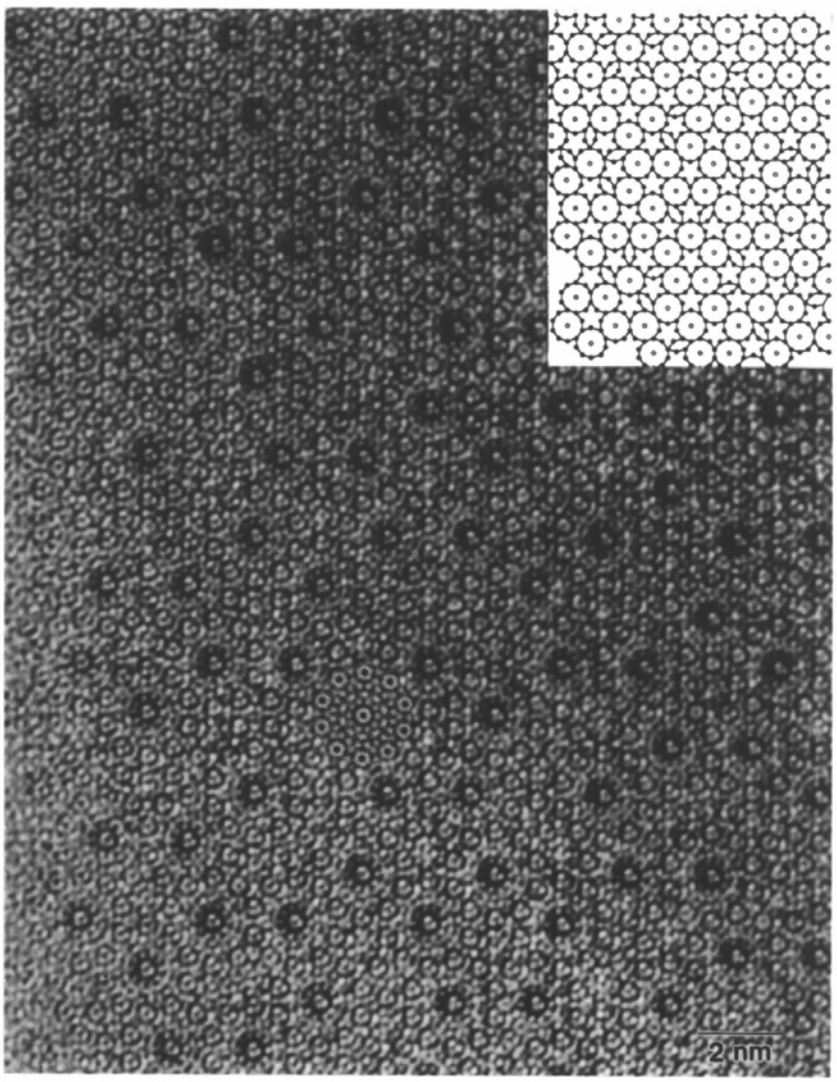

Fig. 40. The HRTEM image of *d*-Al–Pd–Mn and the distribution of the atom clusters (inserted). (Courtesy of K. Hiraga.) The shortest intercluster distance is about 20 Å.

the vertices of the 3D Penrose tiling by the factor τ^{-6}. The first shell of the cluster consists of 12 Al/Cu atoms at the edge centers of 12 bonds in the 3D Penrose tiling. They come from two small triacontahedra at $\mathbf{d}_j/2 \mp \mathbf{d}'_j/2$ within the rhombic icosahedra centered at $\mathbf{d}_j/2$ since the positions of the edge-center atoms $\pm\mathbf{d}'_j/2$ are equivalent to $\mathbf{d}_j/2 \mp \mathbf{d}'_j/2$. The second shell consists of 12 vertices and 20 atoms on the body diagonal of the acute rhombohedron, which divide the diagonal in the ratio $\tau^{-2} : \tau^{-1}$. They are created by the small triacontahedra at $(1, 1, 1, \bar{1}, 1, \bar{1})^{\mathrm{t}}/2 \equiv (1, 1, 1, 1, 1, 1)/2 - (1, 1, 1, \bar{1}, 1, \bar{1})^{\mathrm{t}}/2$ and 19 equivalent positions. These are the small triacontahedra seen in Fig. 38. Most parts of the triacontahedra are in the dodecahedral star but small parts are outshot. This means that the simple decoration discussed in the previous sections gives the atom cluster in most 12-fold vertices but some of them are not complete clusters. Thus, the cluster model modifies the simple decoration model slightly (Yamamoto, 1992*b*). In this model, there exist linking atoms connecting clusters.

On the other hand, a model of *d*-Al–Ni–Co proposed by Burkov (1991) does not include linking atoms but two kinds of atom clusters. The location of the cluster centers is related to the binary tiling given by Lancon & Billard (1988) and Zobetz (1992), where the tiling is generated by three occupation domains as mentioned in §5, two of which are independent (Fig. 20). The occupation domains are located at the same positions as those of the binary tiling but have complicated shapes (Figs. 39*a* and *b*). In order to classify the atoms depending on the different parts of the occupation domains, the structure in 2D space is colored (Fig. 39*c*). This model gives intercluster distances of about 12 Å.

In *d*-Al–Pd–Mn, the cluster arrangement is quite similar to that of the model by Burkov but the intercluster distances are about 20 Å, that is τ times longer than that of the Burkov model of *d*-Al–Ni–Co (Hiraga, Lincoln, & Sun, 1991). This also has two kinds of cluster but the cluster size is τ times larger. The structure of the cluster is deduced from high-resolution electron microscopy and the structure of the approximant Al_3Mn (Hiraga & Sun, 1993; Li, Shi, & Kuo, 1992; Hiraga, Kaneko, Matsuo & Hashimoto, 1993). Fig. 40 shows the HRTEM image and the cluster arrangement of *d*-Al–Pd–Mn. It should be noted that the large clusters with about 20 Å diameter are arranged quasiperiodically, the centers of which are created by the decagon with the corner vector $\tau^{-3}\mathbf{e}_1^i$ ($a \simeq 2.7$ Å). Since this is smaller than that of the binary tiling with the edge length of $|\mathbf{e}_1|$ by the factor τ^{-3}, the intercluster distance is τ^3 times larger than the edge length of the binary tiling, $2a/5^{1/2}$. A model that has similar clusters was proposed by Yamamoto (1993*a*) based on single-crystal X-ray analysis but the structure of the cluster is slightly different. Its large occupation domains are shown in Fig. 41. The shape of the small occupation domain is similar to that of the Burkov model but the size is smaller than that of the latter by the factor τ^{-1} because the intercluster distance is about 20 Å. The occupation domains lead to the structure shown in Figs. 41(*e*) and (*f*) (Yamamoto, 1993*a*). Recently, it was shown that *d*-Al–Ni–Co shows a superstructure (Edagawa, Ichihara, Suzuki & Takeuchi, 1992; Edagawa, Tamura, Suzuki & Takeuchi, 1995). The X-ray analysis of *d*-Al–Ni–Co has been done only for the average structure (Steurer, Haibach, Zhang, Kek & Lück, 1993). Therefore, the result of the X-ray analysis has to be interpreted carefully.

A cluster model of *i*-Al–Pd–Mn was given by Yamamoto, Sato, Kato, Tsai & Masumoto (1994) based on single-crystal X-ray diffraction. This has three complicated occupation domains, which are located at $(0, 0, 0, 0, 0, 0)$, $(1, 0, 0, 0, 0, 0)/2$ and $(3, 1, 1, 1, 1, 1)/4$. Similar to the model for decagonal quasicrystals mentioned above, they consist of small rhombic triacontahedra, small dodecahedral stars and small rhombic icosahedra, which are smaller than those of the simple decoration model of *i*-Al–Cu–Li by a factor of τ^{-3}. This is based on the decoration of the 3D Penrose tiling with the edge length $\tau^3 a$.

The models of *d*-Al–Pd–Mn and *i*-Al–Pd–Mn are refined by introducing a shift from ideal-atom positions. This is quite reasonable because the local environments of atoms are in general different from each other. Then the position of each small occupation domain can be shifted along the external space. Such a refinement method will be discussed in the next section.

Several different symmetries are found in decagonal quasicrystals with different periods. The space groups found so far are: $P10_5/mmc$ for *d*-$Al_{70}Ni_{15}Co_{15}$ ($c = 4.0807$ Å), *d*-$Al_{65}Cu_{20}Co_{15}$ ($c = 4.1481$ Å) and *d*-$Al_{70.5}Mn_{16.5}Pd_{13}$ ($c = 12.4$ Å); $P10/mmm$ for *d*-$Al_{70}Co_{20}Ni_{10}$ ($c = 4.08$ Å); and $P\bar{1}0m2$ for *d*-$Al_{70}Ni_{15}Fe_{15}$ ($c \simeq 17$ Å) (Steurer, Haibach, Zhang, Kek & Lück, 1993; Steurer & Kuo, 1990; Yamamoto & Ishihara, 1988; Beeli, Nissen & Robadey, 1991; Yamamoto, 1993*a*; Saito, Tanaka, Tsai, Inoue & Masumoto, 1992). In *d*-$Al_{70}Ni_{15}Co_{15}$ or *d*-Al–Co, there are diffuse streaks perpendicular to the tenfold axis indicating a doubled (~ 8 Å) period and also satellite reflections suggesting a superstructure in 5D space. The structure analyses made so far neglect such complexity. On the other hand, *d*-$Al_{70}Mn_{17}Pd_{13}$ ($c = 12.04$ Å) shows no diffuse streaks and no satellites.

We discuss the cluster model of *d*-$Al_{70}Mn_{17}Pd_{13}$ in more detail in order to show a modeling of a 5D structure with a given space group. From the crystalline approximants Al_3Mn (Hiraga, Kaneko, Matsuo & Hashimoto, 1993), we assume that it consists of ten layers at around $z = \pm 0.25$, $z = \pm 0.25 \pm 0.12$ and $z = \pm 0.25 \pm 0.19$. The 10_5 screw axis and the mirror plane suggest that one layer is on the mirror plane perpendicular to the screw axis at $z = 0.25$ and the layers at $z \geq 0$ are related to those at $z \leq 0$ by the screw axis. Therefore, there are three independent layers. Furthermore, its HRTEM

image indicates that the arrangement of the cluster centers is quite similar to the tiling obtained from the decagonal occupation domain for the binary tiling (Fig. 20*b*) and that the size of the clusters is about 20 Å (Hiraga, Sun, Lincoln & Matsuo, 1993). This gives a lattice constant of about 2.8 Å and the cluster centers are generated by the decagon with the corner vector $\tau^{-3}\mathbf{e}_1^i$ (Fig. 41).

As discussed above, the occupation domains of the cluster atoms are obtained from that of the center [domain 1 in Fig. 41(*a*)] by shifting it by an appropriate amount along the external space. For example, the atoms at $\mathbf{e}_j^e = 2a/5^{1/2}[c_j\mathbf{a}_1 + s_j\mathbf{a}_2]$ from the center are obtained from the small occupation domains at $\mathbf{e}_j^e$ from the position of the occupation domain of the center. In the present case, the occupation domain of the cluster center is at the origin. Therefore, the shifted occupation domain for the atoms at $\mathbf{e}_j^e$ appears around $-(1, 1, 1, 1, 5z)/5$ since $\mathbf{e}_j^e = \mathbf{d}_j^e - \sum_{l=1}^4 \mathbf{d}_l^e/5 \equiv -\mathbf{e}_j^i - \sum_{l=1}^4 \mathbf{d}_l/5$. Therefore, this is domain 4 in Fig. 41(*b*). Similarly, the atoms at $\mathbf{e}_1^e + \mathbf{e}_2^e$ *etc.* are from the occupation domain at $-(2, 2, 2, 2, 5z)/5$. In the present case, there is another cluster that is located at the center of the pentagon formed by the cluster centers. The center is obtained from a two rhombic star of the occupation domains of the binary tiling by reducing its size by a factor τ^{-3} [domain 1 in Fig. 41(*c*)]. These two are located at $\pm(1, 1, 1, 1, z)/5$ and are related to the tenfold screw axis. The atoms around this cluster are also obtained by shifting the occupation domain of the cluster (the small rhombic star). Such a construction leads to the

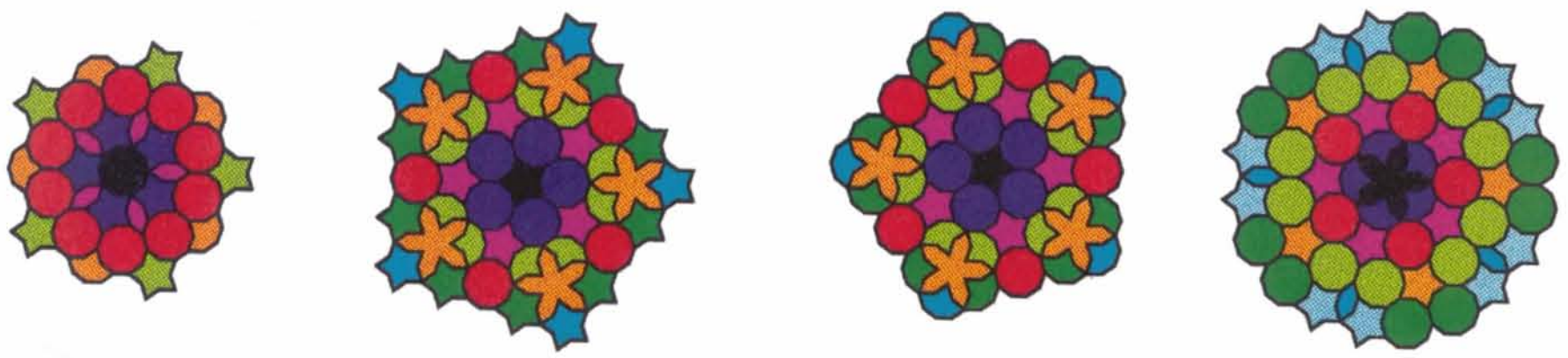

(*a*) (*b*) (*c*) (*d*)

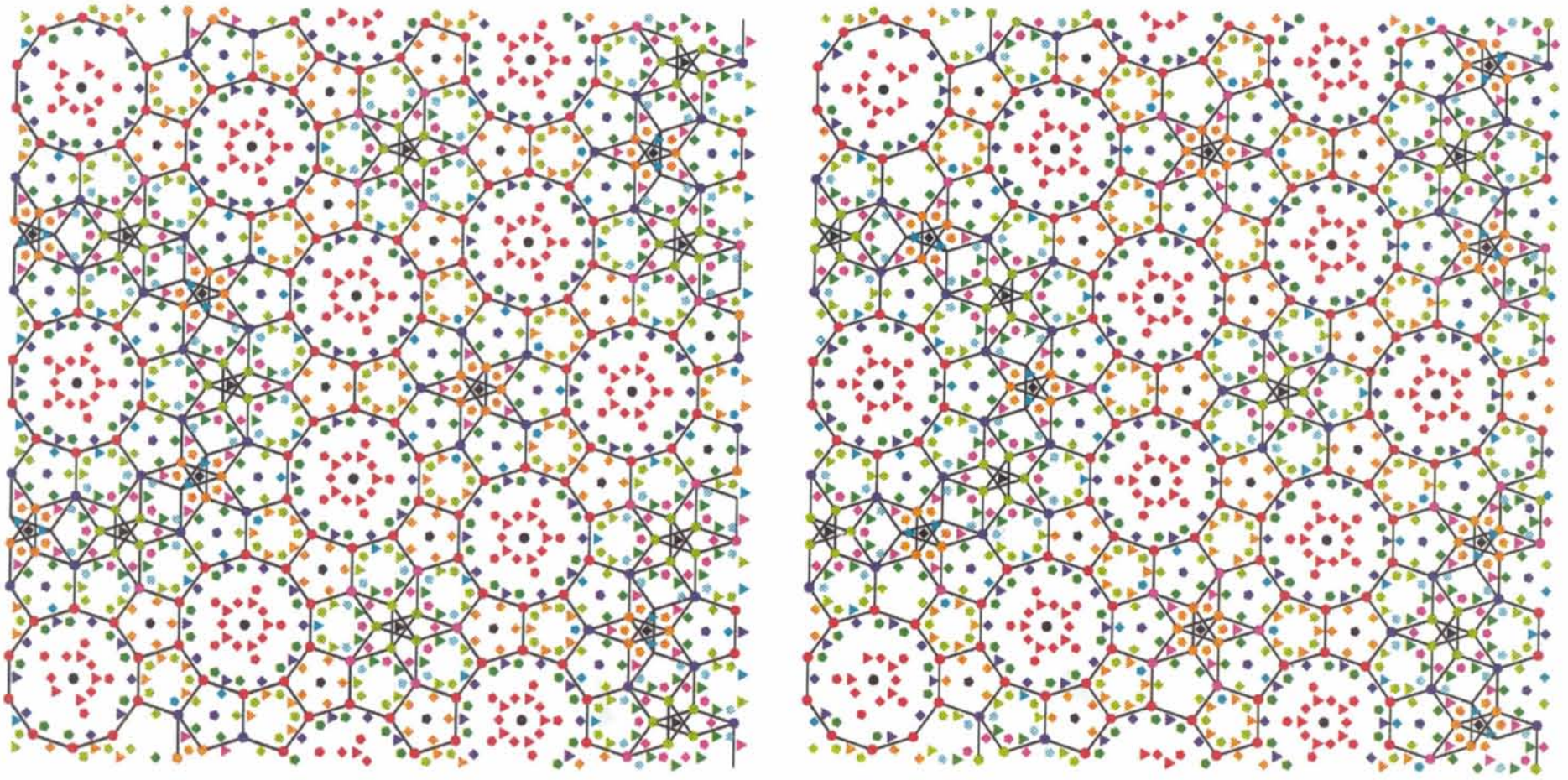

(*e*) (*f*)

Fig. 41. (*a*)–(*d*) Large occupation domains of (*e*), (*f*) the cluster model of *d*-Al–Pd–Mn by Yamamoto (1993*b*). (*a*) The domain *E* located at $(0, 0, 0, 0, 1/4)$. (*b*) The domain *D* at $-(1/5, 1/5, 1/5, 1/5, 1/4)$. (*c*) The domain *A* at $(1/5, 1/5, 1/5, 1/5, \sim 0.38)$. (*d*) the domain *B* at $(2/5, 2/5, 2/5, 2/5, \sim 0.44)$. The structures are projected along the tenfold axis within the range (*e*) $0 \leq z \leq 0.5$ and (*f*) $0.5 \leq z \leq 1$. Atom colors correspond to the occupation domain colors as in Fig. 39. Atoms denoted by circles, triangles, squares and pentagons are obtained from the *E*, *D*, *A* and *B* domains in (*e*), while they come from other domains in (*f*), which are obtained from *E*, *D*, *A* and *B* by the 10_5 screw axis. Small black, violet and red domains are cited as domains 1, 2 and 4 in the text.

occupation domains in Figs. 41(*a*)–(*d*) and the structures in Figs. 41(*e*)–(*f*). In order to see the correspondence between the small occupation domains and the structure in layers perpendicular to the tenfold axis, atoms are plotted with the same color.

As seen above, the cluster model has complicated occupation domains but the structure consists of two clusters and no linking atoms are present. The atoms derived from a small occupation domain have the same local configuration. We can therefore expect the same temperature factor, the shift from the ideal position and the partial occupancies mentioned below to a good approximation. In the structure refinement, it is necessary to take into account the shift. This naturally leads to the refinement method discussed in the next section.

17. Refinement methods

The refinement method is used in the trial-and-error method or in the last stage of the structure determination. This needs a starting model, which is usually obtained from the Patterson or partial Patterson or direct methods discussed in §14 or the theoretical consideration of the structure of crystalline approximants. A rough model can easily be obtained from the Patterson method if there are a few large occupation domains that are located at the special positions. This seems to be true for all quasicrystals found so far except for *i*-Zn–Mg–Y found recently, where there may exist many small occupation domains (Yamamoto, Matsuo, Yamanoi, Tsai, Hiraga & Masumoto, 1995). Then the first task is to determine the size of the large occupation domain since the diffraction intensity is quite sensitive to its size but not so sensitive to its shape (Elser, 1986), provided that an appropriate assignment has been done for the occupation of each domain by constituent atoms. At this stage, we can use spherical occupation domains for icosahedral quasicrystals and circular ones for polyhedral quasicrystals. The radius can be refined by the least-squares method by using the analytic expression of their Fourier integrals [(49) and (50)]. The partial occupancy of each occupation domain can also be refined at the same time if the occupation domain is occupied by two atoms statistically. Then the factor $f^\mu p^\mu$ in (48) is replaced by $[f_1^\mu(1 - s^\mu) + f_2^\mu s^\mu]p^\mu$, where s^μ is the partial occupancy of the second atom sharing the μth site and f_1^μ and f_2^μ are the atomic scattering factors of the first and second atoms. The quasicrystal is usually a ternary alloy. If we try to refine the partial occupancies of three atoms, the same factor is replaced by the factor $[f_1^\mu(1 - s_1^\mu - s_2^\mu) + f_2^\mu s_1^\mu + f_2^\mu s_2^\mu]p^\mu$ with two partial occupancies s_1^μ and s_2^μ (Yamamoto, Matsuo, Yamanoi, Tsai, Hiraga & Masumoto, 1995) but it is impossible to refine these two at the same time by using a single diffraction data set because of the correlation between these two parameters. This is because for a specified value of the factor there are many combinations that give almost same values. If we use two different sets of diffraction data like X-ray and neutron data, it is possible to determine s_1 and s_2 by the refinement (Yamamoto, Kajitani & Morii, 1995).

After the refinement, we can draw difference Fourier maps or the electron-density map by the maximum-entropy method (MEM map) to tailor the shape of the occupation domains or to divide large occupation domains into smaller ones or several shells. In *i*-Al–Pd–Mn, the shell approximation is quite good (Boudard, Boissieu, Janot, Heger, Beeli, Nissen, Vincent, Ibberson, Audier & Dubois, 1992). In order to refine the shape of the occupation domains, the method of Elcoro, Pérez-Mato & Madariaga (1994) mentioned in §10 can be applied, where the deviation from the circle or sphere is expanded in terms of trigonometric functions or spherical harmonics and their amplitudes are refined by the least-squares method. This was successfully applied to *i*-Al–Cu–Li.

It is reasonable to expect a deviation from the ideal atom positions, which are obtained from the occupation domains at special positions with high symmetries. In order to introduce such shifts, it is necessary to subdivide the large occupation domain at the special positions into smaller ones as mentioned in the previous section. Then the center of such occupation domains cannot shift in many cases because of the high site symmetry but the small domains around it can shift along some direction in the external space, since the site symmetry of such subdomains is in general lower than that of the central domain. For example, the domain E_2 in Fig. 41(*a*) is on the mirror plane including $\mathbf{e}_j^i$ and $\mathbf{d}_5$ (the tenfold axis), so that only a shift in the mirror plane is possible. The domain E_2 is on the mirror plane perpendicular to the tenfold axis. This inhibits a shift along the $\mathbf{d}_5$ axis but allows one along $\mathbf{e}_j^e = (2a/5^{1/2})[c_j\mathbf{a}_1 + s_j\mathbf{a}_2]$. On the other hand, the domain A_2 allows a shift along both $\mathbf{d}_5$ and $\mathbf{e}_j^e$. A domain at the general position allows a shift along three independent directions.

The refinement of the shift based on cluster models has been made for *d*-Al–Pd–Mn and *i*-Al–Pd–Mn (Yamamoto, Matsuo, Yamanoi, Tsai, Hiraga & Masumoto, 1995). For both cases, the reduction of the weighted *R* factor (for 1311 and 1137 independent reflections) was about 5% compared to ideal models where the shift is not taken into account. The maximum shift was about 0.3 Å. This means that the the shift is important and not negligible.

18. Maximum-entropy method

The maximum-entropy method (MEM) is known to be efficient in solving normal crystal structures and to determine their electron density (Bricogne & Gilmore, 1990; Sakata & Sato, 1990). Recently, it was applied to quasicrystals and its potential for their structure analysis was discussed (Steurer, 1991). The MEM for quasicrystals in nD space necessitates the calculation technique

discussed below because it requires a large computer memory. For unknown structures, we need to know the phases of several structure factors. The electron density $\rho(\mathbf{r})$ at $\mathbf{r}$ in nD space is calculated from the prior density $\tau(\mathbf{r})$ repeatedly by

$$\rho(\mathbf{r}) = \tau(\mathbf{r}) \exp[\Delta\rho(\mathbf{r})] \tag{70}$$

with

$$\Delta\rho(\mathbf{r}) = \lambda \sum_{\mathbf{h}} [F_{\rm obs}(\mathbf{h}) - F_{\rm cal}(\mathbf{h})] \times \exp(-2\pi i \mathbf{h}\cdot\mathbf{r})/\sigma^2(\mathbf{h}), \tag{71}$$

where λ and $1/\sigma^2(\mathbf{h})$ are the Lagrange multiplier and the weights of the reflections. The phase of a calculated structure factor $F_{\rm cal}(\mathbf{h})$ is used for an observed structure factor $F_{\rm obs}(\mathbf{h})$. The calculated structure factor is given by the Fourier transform of $\tau(\mathbf{r})$:

$$F_{\rm cal}(\mathbf{h}) = V \sum_{\mathbf{r}} \tau(\mathbf{r}) \exp(2\pi i \mathbf{h}\cdot\mathbf{r}), \tag{72}$$

where V is the unit-cell volume. Initial density $\tau(\mathbf{r})$ and structure factors $F_{\rm cal}(\mathbf{h})$ are obtained by the structure refinement based on a model. Phases of several strongest reflections are fixed as known phases in the iteration. The initial density used in the MEM is obtained, for example, from the inverse Fourier transform of $F_{\rm obs}(\mathbf{h})$ for independent reflections and equivalent ones generated by symmetry operations, after truncating its negative parts at a small positive value because MEM requires initial electron density that is positive everywhere. Yamamoto, Weber, Sato, Kato, Ohshima, Tsai, Niikura, Hiraga, Inoue & Masumoto (1996) proposed a slightly modified method with faster convergence, where the following expression is employed instead of (70):

$$\rho(\mathbf{r}) = \tau(\mathbf{r}) \exp\Big(\Delta\rho(\mathbf{r})/\{[\tau(\mathbf{r})]^{1/2} + \varepsilon\}\Big), \tag{73}$$

where ε is a small positive number.

One of the merits of this method is that it provides an electron density that gives a small R factor and is positive everywhere. Since this method estimates the intensities of many unobserved reflections that have large components of diffraction vectors in the internal space, the boundary of the occupation domain is very sharp compared to that of Fourier maps. The peak height of high electron-density regions is also higher. Thus, we can easily see the electron density giving small R factors. This is suitable to tailor the occupation domains or to modify models. There exists one problem in the calculation of MEM maps. This method needs a large computer memory since it calculates the electron density at many grid points in the unit cell of nD space. The nD space necessitates more memory with increasing n, so that the calculations of MEM maps for the icosahedral lattice gives serious problems. The situation is however improved by the application of similarity transformations. The MEM map of *i*-Al–Pd–Mn is shown in Fig. 42(*a*) (Yamamoto, 1995). This map uses 1137 independent reflections. It is noted that the cut-off of the electron density (boundary of the occupation domain) along the internal space is sharp compared to the Fourier map in Fig. 42(*b*).

19. Superstructures in quasicrystals

A superstructure in 5D space was found recently in *d*-$Al_{70}Ni_{15}Co_{15}$ (Edagawa, Ichihara, Suzuki & Takeuchi, 1992). This is the superstructure discussed by Ishihara & Yamamoto (1988). In general, the quasiperiodic tilings

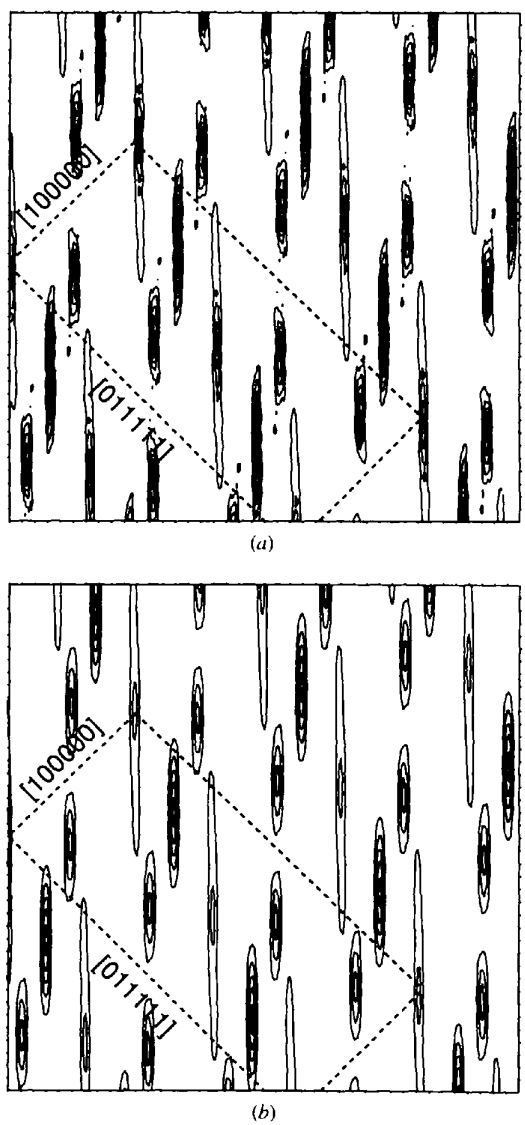

Fig. 42. The electron-density maps of *i*-Al–Pd–Mn obtained from (*a*) the maximum-entropy method and (*b*) Fourier synthesis.

given by the PM can be regarded as superstructures except for the cases where the tilings are obtained from the nD space with minimum dimension by the PM. The exceptional cases are the octagonal Penrose tiling in the 4D octagonal lattice and the 3D Penrose tiling in the 6D icosahedral lattice. In these cases, it should be noted that the tiling is obtained from only one occupation domain at the origin. On the other hand, in the other cases, there are several occupation domains causing the superstructure. The tilings listed in Table 14 can be regarded as superstructures of the tilings given in Table 13.

For example, the rhombic Penrose tiling or binary tiling in the decagonal lattice in 4D space are regarded as the superstructure of the pentagonal Penrose tiling. This is because the occupation domains of the superstructure are located at the lattice points of a smaller cell but their shape and size are different. Therefore, if we place all the lattice points of the smaller cell within the unit cell of the superstructure, we obtain a tiling with a smaller period. In fact, if we place the same decagonal occupation domains at the five special positions $(i, i, i, i)/5$ $(i = 0, 1, 2, 3, 4)$ in a 4D decagonal lattice in contrast to different pentagons in the Penrose tiling, we get the pentagonal Penrose tiling. Then, the five positions are translationally equivalent with the decagonal lattice with $1/5$ cell volume. The diffraction patterns of the pentagonal Penrose and rhombic Penrose tilings are shown by Hiraga, Sun & Yamamoto (1994). Similarly, the dodecagonal Penrose tiling is a superstructure of the Stampfli tiling. In this case, the unit-cell volume of the former is nine times larger than that of the latter (Yamamoto, 1995).

In the Socolar 3D tiling, there are two occupation domains at $(1, 1, 1, 1, 1, 1)/4$ and $(3, 1, 1, 1, 1, 1)/4$ of the face-centered icosahedral lattice (Fig. 24) as mentioned in §6. This is equivalent to the structure with the same occupation domains at the origin and $(1, 0, 0, 0, 0, 0)/2$ of the same face-centered lattice, since the positions are the special positions with site symmetry $m\bar{3}5$ and, therefore, the latter is obtained from the former by just changing the origin. Thus, if we place the same occupation domains at these two positions and equivalent positions to them by the centering translations of the face-centered lattice, we obtain a structure with the primitive icosahedral lattice with a half lattice constant. One such structure is the 3D Penrose tiling, where the occupation domain is a rhombic triacontahedron.

In a real superstructure like d-$Al_{70}Ni_{15}Co_{15}$, the number of occupation domains may be five times larger than that of the normal structure (Hiraga, Sun & Yamamoto, 1994). Some occupation domains are located at positions with low site symmetry. This increases the number of parameters and makes the structure analysis difficult. Hiraga, Lincoln & Sun (1991) proposed a model for the superstructure based on HRTEM images. However, no analysis has been done based on single-crystal X-ray data, though the intensities of satellite reflections can be collected, since there are strong satellite reflections and high-quality single crystals are available.

It is known that there are several superstructures with the face-centered icosahedral lattice with a lattice constant of about 9.6 or 10 Å. They are classified into two types, which are called the Mackay type and Frank–Kasper type. Examples of the former are i-Al–Cu–Fe, i-Al–Pd–Mn and of the latter i-Al–Mg–Li and i-Zn–Mg–Y. For the former, the large occupation domains are located at $(0, 0, 0, 0, 0, 0)$, $(1, 0, 0, 0, 0, 0)/2$, $(3, 1, 1, 1, 1, 1)/4$ (Cornier-Quiquandon, Quivy, Lefebvre, Elkaim, Heger, Katz & Gratias, 1991; Yamamoto, Sato, Kato, Tsai & Masumoto, 1994). On the other hand, in i-Zn–Mg–Y, they are at $(0, 0, 0, 0, 0, 0)$, $(1, 0, 0, 0, 0, 0)/2$, $(1, 1, 1, 1, 1, 1)/4$ and $(3, 1, 1, 1, 1, 1)/4$ but the shifts from the ideal positions seem to be very large compared with the former (Yamamoto, Weber, Sato, Kato, Ohshima, Tsai, Niikura, Hiraga, Inoue & Masumoto, 1996).

The author thanks S. Weber, NIRIM, for drawing Figs. 39 and 41.

References

Aalst, W. van, den Hollander, J., Peterse, W. J. A. M. & de Wolff, P. M. (1976). *Acta Cryst.* B**32**, 47–58.

Audier, M. & Guyot, P. (1988). *Philos. Mag. Lett.* **58**, 17–23.

Bak, P. (1986). *Phys. Rev. Lett.* **56**, 861–864.

Baudour, J. L. & Sanquer, M. (1983). *Acta Cryst.* B**39**, 75–84.

Beeli, C., Nissen, H.-U. & Robadey, J. (1991). *Philos. Mag. Lett.* **63**, 87–95.

Beenker, F. P. M. (1982). Report 82-WSK-04, pp. 1–66. Eindhoven University of Technology, Eindhoven, The Netherlands.

Bendersky, L. (1985). *Phys. Rev. Lett.* **55**, 1461–1463.

Bolotina, N. B., Maximov, R. A., Tamazyan, B. A. & Petříček, V. (1995). *Aperiodic '94*, edited by G. Chapuis & W. Paciorek, pp. 450–454. Singapore: World Scientific.

Boudard, M., Boissieu, M. D., Janot, C., Heger, G., Beeli, C., Nissen, H.-U., Vincent, H., Ibberson, R., Audier, M. & Dubois, J. M. (1992). *J. Phys. Condens. Matter*, **4**, 10149–10168.

Brack, P. J. (1955). *Acta Cryst.* **8**, 175–182.

Bricogne, G. & Gilmore, C. J. (1990). *Acta Cryst.* A**46**, 284–297.

Bronsma, K. D., van Smaalen, S., de Boer, J. L., Wiegers, G. A., Jellinek, F. & Mahy, J. (1987). *Acta Cryst.* B**43**, 305–313.

Brown, H., Bülow, R., Neubüser, J., Wondratschek, H. & Zassenhaus, H. (1978). *Crystallographic Groups of Four-Dimensional Space*. New York: John Wiley.

Bruijn, N. G. de (1981). *Proc. K. Ned. Akad. Wet. Ser. A*, **43**, 39–66.

Budkowski, A., Prodan, A., Marinković, V., Kucharczyk, D., Uszyński, I. & Boswell, F. W. (1989). *Acta Cryst.* B**45**, 529–534.

Burkov, S. E. (1991). *Phys. Rev. Lett.* **67**, 614–617.

Coppens, P., Petříček, V., Levendis, D., Larsen, F. K., Paturle, A., Yan, G. & LeGrand, A. D. (1987). *Phys. Rev. Lett.* **59**, 1695–1697.
Cornier-Quiquandon, M., Quivy, A., Lefebvre, S., Elkaim, G., Heger, E., Katz, A. & Gratias, D. (1991). *Phys. Rev. B*, **44**, 2071–2084.
Dam, B. & Janner, A. (1985). *Phys. Rev. Lett.* **55**, 2301–2304.
Danzer, L. (1989). *Discrete Math.* **76**, 1–7.
Danzer, L. & Talis, A. (1993). *Int. J. Mod. Phys.* B**7**, 1379–1386.
Dehlinger, U. (1929). *Ann. Phys. (Leipzig)*, **2**, 749–755.
Depmeier, W. (1981). *Acta Cryst.* B**37**, 330–339.
Doudin, B. & Chapuis, G. (1990). *Acta Cryst.* B**46**, 180–186.
Dubost, B., Lang, J. M., Tanaka, M., Stainfort, P. & Audier, M. (1986). *Nature (London)*, **324**, 48–50.
Duneau, M. & Katz, A. (1985). *Phys. Rev. Lett.* **54**, 2688–2691.
Ebalard, S. & Spaepen, F. (1989). *J. Mater. Res.* **4**, 39–43.
Edagawa, K., Ichihara, M., Suzuki, K. & Takeuchi, S. (1992). *Philos. Mag. Lett.* **66**, 19–23.
Edagawa, K., Tamura, H., Suzuki, K. & Takeuchi, S. (1995). *Aperiodic '94*, edited by G. Chapuis & W. Paciorek, pp. 351–355. Singapore: World Scientific.
Elcoro, L., Pérez-Mato, J. M. & Madariaga, G. (1994). *Acta Cryst.* A**50**, 182–193; erratum: (1994), A**50**, 550.
Elser, V. (1985). *Phys. Rev. B*, **32**, 4892–4898.
Elser, V. (1986). *Acta Cryst.* A**42**, 36–43.
Elser, V. & Henley, C. (1985). *Phys. Rev. Lett.* **55**, 2883–2886.
Elswijk, H. B., de Hosson, J. T. M., van Smaalen, S. & de Boer, J. L. (1988). *Phys. Rev. B*, **38**, 1681–1685.
Evain, M., van der Lee, A., Monconduit, L. & Petříček, V. (1994). *Chem. Mater.* **6**, 1776–1783.
Fu, Z. Q., Li, F. H. & Fan, H. F. (1993). *Z. Kristallogr.* **206**, 57–68.
Fung, K. K., Yang, C. Y., Zhou, Y. Q., Zhan, W. S. & Shen, B. G. (1986). *Phys. Rev. Lett.* **56**, 2060–2063.
Gähler, F. (1990). *Quasicrystals and Incommensurate Structures in Condensed Matter*, edited by J. Yacaman, pp. 69–78. Singapore: World Scientific.
Gähler, F. & Rhyner, J. (1986). *J. Phys. A: Math. Nucl. Gen.* **19**, 267–277.
Gaillard, V. B., Paciorek, W. & Chapuis, G. (1995). *Aperiodic '94*, edited by G. Chapuis & W. Paciorek, pp. 478–482. Singapore: World Scientific.
Gao, Y., Gajhede, M., Mallinson, P., Petříček, V. & Coppens, P. (1988). *Phys. Rev. B*, **37**, 1825–1831.
Gratias, D., Cahn, J. W. & Mozer, B. (1988*a*). *J. Phys. (Paris)*, **49**, 1225–1233.
Gratias, D., Cahn, J. W. & Mozer, B. (1988*b*). *Phys. Rev. B*, **38**, 1638–1642.
Hardy, H. K. & Silcock, J. M. (1955). *J. Inst. Met.* **24**, 423–428.
Harris, P., Larsen, F. K., Lebech, B. & Achiwa, N. (1994). *Acta Cryst.* B**50**, 676–684.
Hedoux, A., Grebille, D. & Garnier, P. (1989). *Phys. Rev. B*, **40**, 10653–10656.
Henley, C. L. (1986). *Phys. Rev. B*, **34**, 797–816.
Henley, C. L. (1987). *J. Phys. A*, **21**, 1649.
Henley, C. L. (1988). *Philos. Mag. Lett.* **58**, 87–89.
Henley, C. L. & Elser, V. (1986). *Philos. Mag.* B**53**, L59–L66.
Hiraga, K. (1995). *Aperiodic '94*, edited by G. Chapuis & W. Paciorek, pp. 341–350. Singapore: World Scientific.
Hiraga, K., Kaneko, M., Matsuo, Y. & Hashimoto, S. (1993). *Philos. Mag.* B**67**, 193–205.
Hiraga, K., Lincoln, F. J. & Sun, W. (1991). *Mater. Trans. Jpn. Inst. Met.* **32**, 308–314.
Hiraga, K. & Sun, W. (1993). *Philos. Mag. Lett.* **67**, 117–123.
Hiraga, K., Sun, W., Lincoln, F. J. & Matsuo, Y. (1993). *Phase Transit.* **44**, 163–172.
Hiraga, K., Sun, W. & Yamamoto, A. (1994). *Mater. Trans. Jpn. Inst. Met.* **35**, 657–662.
Ishihara, K. N., Nishitani, S. R. & Shingu, P. H. (1987). *Trans. Iron Steel Inst. Jpn*, **28**, 2–6.
Ishihara, K. N. & Shingu, P. H. (1986). *J. Phys. Soc. Jpn*, **55**, 1795–1798.
Ishihara, K. N. & Yamamoto, A. (1988). *Acta Cryst.* A**44**, 508–516.
Ishii, Y. (1989). *Phys. Rev. B*, **39**, 11862–11871.
Ishimasa, T., Fukano, Y. & Tsuchimori, M. (1988). *Philos. Mag. Lett.* **58**, 157–165.
Ishimasa, T., Nissen, H. U. & Fukano, Y. (1985). *Phys. Rev. Lett.* **55**, 511–513.
Janner, A. & Janssen, T. (1977). *Phys. Rev. B*, **15**, 643–658.
Janner, A. & Janssen, T. (1979). *Physica (Utrecht)*, **99**A, 47–76.
Janner, A. & Janssen, T. (1980*a*). *Acta Cryst.* A**36**, 399–408.
Janner, A. & Janssen, T. (1980*b*). *Acta Cryst.* A**36**, 408–415.
Janot, C., de Boissieu, M., Dubois, J. M. & Pannetier, J. (1989). *J. Phys. Condens. Matter*, **1**, 1029–1048.
Janot, C., Pannetier, J., Dubois, J. M. & de Boissieu, M. (1989). *Phys. Rev. Lett.* **62**, 450–453.
Janssen, T. (1986). *Acta Cryst.* A**42**, 261–271.
Janssen, T. (1992). *Philos. Mag. Lett.* **66**, 125–134.
Janssen, T. & Janner, A. (1987). *Adv. Phys.* **36**, 519–624.
Janssen, T., Janner, A., Looijenga-Vos, A. & de Wolff, P. M. (1992). *International Tables for Crystallography*, Vol. C, edited by A. J. C. Wilson, pp. 797–835. Dordrecht: Kluwer Academic Publishers.
Jarić, M. V. (1986). *Phys. Rev. B*, **34**, 4685–4698.
Jarić, M. V. & Nelson, D. R. (1988). *Phys. Rev. B*, **37**, 4458–4472.
Jarić, M. V. & Quin, S. Y. (1990). *Quasicrystals*, edited by T. Fujiwara & T. Ogawa, pp. 48–56. Berlin: Springer-Verlag.
Kalugin, P. A., Kitayev, A. Y. & Levitov, L. S. (1985*a*). *JETP Lett.* **41**, 145–149.
Kalugin, P. A., Kitayev, A. Y. & Levitov, L. S. (1985*b*). *J. Phys. Lett.* **46**, L601–L607.
Kato, K. (1990). *Acta Cryst.* B**46**, 39–44.
Katz, A. & Duneau, M. (1986). *J. Phys. (Paris)*, **47**, 181–196.
Komdeur, A. J. H., de Boer, J. & van Smaalen, S. (1990). *J. Phys. Condens. Matter*, **2**, 45–54.
Korepin, V. E., Gähler, F. & Rhyner, J. (1988). *Acta Cryst.* A**44**, 667–672.
Kramer, P. (1987). *Acta Cryst.* A**43**, 486–489.
Kramer, P. & Neri, R. (1984). *Acta Cryst.* A**40**, 580–587.
Kramer, P., Papadopolos, Z., Schlottmann, M. & Zeidler, D. (1994). *J. Phys. A: Math. Nucl. Gen.* **27**, 4505–4517.
Krumeich, F., Conrad, M. & Harbrecht, B. (1994). Proceedings of ICEM 13, Paris, France, pp. 751–752.
Kucharczyk, D., Budkowski, A., Boswell, F. W., Prodan, A. & Marinković, V. (1990). *Acta Cryst.* B**46**, 153–159.
Lancon, F. & Billard, L. (1988). *J. Phys. (Paris)*, **49**, 249–256.
Lee, A. van der, Evain, M., Mansuetto, M., Monconduit, L., Brec, R. & Rouxel, J. (1994). *J. Solid State Chem.* **111**, 75–82.
Lee, A. van der, Evain, M., Monconduit, L., Brec, R., Rouxel, J. & Petříček, V. (1994). *Acta Cryst.* B**50**, 119–128.

Lee, A. van der, Evain, M., Monconduit, L., Brec, R. & van Smaalen, S. (1994). *J. Phys. Condens. Matter*, **6**, 933–944.
Lee, A. van der, van Smaalen, S., Wiegers, G. A. & de Boer, J. L. (1991). *Phys. Rev. B*, **43**, 9420–9430.
Leligny, H., Durcok, S., Labbe, P., Ledesert, M. & Raveau, B. (1992). *Acta Cryst.* B**48**, 407–418.
Leligny, H., Labbe, P., Ledesert, M., Hervieu, M., Raveau, B. & McCarroll, W. H. (1993). *Acta Cryst.* B**49**, 444–454.
Leligny, H., Labbe, P., Ledesert, M., Raveau, B., Valdez, C. & McCarroll, W. H. (1992). *Acta Cryst.* B**48**, 134–144.
Levitov, L. S. & Rhyner, J. (1988). *J. Phys. (Paris)*, **49**, 1835–1849.
Li, J. Q., Li, F. H. & Zhao, Z. X. (1993). *Phys. Rev. B*, **48**, 1333–1336.
Li, X. Z., Shi, D. & Kuo, K. H. (1992). *Philos. Mag.* B**66**, 331–340.
Li, X. Z., Shi, N. C., Ma, Z. S., Ma, X. L. & Kuo, K. H. (1995). *Philos. Mag. Lett.* **72**, 79–86.
Mackay, A. (1981). *Sov. Phys. Crystallogr.* **26**, 517–522.
Mai, Z. H., Tao, S. H., Zeng, L. Z. & Zhang, B. (1988). *Phys. Rev. B*, **38**, 12913–12916.
Makovicky, E. & Hyde, B. G. (1981). *Struct. Bonding (Berlin)*, **46**, 101–176.
Matthew, A. M. & Elser, V. (1986). *Philos. Mag. Lett.* **53**, L101–L104.
Maximov, B. A., Bolotina, N. B., Simonov, V. I., Petříček, V. & Schulz, H. (1994). *Acta Cryst.* B**50**, 261–268.
Meyer, M., Paciorek, W., Schenk, K. & Chapuis, G. (1995). *Aperiodic '94*, edited by G. Chapuis & W. Paciorek, pp. 483–487. Singapore: World Scientific.
Meyer, M., Paciorek, W. A., Schenk, K. J., Chapuis, G. & Depmeier, W. (1994). *Acta Cryst.* B**50**, 333–343.
Motai, K., Watanabe, Y. & Hashimoto, S. (1993). *Acta Cryst.* B**49**, 655–661.
Niizeki, K. (1989). *J. Phys. A: Math. Nucl. Gen.* **22**, 1859–1869.
Niizeki, K. (1991). *J. Phys. A: Math. Nucl. Gen.* **24**, 3641–3654.
Ogawa, T. (1985). *J. Phys. Soc. Jpn*, 3205–3208.
Ohmasa, M., Hiraga, K., Tomeoda, K. & Ueda, A. (1995). *Aperiodic '94*, edited by G. Chapuis & W. Paciorek, pp. 475–477. Singapore: World Scientific.
Onoda, G. Y., Steinhardt, P. J., DiVincenzo, D. P. & Socolar, J. E. (1988). *Phys. Rev. Lett.* **60**, 2653–2656.
Onoda, M. & Kato, K. (1991). *Acta Cryst.* B**47**, 630–634.
Onoda, M., Saeki, M., Yamamoto, A. & Kato, K. (1993). *Acta Cryst.* B**49**, 929–936.
Pavlovitch, A. & Kléman, M. (1987). *J. Phys. A: Math. Nucl. Gen.* **20**, 687–702.
Penrose, R. (1974). *Bull. Inst. Math. Appl.* **10**, 266–271.
Penrose, R. (1977). *Math. Intel.* **2**, 32–37.
Perez, O., Leligny, H., Grebille, D., Labbe, D. P., Groult, D. & Raveau, B. (1995). *Aperiodic '94*, edited by G. Chapuis & W. Paciorek, pp. 465–469. Singapore: World Scientific.
Petříček, V., Cisarova, I., de Boer, J. L., Zhou, W., Meetsma, A., Wiegers, G. A. & van Smaalen, S. (1993). *Acta Cryst.* B**49**, 258–266.
Petříček, V., Coppens, P. & Becker, P. (1985). *Acta Cryst.* A**41**, 478–483.
Petříček, V., Maly, K., Coppens, P., Bu, X., Cisarova, I. & Frost-Jenssen, A. (1991). *Acta Cryst.* A**47**, 210–216.
Prodan, A. & Boswell, F. W. (1987). *Acta Cryst.* B**43**, 165–170.
Rabson, D. A., Mermin, N. D., Rokhsar, D. S. & Wright, D. C. (1991). *Rev. Mod. Phys.* **63**, 699–733.
Rokhsar, D. S., Wright, D. C. & Mermin, N. D. (1988). *Phys. Rev. B*, **37**, 8145–8149.
Roth, J. (1993). *J. Phys. A: Math. Nucl. Gen.* **26**, 1455–1461.
Sadanaga, R. & Ohsumi, K. (1979). *Acta Cryst.* A**35**, 115–122.
Saito, M., Tanaka, M., Tsai, A. P., Inoue, A. & Masumoto, T. (1992). *J. Appl. Phys.* **31**, L109–L112.
Sakata, M. & Sato, M. (1990). *Acta Cryst.* A**46**, 263–270.
Schmid, S. & Withers, R. L. (1995). *Aperiodic '94*, edited by G. Chapuis & W. Paciorek, pp. 455–459. Singapore: World Scientific.
Schmid, S., Withers, R. L. & Thompson, J. G. (1992). *J. Solid State Chem.* **99**, 226–242.
Schutte, W. J. & de Boer, J. L. (1988). *Acta Cryst.* B**44**, 486–494.
Schutte, W. J. & de Boer, J. L. (1993*a*). *Acta Cryst.* B**49**, 398–403.
Schutte, W. J. & de Boer, J. L. (1993*b*). *Acta Cryst.* B**49**, 579–591.
Schutte, W. J., Disselborg, F. & de Boer, J. L. (1993). *Acta Cryst.* B**49**, 787–794.
Sciau, P. & Grebille, D. (1989). *Phys. Rev. B*, **39**, 11982–11992.
Sciau, P., Lapasset, J., Grebille, D. & Berar, J. F. (1988). *Acta Cryst.* B**44**, 108–116.
Shechtman, D., Blech, I., Gratias, D. & Cahn, J. W. (1984). *Phys. Rev. Lett.* **53**, 1951–1954.
Shen, Y., Poon, S. J., Dmowski, W., Egami, T. & Shiflet, G. J. (1987). *Phys. Rev. Lett.* **58**, 1440–1443.
Smaalen, S. van (1989). *J. Phys. Condens. Matter*, **1**, 2791–2800.
Smaalen, S. van (1991). *J. Phys. Condens. Matter*, **3**, 1247–1263.
Smaalen, S. van (1995). *Crystallogr. Rev.* **4**, 79–202.
Smaalen, S. van & George, T. F. (1987). *Phys. Rev. B*, **35**, 7939–7951
Smaalen, S. van & Haas, C. (1985). *Solid State Commun.* **55**, 1027–1029.
Socolar, H. E. S. (1989). *Phys. Rev. B*, **39**, 10519–10551.
Socolar, H. E. S., Lubensky, T. C. & Steinhardt, P. J. (1986). *Phys. Rev. B*, **34**, 3345–3360.
Socolar, P. J., Steinhardt, J. E. S. & Levine, D. (1985). *Phys. Rev. B*, **32**, 5547–5550.
Soma, T. & Watanabe, Y. (1992). *Acta Cryst.* A**48**, 470–475.
Speziali, N. L. & Chapuis, G. (1989). *Acta Cryst.* B**45**, 20–26.
Steurer, W. (1987). *Acta Cryst.* A**43**, 36–42.
Steurer, W. (1989). *Acta Cryst.* B**45**, 534–542.
Steurer, W. (1991). *Methods of Structural Analysis of Modulated Structures and Quasicrystals*, edited by J. M. Pérez-Mato, F. J. Zúñiga & G. Madariaga, pp. 344–349. Singapore: World Scientific.
Steurer, W. & Adlhart, W. (1983*a*). *Acta Cryst.* B**39**, 349–355.
Steurer, W. & Adlhart, W. (1983*b*). *Acta Cryst.* B**39**, 721–724.
Steurer, W. & Depmeier, W. (1989). *Acta Cryst.* B**45**, 555–562.
Steurer, W., Haibach, T., Zhang, B., Kek, S. & Lück, R. (1993). *Acta Cryst.* B**49**, 661–675.
Steurer, W. & Jagodzinski, H. (1988). *Acta Cryst.* B**44**, 344–351.
Steurer, W. & Kuo, H. (1990). *Acta Cryst.* B**46**, 703–712.
Steurer, W., Visser, R. J. J., van Smaalen, S. & de Boer, J. L. (1987). *Acta Cryst.* B**43**, 567–574.

Strandburg, K. J., Tang, L. & Jarić, M. V. (1989). *Phys. Rev. Lett.* **63**, 314–317.
Terauchi, M., Takahashi, M. & Tanaka, M. (1994). *Acta Cryst.* A**50**, 566–574.
Thompson, J. G., Withers, R. L. & Kepert, C. J. (1991). *J. Solid State Chem.* **95**, 111–125.
Torres, M., Pastor, G., Jimenez, I. & Fayos, J. (1989). *Philos. Mag. Lett.* **59**, 181–188.
Tsai, A. P., Inoue, A. & Masumoto, T. (1987). *Jpn. J. Appl. Phys.* Part 2, **26**, L1505–L1507.
Tsai, A. P., Inoue, A. & Masumoto, T. (1989). *Mater. Trans. Jpn. Inst. Met.* **30**, 463–473.
Ukei, K., Shishido, T. & Fukuda, T. (1994). *Acta Cryst.* B**50**, 42–45.
Ukei, K., Yamamoto, A., Watanabe, Y., Shishido, T. & Fukuda, T. (1993). *Acta Cryst.* B**49**, 67–72.
Valentine, D. Y., Cavin, O. B. & Yakel, H. L. (1977). *Acta Cryst.* B**33**, 1389–1396.
Wang, N., Chen, H. & Kuo, K. H. (1987). *Phys. Rev. Lett.* **59**, 1010–1013.
Wang, R. H., Quin, C. S., Lu, G. H., Feng, Y. C. & Xu, S. Q. (1994). *Acta Cryst.* A**50**, 366–375.
Wang, Z. M. & Kuo, K. H. (1988). *Acta Cryst.* A**44**, 857–863.
Watanabe, Y., Ito, M. & Soma, T. (1987). *Acta Cryst.* A**43**, 133–134.
Whittaker, J. W. & Whittaker, R. M. (1988). *Acta Cryst.* A**44**, 105–112.
Widom, M., Deng, D. P. & Henley, C. L. (1989). *Phys. Rev. Lett.* **63**, 310–313.
Willson, J. A., Di Salve, F. J. & Mahajan, S. (1975). *Advances in Physics*, edited by D. H. Martin, pp. 117–201. New York: Taylor & Francis.
Withers, R. L., Feng, Y. C. & Lu, G. H. (1990). *J. Phys. Condens. Matter*, **2**, 3187–3200.
Withers, R. L., Hyde, B. G., Prodan, A. & Boswell, F. W. (1990). *J. Phys. Condens. Matter*, **2**, 4051–4058.
Withers, R. L., Thompson, J. G. & Hyde, B. G. (1991). *Acta Cryst.* B**47**, 166–174.
Wolff, P. M. de (1974). *Acta Cryst.* A**30**, 777–785.
Wolff, P. M. de, Janssen, T. & Janner, A. (1981). *Acta Cryst.* A**37**, 625–636.
Xiang, S., Fan, H., Wu, X., Li, F. & Pan, Q. (1990). *Acta Cryst.* A**46**, 929–934.
Yamamoto, A. (1981). *Acta Cryst.* A**37**, 838–842.
Yamamoto, A. (1982*a*). *Acta Cryst.* A**38**, 87–92.
Yamamoto, A. (1982*b*). *Acta Cryst.* B**38**, 1446–1451.
Yamamoto, A. (1982*c*). *Acta Cryst.* B**38**, 1451–1456.
Yamamoto, A. (1983*a*). *Phys. Rev. B*, **27**, 7823–7826.
Yamamoto, A. (1983*b*). *Acta Cryst.* B**39**, 17–20.
Yamamoto, A. (1985*a*). *Phys. Rev. B*, **31**, 5941–5945.
Yamamoto, A. (1985*b*). *Kesshou Gakkai Kouen Yokoushyu*, p. 2027. (In Japanese.)
Yamamoto, A. (1990). *Quasicrystals*, edited by T. Fujiwara & T. Ogawa, pp. 57–67. Berlin: Springer-Verlag.
Yamamoto, A. (1992*a*). *Acta Cryst.* A**48**, 476–483.
Yamamoto, A. (1992*b*). *Phys. Rev. B*, **45**, 5217–5227.
Yamamoto, A. (1993*a*). *Acta Cryst.* A**49**, C337.
Yamamoto, A. (1993*b*). *Acta Cryst.* A**49**, 831–846.
Yamamoto, A. (1995). Unpublished.
Yamamoto, A. & Hiraga, K. (1988). *Phys. Rev. B*, **37**, 6207–6214.
Yamamoto, A. & Inoue, Z. (1982). *Acta Cryst.* B**38**, 1703–1706.
Yamamoto, A. & Ishihara, K. N. (1988). *Acta Cryst.* A**44**, 707–714.
Yamamoto, A., Janssen, T., Janner, A. & de Wolff, P. M. (1985). *Acta Cryst.* A**41**, 528–530.
Yamamoto, A., Kajitani, T. & Morii, Y. (1995). *Proc. 2nd AsCA Meeting*. To be published.
Yamamoto, A., Kato, K., Shibuya, T. & Takeuchi, S. (1990). *Phys. Rev. Lett.* **65**, 1603–1605.
Yamamoto, A., Matsuo, Y., Yamanoi, T., Tsai, A. P., Hiraga, K. & Masumoto, T. (1995). *Aperiodic '94*, edited by G. Chapuis & W. Paciorek, pp. 393–398. Singapore: World Scientific.
Yamamoto, A. & Nakazawa, H. (1982). *Acta Cryst.* B**38**, 79–86.
Yamamoto, A., Nakazawa, H., Kitamura, M. & Morimoto, N. (1984). *Acta Cryst.* B**40**, 228–237.
Yamamoto, A., Sato, A., Kato, K., Tsai, A. P. & Masumoto, T. (1994). *Mater. Sci. Forum*, **150**, 211–222.
Yamamoto, A., Takayama-Muromachi, E., Izumi, F., Ishigaki, T. & Asano, H. (1992). *Physica (Utrecht)*, C**201**, 137–144.
Yamamoto, A., Weber, S., Sato, A., Kato, K., Ohshima, K., Tsai, A. P., Niikura, A., Hiraga, K., Inoue, A. & Masumoto, T. (1996). *Philos. Mag. Lett.* In the press.
Yamamoto, A., Yamada, T., Ikawa, H., Fukunaga, O., Tanaka, K. & Marumo, F. (1991). *Acta Cryst.* C**47**, 1588–1591.
Yamamoto, N., Hirotsu, Y., Nakamura, Y. & Nagakura, S. (1989). *Jpn. J. Appl. Phys.* Part 2, **28**, L598–L601.
Yao, J. X. (1981). *Acta Cryst.* A**37**, 642–644.
Zobetz, E. (1992). *Acta Cryst.* A**48**, 328–335.
Zobetz, E. & Preisinger, A. (1990). *Acta Cryst.* A**46**, 962–969.
Zúñiga, F. J., Madariaga, G., Paciorek, W. A., Pérez-Mato, J. M., Ezpeleta, J. M. & Etxebarria, I. (1989). *Acta Cryst.* B**45**, 566–576.